

Santa Clara University

Scholar Commons

Mechanical Engineering Senior Theses

Engineering Senior Theses

6-2021

Bi-directional Kerr-Lens Mode-Locked Titanium Sapphire Laser

Ricky Arnold

Stratos Koutroulis

Dylan Meyer

Follow this and additional works at: https://scholarcommons.scu.edu/mech_senior



Part of the [Mechanical Engineering Commons](#)

SANTA CLARA UNIVERSITY

Department of Mechanical Engineering

I HEREBY RECOMMEND THAT THE THESIS PREPARED
UNDER MY SUPERVISION BY

Ricky Arnold, Stratos Koutroulis, Dylan Meyer

ENTITLED

**Bi-directional Kerr-Lens Mode-Locked
Titanium Sapphire Laser**

BE ACCEPTED IN PARTIAL FULFILLMENT OF THE REQUIREMENTS
FOR THE DEGREE OF

**BACHELOR OF SCIENCE
IN
MECHANICAL ENGINEERING**

DocuSigned by:

Dr. Bachana Lomsadze

9F93B6E69C94484...

6/10/2021

Dr. Bachana Lomsadze, Physics Advisor

Date

Drazen Fabris

6/10/21

Dr. Drazen Fabris, Mechanical Engineering Advisor

Date

Drazen Fabris

6/10/2021

Dr. Drazen Fabris, Mechanical Engineering Department Chair

Date

Bi-directional Kerr-Lens Mode-Locked Titanium Sapphire Laser

By

Ricky Arnold, Stratos Koutroulis, Dylan Meyer

SENIOR DESIGN PROJECT REPORT

Submitted to
the Department of Mechanical Engineering

of

SANTA CLARA UNIVERSITY

in Partial Fulfillment of the Requirements
for the degree of
Bachelor of Science in Mechanical Engineering

Santa Clara, California

2021

Bi-directional Kerr-Lens Mode-Locked Titanium Sapphire Laser

Ricky Arnold, Stratos Koutroulis, Dylan Meyer

Department of Mechanical Engineering
Santa Clara University
Santa Clara, California
2021

ABSTRACT

Precision near-infrared absorption spectroscopy is a highly desired scientific method, but the blooming technology has not yet come to fruition. Field deployments are limited, and some methods come with limitations that hamper the viability. The laser cavity completed for this thesis project is a single cavity Dual Comb Spectroscopy laser, which improves myriad limiting characteristics of previous lasers in this application. Crucially, it can produce two simultaneous pulse trains with unique repetition rates. The laser cavity has been designed, built, and aligned for improved stability, including vibrational, noise, and thermal control. The design, analysis, and results of a dual comb spectroscopy laser which successfully maintains two combs, 750 MHz repetition rate, with a bandwidth of 30 nm centered at 835 nm is presented.

Acknowledgements

We would like to thank both of our faculty advisors, Dr. Bachana Lomsadze and Dr. Drazen Fabris, for their immense support and encouragement throughout the duration of our project. Had it not been for their experience and insight, this project would not have been possible. Additionally, both Mr. Gary Sloan and Mr. Rodney Broome contributed a huge amount of their time to make sure that we could manufacture the parts necessary for our project's success, and for that we are extremely appreciative. We would also like to thank Dr. Betty Young for help with the preparation of the thesis.

Table of Contents

ABSTRACT	iii
Acknowledgements	iv
Table of Contents	v
List of Figures	xi
List of Tables	xv
Nomenclature	xvi
1 Introduction	1
1.1 Motivation	1
1.2 Absorption Spectroscopy background	2
1.3 Background Information	5
1.3.1 Lasing	5
1.3.2 Four Mirror Cavity	6
1.3.3 Bi-directionality of a Cavity	7
1.3.4 Absorption/Emission & Stimulated Emission	8
1.3.5 Bandwidth	9
1.3.6 Mode-locked operation	10
1.3.7 Frequency Combs	10
1.3.8 Titanium Sapphire Crystal	11
1.3.9 Kerr-Lensing/Refractive Index	13
1.3.10 Chirp	14
1.3.11 Drifting	14
1.4 Review of Literature	15
1.5 Core Characteristics Condensed	15
1.6 Goals and Objectives	17
Chapter 2 Project Overview	18
2.1 Recipient Needs	18
2.2 Core Requirements	18
2.3 Conceptual System Layout	19
2.4 Functional Analysis	20
2.6 Key system level issues	21
2.7 Team and project management	22
2.7.1 Challenges	22
2.7.2 Budget	22

2.7.3 Safety	22
2.7.4 Design process	23
Chapter 3 Pre-Cavity	24
3.1 Overview and Requirements	24
3.2 Pre-existing Setup	24
3.2.1 Sprout G Pump Laser	25
3.2.2 Half Wave Plate and Beam Splitter	25
3.3 Redirecting Mirrors	27
3.3.1 Pump-Height Mirrors	27
3.3.2 Periscope Mirrors	28
3.4 Periscope	29
3.4.1 Periscope Tower	30
3.4.2 Periscope Mounting Plate	30
3.4.3 PeriscopeVariable Mount	31
3.4.2 Periscope Container	32
3.5 Optical Analysis	33
3.5.1 Mount Integrity	33
3.5.2 Beam Direction	33
3.5.3 Optical Power	34
3.6 Problems, Revisions, and Future Changes	35
Chapter 4 Physical Build Components	36
4.1 Introduction to Physical Build	36
4.2 Initial Design Decisions	36
4.3 Breadboard	38
4.3.1 Implementation Trade-offs	38
4.3.2 Material	41
4.3.3 Breadboard Clamps	42
4.4 Optical Stages	42
4.5 Posts	43
4.6 Mounting Spacers	43
4.6.1 Focusing Lens:	43
4.6.2 Heat sink spacers:	45
4.7 Proof of Worth Analysis	46
4.8 PID Implementation	46
4.9 Problems Encountered and Adaptations	47
Chapter 5 Optics	48
5.2 Requirements	48

5.2.1 Assembly Requirements	48
5.2.2 Optical Requirements	49
5.3 Component Selection	49
5.3.1 Redirecting Mirrors	49
5.3.2 Focus Lens	50
5.3.3 Crystal	50
5.3.4 Curved Mirrors	50
5.3.5 Output Mirror	52
5.3.6 Chirped Mirror	52
5.4 Cavity	53
5.5 Post-Cavity Components	53
Chapter 6 Thermal Regulation	54
6.1 Overview	54
6.2 Requirements	54
6.3 Design	55
6.3.1 Tubing Setup	57
6.3.2 Flow Source	58
6.4 Analytical Solution	60
6.5 CFD analysis	66
6.6 Thermal Performance Verification	68
6.7 Problems and Revisions	68
Chapter 7 Manufacturing and Preliminary Assembly	69
7.1 Overview and Requirements	69
7.2 Materials Selection	69
7.3 Stainless Steel	69
7.3.1 Posts	69
7.4 Aluminum	70
7.4.1 Spacers	70
7.4.2 Periscope	71
7.5 Acrylic	71
7.5.1 Cavity Containment	71
7.5.2 Periscope Containment	72
7.5.3 Other Improvements	72
7.6 Screws	72
7.7 Timeline considerations	73
Chapter 8 Laser Alignment and Results	74
8.1 Overview	74

8.2 Challenges & Solutions	74
8.3 Component Placement	75
8.4 Initial Alignment	75
8.4.1 Hazard Awareness	76
8.5 Feedback Alignment	76
8.6 Lasing Alignment	77
8.7 Mode Locking Alignment	79
8.8 Iterations, Power, Appearance	80
8.8.1 Green	82
8.8.2 Red/Near Infrared	82
8.9 Laser Qualitative Analysis	83
8.9.1 Mode Locking Quality	85
8.9.2 Pulse Repetition Rates	85
8.9.3 Dual Comb Status	85
8.9.4 Absorption Spectroscopy Test	85
8.9.5 Frequency Combs	85
8.10 Aligning Summary	85
8.11 Future Plans	85
Chapter 9 Budget Analysis	86
9.1 Presecured Components	86
9.2 Directly Funded Components	87
9.2.1 Funding	87
9.2.2 Budget Dedication	87
9.2.3 Retrospective	87
9.3 Other Components	88
Chapter 10 Team and Project Management	89
10.1 Project Challenges	89
10.2 Laser Protocol	89
10.2.1 Hazards	89
10.2.2 Mitigations	90
10.2.3 In Lab Procedure	90
10.3 Timeline	90
10.4 Design Process	92
10.5 Major Breakthroughs and Successes	92
Chapter 11 Patent Search	94
11.1 Invention Overview	94
11.2 Summary of Patent Classifications	94

11.3 Sketch	95
11.4 Review of Prior “Art”	95
11.5 Preliminary Patent Search Choice: Heat Sink	96
11.6 Conclusion	96
Chapter 12 Realistic Constraints & Engineering Standards	98
12.1 Manufacturability	98
12.1.1 Project Unique Components	98
12.1.2 Component Assembly	98
12.1.3 Laser Alignment Skills	98
12.2 Economic Impact	99
12.3 Environmental Impact	99
12.4 Sustainability	99
12.5 Health and Safety	100
12.6 Ethical Considerations	100
12.7 Engineering Standards	101
12.7.1: Introduction	101
12.7.2 Drawing standards	101
12.7.3 Safety Standards	102
12.7.3.1 Identification	102
12.7.3.2 Classification	102
12.7.3.3 Hazard Zone	103
12.7.3.4 Summary/ Safety Agreement	104
Chapter 13 Conclusion	107
13.1 Summary	107
13.2 Focus on the Future	107
13.2.1 Spectroscopy	107
13.2.2 Two Unidirectional Cavities	107
13.2.3 Quad Comb	107
13.3 Reproducibility	108
13.4 Lessons Learned	108
13.5 Reflections	108
Bibliography	110
Appendices	113
Appendix A : Detailed Calculations	113
A.1: cavity expansion	113
A.2: heat sink calculation	114
A.3 CFD model	121

Appendix B : PDS	123
Crystal cooling:	124
PID system:	124
Pump laser:	124
Overview:	124
Appendix B.1: Product Design Specification	126
Appendix B.1.1: Attributes	126
Appendix B.1.2: Performance Criteria	128
Appendix B.1.3: Flow Down Chart	129
Appendix B.1.4: Detailed Timeline	129
Appendix C : Customer Needs	131
Appendix D : Sketches	132
D.1: Heat Sink:	132
D.2: Focus Lens:	136
D.3 Chirped mirror:	138
D.4 BreadBoard Clamps	139
Appendix E : Gantt Chart	140
Appendix F : Budget	141
Appendix G : safety requirements	143
G.1: OSHA Control Measures	143
G.2 Laser Safety Goggles:	144
Appendix H : Senior Design Presentation Slides	145
Appendix I: Optical Equipment used	152
Appendix J: Crystal Background Information	153
Thermal Behavior	153
Medium Characteristics e.g. Wavelength Bands	153
Doping Level	154
Brewster Angle	154
Appendix K: Power Extraction Efficiency	154

List of Figures

Figure 1.1: Example of FTIR working principle.	2
Figure 1.2: Scanning effect due to offsets in time/frequency.	3
Figure 1.3: Light absorption detected as dips in optical intensity.	3
Figure 1.4: Representation of outputs needed for dual comb spectroscopy via two cavities.	4
Figure 1.5: Two mirror optical resonator which supports lasing.	5
Figure 1.6: Standing waves or modes in a cavity configuration with two mirrors.	6
Figure 1.7: Four mirror cavity configuration in a bowtie design.	6
Figure 1.8: Bi-directional cavity configuration where 2 arms are supported.	7
Figure 1.9: Emission spectrum for a Ti:Sapphire crystal.	8
Figure 1.10: Electrons in the ground state are stimulated to higher energy e_1 .	9
Figure 1.11: Absorption spectrum of various Ti:Sapphire crystals.	9
Figure 1.12: Summation of standing waves.	11
Figure 1.13: Frequency comb of a pulse within a mode locked laser.	12
Figure 1.14: Ti:Sapphire crystal (left) with crystal mount (right).	13
Figure 1.15: Heat sink assembly.	13
Figure 1.16: Energy splitting of free Ti^{3+} ion levels.	14
Figure 1.17: Path length experienced by each arm of the Ti:Sapphire infrared laser.	15
Figure 1.18: Beating pattern in the frequency domain produced from the overlap of two different pulse trains.	17
Figure 2.1: Total system overview, simplified for clarity.	20
Figure 2.2: System layout for a generic infrared absorption spectroscopy measurement.	21
Figure 2.3: Pump beam enters the cavity from the right, hits the crystal, then travels in both directions through the cavity.	22
Figure 3.1: Pre-existing pump laser setup is visible left of the dashed line, as well as a half wave plate($1/2$ WP) and polarizing beam splitter (BS).	26
Figure 3.2: (View from above) The existing setup diverts light from the pump laser beam “downward” (as shown) towards a Ti:Sapphire crystal.	27

Figure 3.3: Thorlabs WPHSM05-532, 532 nm half-wave plate used to provide fine-scale control over the electric field polarization of the pump beam.	27
Figure 3.4: Silver mirrors are used to redirect the pump beam to the new Dual Comb system.	28
Figure 3.5: Mirror configuration in the original pump beam containment box.	29
Figure 3.6: Bottom periscope mirror.	29
Figure 3.7: Custom built, adjustable periscope used to raise the optical axis of the pump beam to the height of the Si-Sapphire crystal at the heart of our Dual Comb Spectroscopy (DCS) system.	30
Figure 3.8: Left: Machined 6061 Al periscope tower, mounting plate and variable mirror mount. Right: The 6" tall x 1" diameter design model of the periscope tower.	31
Figure 3.9: Periscope mounting plate used to clamp the periscope tower to the optical breadboard with four 1/4"-20 screws.	32
Figure 3.10: Variable mount for the lower mirror of the periscope.	33
Figure 3.11: Top view of the periscope containment (shielding) box, with lid removed.	34
Figure 3.12: Green beam path from pump laser to DCS system.	35
Figure 3.13: Mirror configuration in the pump beam containment box.	36
Figure 4.1: SolidWorks model of the completed cavity design.	37
Figure 4.2: Cavity component locations.	38
Figure 4.3: Bowtie cavity design.	40
Figure 4.4: Cavity design on a 18"x18" breadboard.	40
Figure 4.5: Steel optical breadboard.	41
Figure 4.6: Steel clamps which clamp to the breadboard.	43
Figure 4.7: Clamp configuration of the board.	43
Figure 4.8: Custom manufactured post, standard mount, output mirror at design height.	44
Figure 4.9: Focus lens spacers and linear stage.	45
Figure 4.10: Top view of the focusing lens in its 2" long cylindrical mount.	45
Figure 4.11: Heat sink top spacer during manufacturing (left), top and bottom spacers after full installation (right).	46

Figure 4.12. <i>Left:</i> Bottom heat spacer successfully raises crystal mount above the height of the mirror stage, (visible bottom right). <i>Right:</i> Close up of heat sink assembly, showcasing the maximized protrusion of the copper neck, and thereby the crystal.	47
Figure 4.13: Block diagram of PID system.	48
Figure 5.1: The pair of mirrors on the breadboard used to perfect the output from the periscope, as seen during early stages of the build.	51
Figure 5.2: Curved mirrors within cavity.	52
Figure 5.3: The curved mirrors are angled at 9.8° with respect to the optical axis to compensate for astigmatism (half of 19.6° astigmatism compensation angle).	52
Figure 5.4: Output mirror in mirror mount.	53
Figure 5.5: Extra pair of mirrors.	54
Figure 6.1: Quantum emission efficiency of a Ti:Sapphire crystal.	55
Figure 6.2: Heat sink subassembly drawings.	56
Figure 6.3: Ti:Sapphire crystal mount and heat sink.	57
Figure 6.4: Close up of heat sink cross section.	57
Figure 6.5: Crystal clamp (right) with Ti:Sapphire crystal (left).	58
Figure 6.6: Tubing setup for heatsink.	59
Figure 6.7: Flow regulator which controls the flow to the heat sink.	59
Figure 6.8: Sprout G pump laser power supply and liquid cooling pump (chiller).	60
Figure 6.9: Junction for fluid pump that directs 0.17 L/min of cooling fluid to the OFHC heatsink of our Ti:Sapphire laser crystal.	60
Figure 6.10: Heat sink labeled according to thermal sections based on most significant heat transfer.	61, 66, 67
Figure 6.11: Water pipe approximation.	62
Figure 6.12: Section 4 simplified geometry.	65
Figure 6.13: CFD temperature gradient graph solution of heat sink model.	68
Figure 6.14: CFD solution streamlines for internal flow within the heat sink.	68
Figure 7.1: Custom machined post for output coupler mirror.	70
Figure 7.2: Aluminum during manufacturing, which was used to make all the	71

breadboard clamps.	
Figure 7.3: Periscope (side and front view).	72
Figure 7.4: Stay-hinge-lid container.	73
Figure 8.1: Pump beam passing through the periscope.	75
Figure 8.2: Power meter and sample reading.	78
Figure 8.3: Close-up of the two curved mirrors angled at half the astigmatism angle, 9.8° .	78
Figure 8.4: Cavity with micrometers for optical components.	79
Figure 8.5: First evidence of mode locking, solely in one arm, and with static and CW noise. FWHM bandwidth appears to be around 30 nm.	80
Figure 8.6: Mode locked cavity	81
Figure 8.7: Mode locking progress in a single arm, improving signal to noise ratio and eliminating some CW waves within the cavity.	81
Figure 8.8: Green beam. To the naked eye, the laser would appear like this, as the emittance of the crystal is mostly in the infrared	83
Figure 8.9: Red/Near Infrared appearance.	83
Figure 8.10: Mode locked cavity under testing. The infrared beams can be seen striking the power meter located in the top right, as well as the spectrum analyzer directed at the point of contact.	84
Figure 8.11: Repetition rate testing equipment, Agilent Frequency Counter 5-3181A, showing the f_{rep} from one arm of the mode locked laser. This number indicates a cavity length of around 40.02 cm.	85
Figure 8.12: Spectrum overlay graph, as shown in SpectraSuite. Visible are both combs, now with greatly reduced CW noise, with FWHM bandwidths of around 40 nm.	85
Figure 10.1: The image demonstrates the focal point of the pump beam in the center of the crystal.	92
Figure 10.2: Fluorescence in the red/infrared range from the crystal. Green light has been filtered.	93
Figure 11.1: Sketch of heat sink.	95

List of Tables

Table 1.1: Important crystal and laser characteristics.	18
Table 4.1: Components in cavity.	38
Table 4.2: Thermal expansion coefficients for potential breadboard materials.	42
Table 4.3: Approximate frequency shift given a 1°C fluctuation in temperature.	42
Table 5.1: Detailed info on each optical part.	50
Table 6.1: Resistance method of analytical heat transfer.	62
Table 6.2: Nusselt number formulas for each plate.	64
Table 6.3: Heat sink resistances values calculated ($\text{Wm}^{-1}\text{k}^{-1}$).	66
Table 6.4: Temperature change at each location in heat sink assembly.	67
Table 8.1: Output values for different power settings.	82
Table 9.1: Pre secured covered costs.	87
Table 9.2: Mechanical engineering department funding.	88
Table 9.3: Purchased parts costs.	88
Table 11.1: Descriptions of preliminary patent searches.	96
Table 12.1: List of tools used	98
Table 12.2: Team based ethical considerations.	100
Table 12.3: Design based ethical considerations.	101

Nomenclature

\dot{Q}	Heat transfer per unit time
k	Thermal conductivity
A_c	Contact area
A_s	Surface area
h	Heat transfer coefficient
R_{cond}	Thermal resistance for conduction
R_{conv}	Thermal resistance for convection
R_{tc}	Thermal resistance for contact
Nu	Nusselt number
Ra_L	Rayleigh number
g	Gravity
β	Volumetric expansion
ν	Kinematic viscosity
L_c	Characteristic length
α	Thermal diffusivity
p	Perimeter
K	Deans number
Pr	Prandtl number
Re	Reynolds number
ζ	Ratio of thermal to hydrodynamic boundary layer thickness

1 Introduction

Pushing the limits of science and technology has and will continue to be one of the defining impacts of engineering on society at large. The application of technology leveraging electromagnetic waves continues to be at the forefront of this push, stretching from the study of gravitational waves to global satellite communications. Controlled, high power electromagnetic emissions enable scientists and engineers to control rovers on Mars, but also probe, identify, and examine the world we live in. Currently, laser enabled science is spearheaded by developments in various pulsed laser systems. More specifically, systems which use the overlapping of two distinct but similar lasers to perform measurements beyond what was possible only 30 years ago. One such system is known generally as a Dual Comb Laser. This project, at the crossroads of optical physics and mechanical engineering, has sought to build this type of system by designing, manufacturing, and assembling a Bi-Directional Kerr-Lens Mode-Locked Dual Comb Laser.

1.1 Motivation

The motivation for this project can be broken down into two major categories: delivering a functioning Dual Comb Laser to the SCU physics research lab of Prof. Bachana Lomzadse, and contributing to the further development of the Dual Comb technology for use in applied optics.

Primarily, this project presented an opportunity for our team of three to take full responsibility for a complete and functioning laser system. By chance, the Santa Clara University Physics Department, specifically Dr. Bachana Lomsadze, was planning on adding a second Dual Comb Laser to his laser lab on campus. Accepting responsibility for this would incorporate applied engineering, from intentional systems design through iterative manufacturing and assembly, paired with applied optics, which involved crucial, extensive research, and guided implementation and refinement of all components to complete the whole. As will be expanded on throughout this report, such a pulse laser is best classified as: incredibly more capable than previous lasers within the same application, rated in the highest hazard category, and requiring precise assembly and alignment to function. Despite the significant challenges that taking on this project entailed, the opportunity had too much potential to pass up.

Secondarily, the state of development of Dual Comb Lasers and their potential applications has motivated a myriad of exploration. Interest in this class of ultra-short pulsed laser systems is increasing, especially, but not limited to, their primary use in absorption spectroscopy. Much potential exists for a laser system that can provide quick bursts of energy in the femtosecond(10^{-15}) time scale. For instance, atomic interactions within chemical reactions often happen at the femtosecond time scale and discerning between processes within these reactions could provide valuable information. The absorption line resolution of ultra short pulse lasers is the other characteristic feature

that merits their continued development. Demand for scientific tools to measure at this time scale and precision is well-warranted.

Authors' Note: Sections 1.2 through 1.4 constitute critical background information, along with more detailed information in the Appendix. For a more pared-down view of the project, skip to 1.5 and continue from there.

1.2 Absorption Spectroscopy background

Absorption spectroscopy itself is not new, and various methods have been used to perform optical based materials identification. One of the widely used methods is fourier transform infrared spectroscopy, a.k.a. FTIR. This method involves splitting a pulsed beam, whereby a portion travels at a fixed mirror and remainder at a mirror on a moving stage.

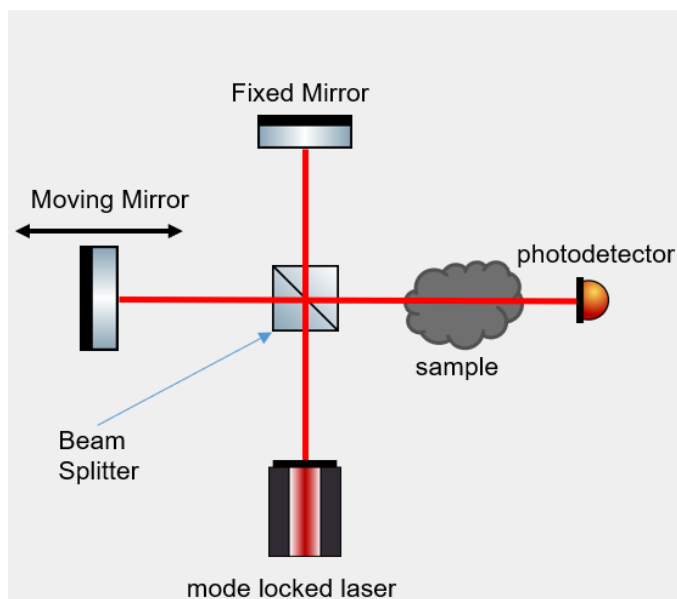


Figure 1.1: Example of FTIR working principle.

A. Franzen, "ComponentLibrary," ComponentLibrary: a free vector graphics library for optics. [Online]. Available: <http://www.gwoptics.org/ComponentLibrary/>. [Accessed: 10-Jun-2021].

Images were made using the optics component library

<https://creativecommons.org/licenses/by-nc/3.0/>

A moving mirror is used to cause a slight offset in phase and frequency with respect to the unaltered pulses. These changes affect the pulse such that when overlapped with the unchanged pulse from the fixed mirror, an interference pattern occurs.

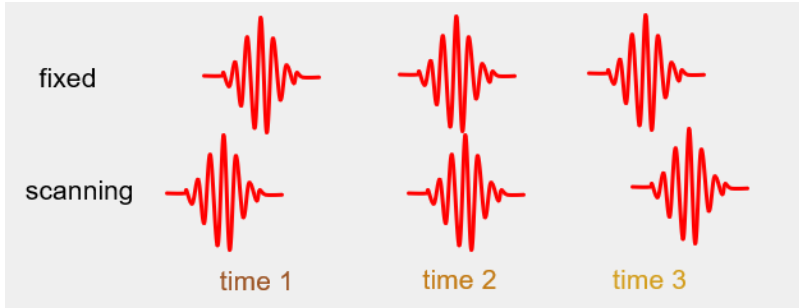


Figure 1.2: Scanning effect due to offsets in time/frequency. At any one point in time, the fixed and the altered pulses, which have different frequencies, will also be at different stages in their propagations.

This interference can be considered as a scanning effect over the entire frequency spectrum. When these overlapped pulses are shot through a sample and collected via photodetector, a fourier transform can be performed to rebuild the absorption spectrum of the sample. Fig. 1.3 below completes the outline of the working principles behind FTIR.

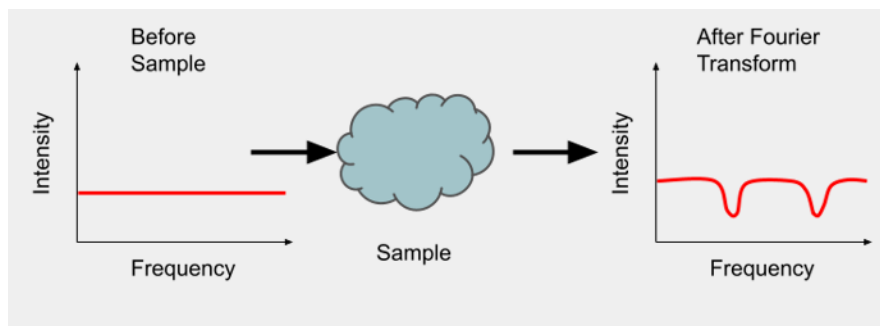


Figure 1.3: Light absorption detected as dips in optical intensity. Fast fourier transforms reveal these dips as results of overlap of the pulses in the sample. Samples are normally gaseous, but can be solid in composition.

This method, however, is tied to the mechanical stage that causes the pulse shifting, and this reliance on a stably moving stage limits field applications.

Alternatively, a similar effect can be achieved by utilizing two similar mode-locked cavities, in a method known as dual comb spectroscopy, or DCS. Instead of relying on a moving mirror to achieve the scanning effect, one can build two laser cavities with slightly different repetition rates. This method produces the same scanning effect, but without the need for actively moving components.

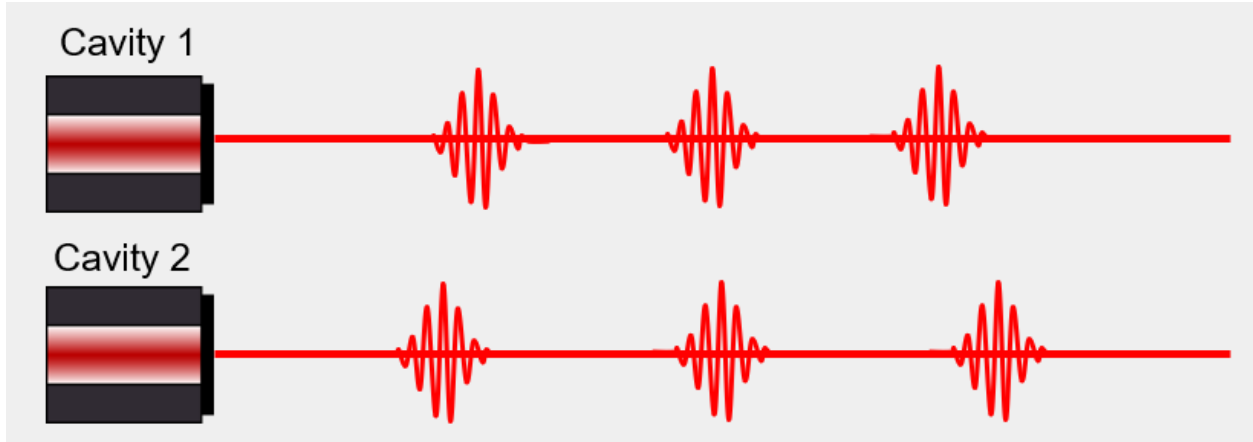


Figure 1.4: Representation of outputs needed for dual comb spectroscopy via two cavities. These outputs represent scanning without the necessity for moving parts that FTIR has. Instead of splitting one beam and using a moving stage, scanning is achieved in DCS using two completely separate beams.

A. Franzen, "ComponentLibrary," ComponentLibrary: a free vector graphics library for optics. [Online]. Available: <http://www.gwoptics.org/ComponentLibrary/>. [Accessed: 10-Jun-2021].
 Images were made using the optics component library
<https://creativecommons.org/licenses/by-nc/3.0/>

In DCS, one frequency comb is used to conduct an infrared absorption spectroscopy test on a sample. Passing through a sample with absorption in the near-infrared (250-400THz) does yield absorption spectrum information, but when shone on a photodetector, the information in the comb structure remains inaccessible. To extract the information, the second comb with its slightly different repetition rate must be overlapped with the first, resulting in a beating pattern in the radio frequency domain which correlates to absorption in the infrared region. A photodetector can now discern the high resolution of the test absorption spectrum. Fig. 1.2 above illustrates how the working principle behind DCS is similar to FTIR but the moving mirror is replaced by a second cavity. This method has high precision and accuracy stemming from the fine tuning of two independent cavities. However, there is still room for improvement, as this method requires two nearly identical lasers, doubling parts, cost, and space requirements, which also limits field applications.

In pursuit of field deployability, on top of the significant performance boosts of DCS over FTIR spectroscopy, this project intended to design and build a DCS system inside of a single cavity.

1.3 Background Information

The acronym LASER stands for Light Amplification by Stimulated Emission of Radiation. Invented in December 1958, lasers have since revolutionized many aspects of science and engineering. The two main classifications of lasers are continuous wave (CW) and pulsed lasers. This project involves both; our goal is to produce two pulsed lasers using a single CW laser as a power source.

1.3.1 Lasing

A simplified schematic of a laser cavity is shown in Fig 1.5. It contains a pair of mirrors and a gain medium which is continuously excited by another form of energy (in our case using a green light source). The excited medium then emits near infrared light which is amplified using cavity mirrors that reflect the light back to the gain medium. In the cavity one mirror is 100% reflective and the other is only partially reflective that allows the light to leave the laser cavity.



Figure 1.5: Two mirror optical resonator which supports lasing. The green beam is turned to infrared when it contacts the gain medium. The gain medium sends infrared light to the output mirror as well as back to the reflective mirror.

A. Franzen, “ComponentLibrary,” ComponentLibrary: a free vector graphics library for optics. [Online]. Available: <http://www.gwoptics.org/ComponentLibrary/>. [Accessed: 10-Jun-2021].

Images were made using the optics component library

<https://creativecommons.org/licenses/by-nc/3.0/>

It is important to note that a laser gain medium can emit light that covers a wide range of frequencies but only the ones that are resonant (create standing waves) with the laser cavity are amplified. Fig. 1.6 demonstrates the first 3 standing waves in a cavity (which are outside of the gain medium spectrum) but there are many more standing

waves. The laser system discussed in this thesis uses a titanium sapphire (Ti:Sapphire) crystal as its gain medium, which amplifies waves in the near infrared region.

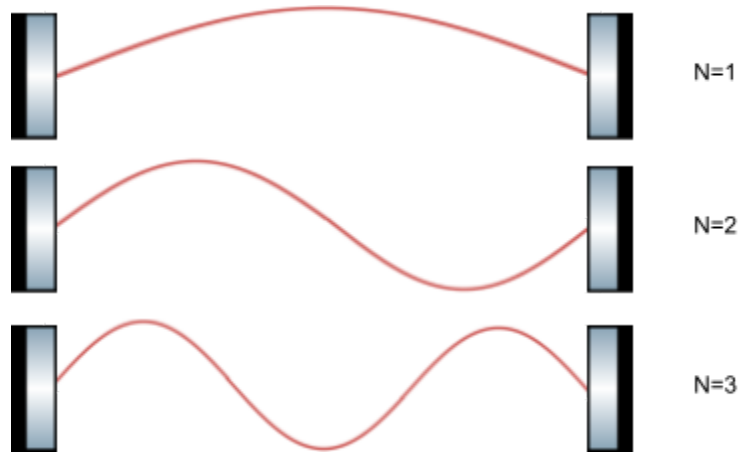


Figure 1.6: Standing waves or modes in a cavity configuration with two mirrors. The number of antinodes, points where the amplitude of a wave is at a maximum, is directly related to the “N” value for each standing wave.

A. Franzen, “ComponentLibrary,” ComponentLibrary: a free vector graphics library for optics. [Online]. Available: <http://www.gwoptics.org/ComponentLibrary/>. [Accessed: 10-Jun-2021].

Images were made using the optics component library

<https://creativecommons.org/licenses/by-nc/3.0/>

1.3.2 Four Mirror Cavity

As opposed to the cavity in Fig. 1.5, the cavity for this project uses four mirrors, which is shown in Fig. 1.7. Fig. 1.7 demonstrates a bowtie design where two counter propagating beams are generated from a single cavity.

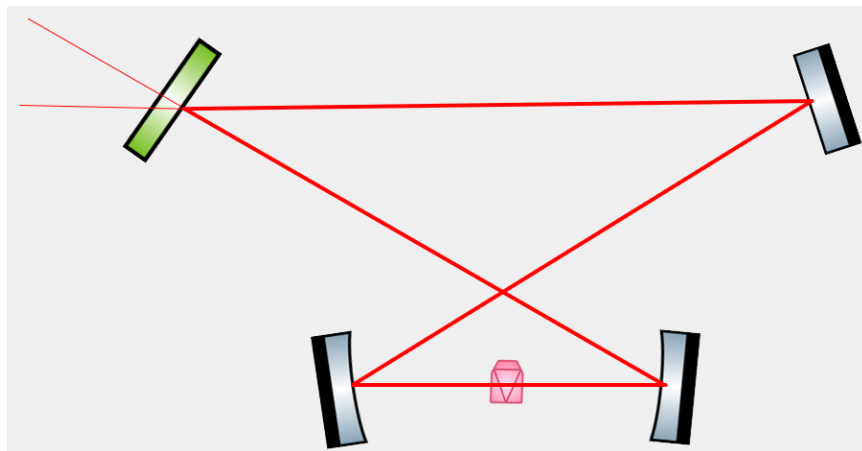


Figure 1.7: Four mirror cavity configuration in a bowtie design. Two separate beam pulses setup traverse the cavity in opposing directions.

A. Franzen, “ComponentLibrary,” ComponentLibrary: a free vector graphics library for optics. [Online]. Available: <http://www.gwoptics.org/ComponentLibrary/>. [Accessed: 10-Jun-2021].

Images were made using the optics component library

<https://creativecommons.org/licenses/by-nc/3.0/>

Most importantly, four mirrors does not impact the discussed basics of lasing discussed in the previous section. However, as will be discussed at various intervals, other unique specifications of the mirrors, as well as our lasing medium, and the cavity arrangement itself has further impacts on the overall behaviour of the system. If, for any reason, there is a good reason to skip specifics, and you'd like to get more to the project, skip to 1.5, Core Characteristics Condensed, then move on to Chapter 2.

Our laser system utilizes the bowtie design. The center of the cavity contains a Ti:Sapphire crystal as the gain medium for the cavity. The Ti:Sapphire crystal is excited by a green pump laser and the bowtie design produces 2 outputs from a single cavity. The bowtie design is a bi-directional design which will be described below.

1.3.3 Bi-directionality of a Cavity

A bi-directional cavity consists of two counterpropagating beams within a single cavity. Fig. 1.8 describes how a bi-directional cavity produces 2 outputs from a single cavity. The mirrors must support light traveling in both directions. The implications of having opposing beams traveling within a single cavity are some of the most important factors when doing spectroscopy. Everything from initial alignment to mode locking is dependent on the bi-directionality of the cavity. The fact that each of the two beams hits each optical component means that alignment of the optics is extremely sensitive to even the smallest of adjustments.

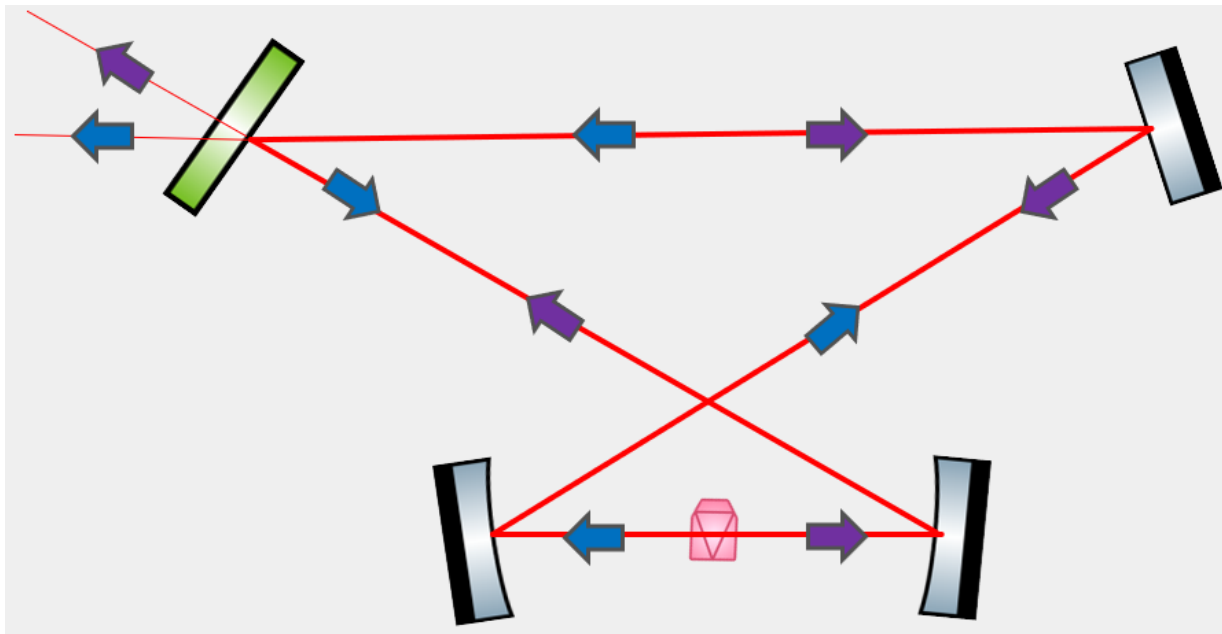


Figure 1.8: Bi-directional cavity configuration where 2 arms are supported.

A. Franzen, "ComponentLibrary," ComponentLibrary: a free vector graphics library for optics. [Online]. Available: <http://www.gwoptics.org/ComponentLibrary/>. [Accessed: 10-Jun-2021].

Images were made using the optics component library

<https://creativecommons.org/licenses/by-nc/3.0/>

1.3.4 Absorption/Emission & Stimulated Emission

As seen by Fig. 1.9 below, the Ti:Sapphire crystal emits a spectrum of light between 600 nm and 1050 nm. If the cavity is properly aligned, the red/infrared light which is emitted by the crystal will continuously cycle around the cavity. The infrared light that returns to the Ti:Sapphire crystal can act as a catalyst for stimulated emission where electrons which are sitting in the lasing energy level emit a photon of the same frequency in the same direction.

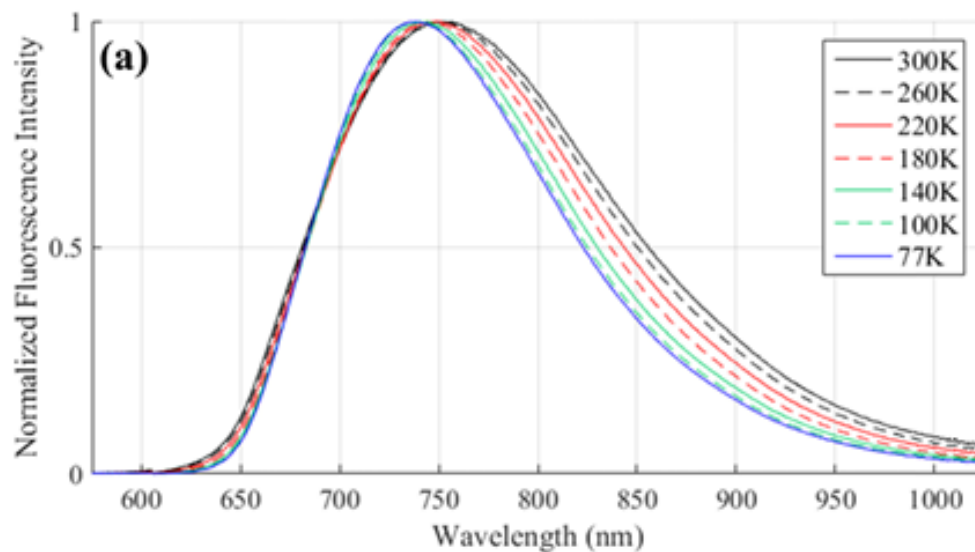


Figure 1.9: Emission spectrum for a Ti:Sapphire crystal. The Ti:Sapphire crystal has an emission profile that is related to its temperature.

Harry Burton, Christopher Debardeleben, Wafa Amir, Thomas A. Planchon, "Temperature dependence of Ti:Sapphire fluorescence spectra for the design of cryogenic cooled Ti:Sapphire CPA laser," *Opt. Express* **25**, 6954-6962 (2017); <https://www.osapublishing.org/oe/abstract.cfm?uri=oe-25-6-6954>

In the gain medium, electrons are excited by a green pump laser up to a higher energy level. These electrons sit in the 'lasing energy level' where the population of electrons builds up. Another photon emission in this state allows the electron to return to ground level, which in our case is a red/infrared photon. Stimulated emission, specifically, occurs when excited electrons struck by a photon emit another photon of the same frequency and direction.

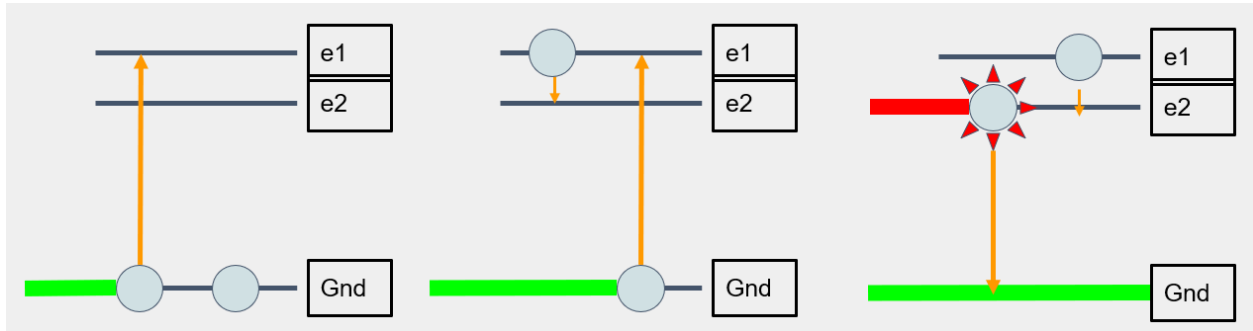


Figure 1.10: Electrons in the ground state are stimulated to higher energy e1. e1 is unstable, and the electron drops to a lower energy state e2. The e2 state is semi stable and is the 'lasing level.'

In our system a pump beam at 532 nm is used to excite our gain medium(Ti:Sapphire crystal). The pump beam operates at near the optimum wavelength for a Ti:Sapphire crystal(see Fig 1.6). Once it passes through the crystal and the crystal fluoresces in all directions, most of the beam's energy is turned into the near infrared range with a wavelength of around 780 nm. The amount of green light that is converted into the IR depends on the doping percentage (0.15 to 0.25%) of the crystal. More information on the doping percentage is included in Appendix J.

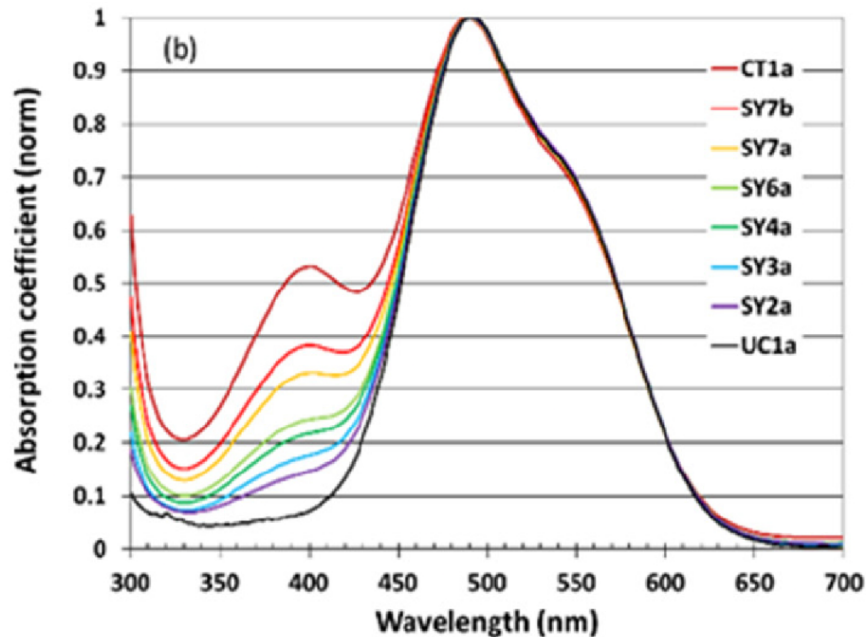


Figure 1.11: Absorption spectrum of various Ti:Sapphire crystals. The pump that is used to excite our Ti:Sapphire crystal operates at 532 nm.

Harry Burton, Christopher Debardeleben, Wafa Amir, Thomas A. Planchon, "Temperature dependence of Ti:Sapphire fluorescence spectra for the design of cryogenic cooled Ti:Sapphire CPA laser," *Opt. Express* **25**, 6954-6962 (2017);

<https://www.osapublishing.org/oe/abstract.cfm?uri=oe-25-6-6954>

1.3.5 Bandwidth

Bandwidth is the measure of the range of frequencies emitted by a laser system. As will be discussed later, the pump beam, which is used to stimulate the system, has a very small bandwidth. The pump beam for this project emits a beam of 532 nm, i.e. a single 'band' of green light.

On the other hand, the Dual Comb system is desired to have a high bandwidth that spans over hundreds of nm. Materials absorb unique wavelengths which can be used to identify the material. It is important for an absorption spectroscopy system to utilize a wide bandwidth so that it can be used to identify many samples.

1.3.6 Mode-locked operation

A mode locked laser cavity is one which produces extremely short pulses of light. This occurs when many wavelengths that are resonant (standing waves) constructively interfere with each other to produce pulses. Fig. 1.12 demonstrates the overlap of a few wavelengths inside a single cavity that form pulses. The time it takes the pulses to travel one full roundtrip is $T=1/f_{rep}$. (repetition rate).

As we described earlier, the Ti:Sapphire crystal has a large emission bandwidth which can be used to produce pulses that are extremely high in intensity. The duration of these pulses is also tied to the bandwidth; the Ti:Sapphire crystal can produce pulses that are in the range of femtoseconds in duration.

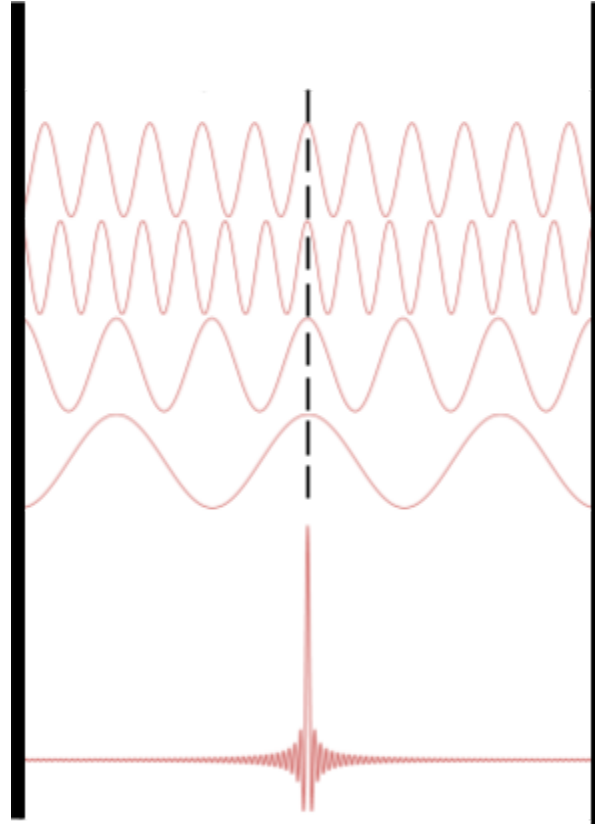


Figure 1.12: Summation of standing waves. More frequencies cause more intense pulses. The time it takes a pulse to travel the length of the cavity is $T = 2L/c = 1/f_{rep}$.

1.3.7 Frequency Combs

A mode locked laser can be represented in the frequency domain by a specific structure, called a frequency comb Fig.1.13. This structure can be obtained by taking a Fourier transform of a pulse train. The spacing between the modes equals to f_{rep} (the repetition rate of the cavity)[1]. The repetition rate and thereby the frequency comb structure, is a function of the cavity length, where any variation in cavity length shifts the distance between each spike.

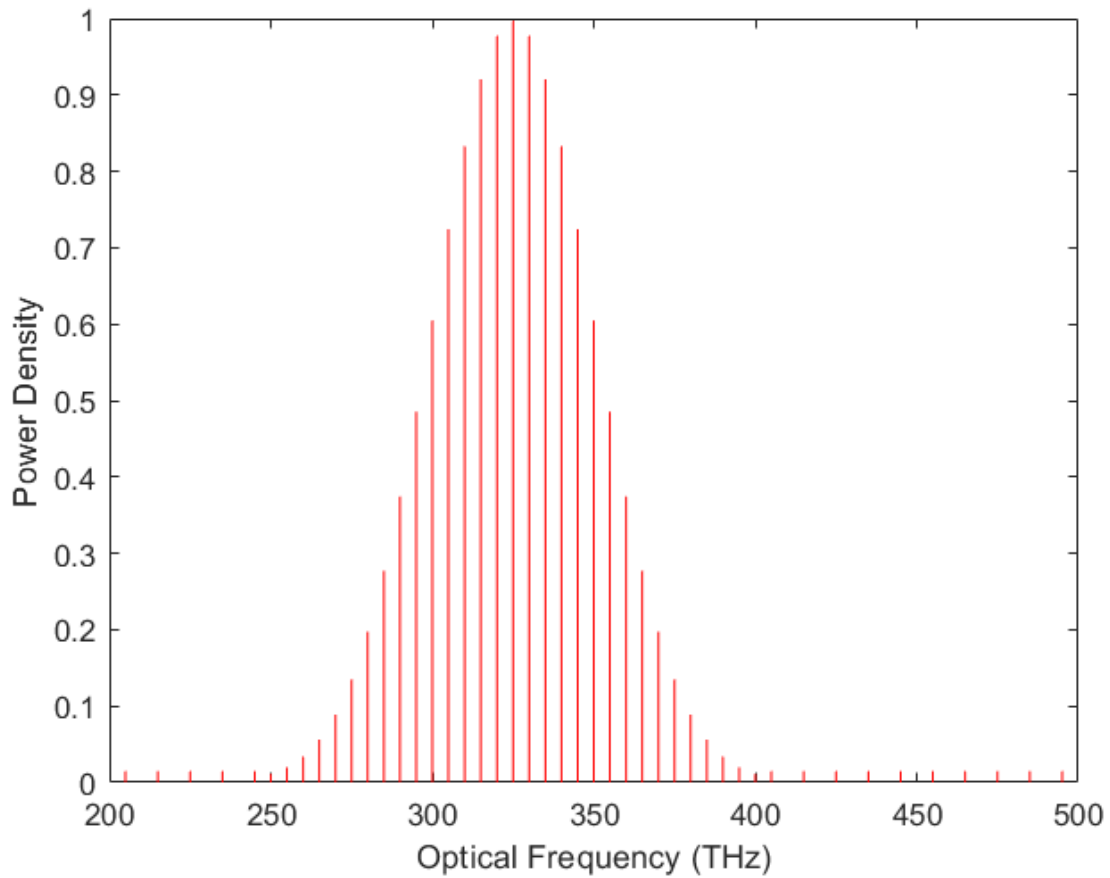


Figure 1.13: Frequency comb of a pulse within a mode locked laser. The red lines indicate a set, equidistant spacing in the frequency domain.

1.3.8 Titanium Sapphire Crystal

The gain medium in our cavity is a Ti:Sapphire crystal. To minimize reflections off of the crystal, the crystal is cut at a Brewster angle. More information about the Brewster angle is included in Appendix J.



Figure 1.14: Ti:Sapphire crystal (left) with crystal mount (right). The adjustable clamp was machined from oxygen-free high-conductivity (OFHC) copper.

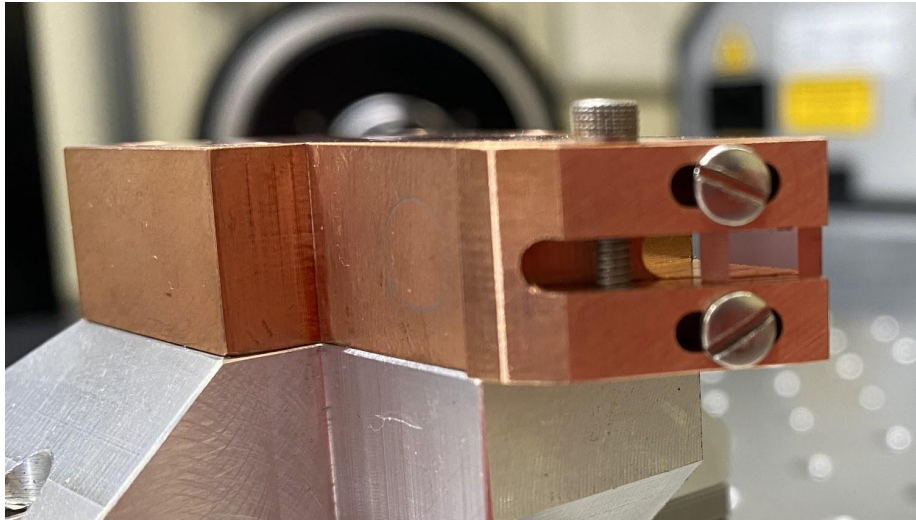


Figure 1.15: Heat sink assembly. The copper Ti:Sapphire crystal mount is attached to a OFHC copper heat sink, and then to the beveled aluminum mount. The crystal is mounted using the two screws found at the front and held in place by gently tightening the vertical screw.

The crystal chemical formula is $\text{Ti}^{3+}:\text{Al}_2\text{O}_3$, from which we can tell that it is a sapphire *doped* with titanium 3+ ions, in our case around 0.15 - 0.25% concentration. For more information on doping level, see Appendix J. In his article, *Spectroscopic and Laser Characteristics of Ti:Al₂O₃*, P.F. Moulton explains that the titanium ion, Ti^{3+} , in the crystal has an electronic structure of a 3d single electron [2]. Through various processes involving interactions between electric fields and the ion, this Ti ion can be broken down into five different 3d-orbital arrangements: 3 Ti ground states and 2 excited states [3]. These arrangements represent different energy levels and are critical

when discussing energy conversion and the connections between the lattice structure and the absorption band of the crystal, which can be found in Appendix J. Additionally, an explanation of the power extraction efficiency for our crystal and the laser are discussed in Appendix K.

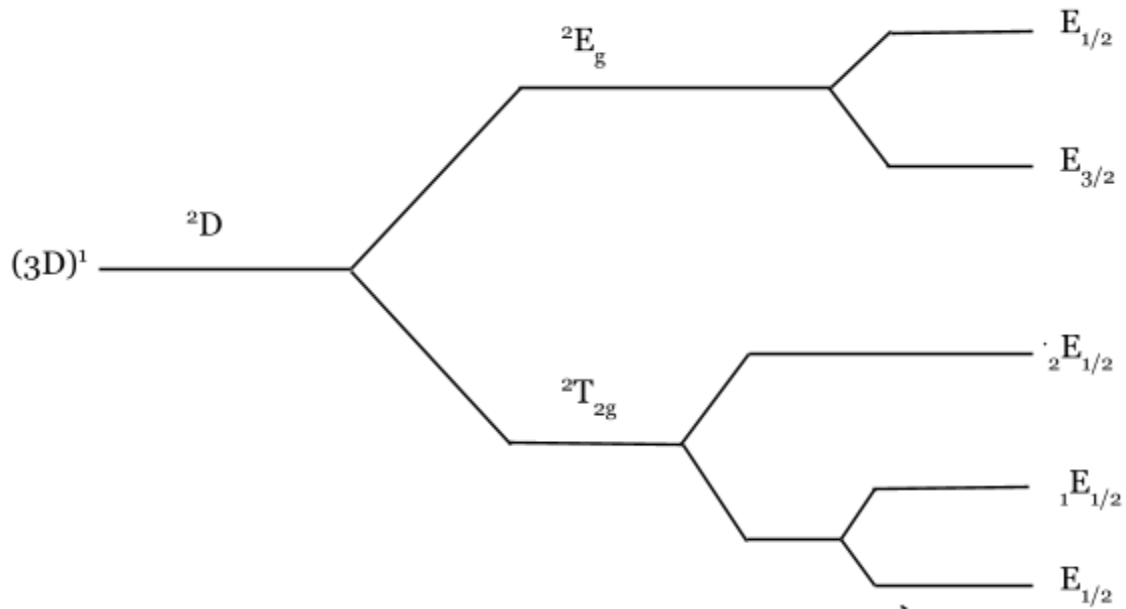


Figure 1.16: Energy splitting of free Ti^{3+} ion levels. As you move from left to right in the diagram, the energy level of the single 3d ion is continuously split until there are five different states, three at low energy and two excited states.

1.3.9 Kerr-Lensing/Refractive Index

Our goal was to generate two laser outputs from a single cavity that has different repetition rates. At first it seems impossible because the repetition rate is determined by the cavity length which is the same for both arms. However the refractive index of the Ti:Sapphire crystal is a strong function of the light intensity. This is also referred to as the Kerr-effect, more specifically the Kerr-lens effect is a phenomenon by which an applied electromagnetic field changes the refractive index of a material.

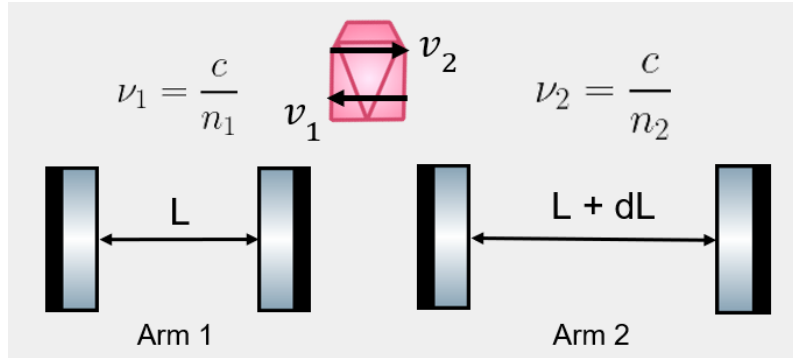


Figure 1.17: Path length experienced by each arm of the Ti:Sapphire infrared laser. The change in path length is represented by “dL.”

A. Franzen, “ComponentLibrary,” ComponentLibrary: a free vector graphics library for optics. [Online]. Available: <http://www.gwoptics.org/ComponentLibrary/>. [Accessed: 10-Jun-2021].

Images were made using the optics component library

<https://creativecommons.org/licenses/by-nc/3.0/>

If the cavity has the ability to produce two separate pulses with slightly different intensity profiles, the Kerr-lens medium has a slightly different effect on each of the pulses, experienced as different indices of refraction. The index of refraction governs how quickly light can move through the medium, i.e. each pulse moves at a different rate through the crystal. This varying speed causes each pulse to experience a slightly different cavity length, and manifests itself as a slightly different repetition rate, aka f_{rep} .

1.3.10 Chirp

Chirp, which is the time-dependence of the instantaneous frequency of an optical pulse, is an optical phenomenon that must be compensated for to make a laser function properly.

The speed of light in a medium depends on wavelength. All colors travel at essentially the same speed in air but this is not the case in Ti:Sapphire. The result is that the components of the pulse spread out in time when travelling through a crystal. This phenomenon is called chirp.

Chirp can be compensated for by using mirrors coated with a dielectric thin-film that provides a negative chirp. Each individual wavelength is reflected at a slightly different depth within the mirror, which effectively reverses the effects of chirp and keeps the pulse spectral components (wavelengths) aligned.

1.3.11 Drifting

After continuous operation in a mode-locked configuration, the repetition rate of the pulses is expected to drift. Factors such as vibration, thermal expansion, air density changes, and even intensity profile changes can cause the repetition rate of the two arms to drift. If both arms are drifting apart, this can cause issues with the stability of

mode-locked operation. The external factors that can influence the f_{rep} need to be compensated for; this can be done through vibrational isolation, material selection, ambient environment stabilization, and in some cases, active feedback systems.

1.4 Review of Literature

DCS is an emerging field that utilizes the beating pattern of two slightly different frequency combs to read information from an infrared spectroscopy test which is encoded in the frequency domain. Coddington *et al.* noted that “at 100 MHz comb tooth spacing, a single spectrum having over a million spectral elements can be acquired in milliseconds” [4]. DCS is thus an optimal method for conducting a quick and accurate spectroscopy test.

Many teams have implemented Dual comb spectroscopy systems. Kerber *et al.* maintained two cavities in which the mode locked cavities are actively stabilized which hold a repetition rate difference of 38 Hz between the two cavities [5]. The team was able to measure an absorption spectrum for an acetone sample which has absorption features in the near infrared spectrum. Additionally Yang *et al.* utilized two er-doped femtosecond fiber lasers to measure the absorption spectrum of water vapor [6]. The two laser cavities were actively stabilized and maintained a repetition frequency difference of 180 Hz with a fundamental repetition frequency of 66 MHz. A nonlinear fiber was used to broaden the spectrum to include the absorption spectrum of water vapor.

Our team implements a DCS system that is similar to the two listed above but a single cavity is stabilized and maintained, instead of a two cavity DCS system, which greatly reduces cost and size.

1.5 Core Characteristics Condensed

The single laser cavity can produce two dissimilar counterpropagating beams, each exhibiting a unique repetition rate, owing to their respective intensities within the solid state gain medium, a titanium sapphire crystal ($\text{Ti:Al}_2\text{O}_3$). The titanium sapphire has an intensity dependent index of refraction; any slight difference in beam intensity changes the speed of light each beam experiences while it travels through the crystal. As a result of this difference, when the two beams are overlapped while each is mode locked and thereby made up of a wide band of frequencies in the infrared (280-400 THz), they produce a beating signal measured in the MHz-scale radio frequency domain (see fig 1.18 for beating signal example). Critically, this shift from optical to radio frequency (RF) allows accurate “reading” of the results; it is possible to directly correlate between the absorption displayed in the RF domain and the associated absorption of NIR light within a sample. Table 1 summarizes the most important characteristics of the laser and Ti:Sapphire crystal.

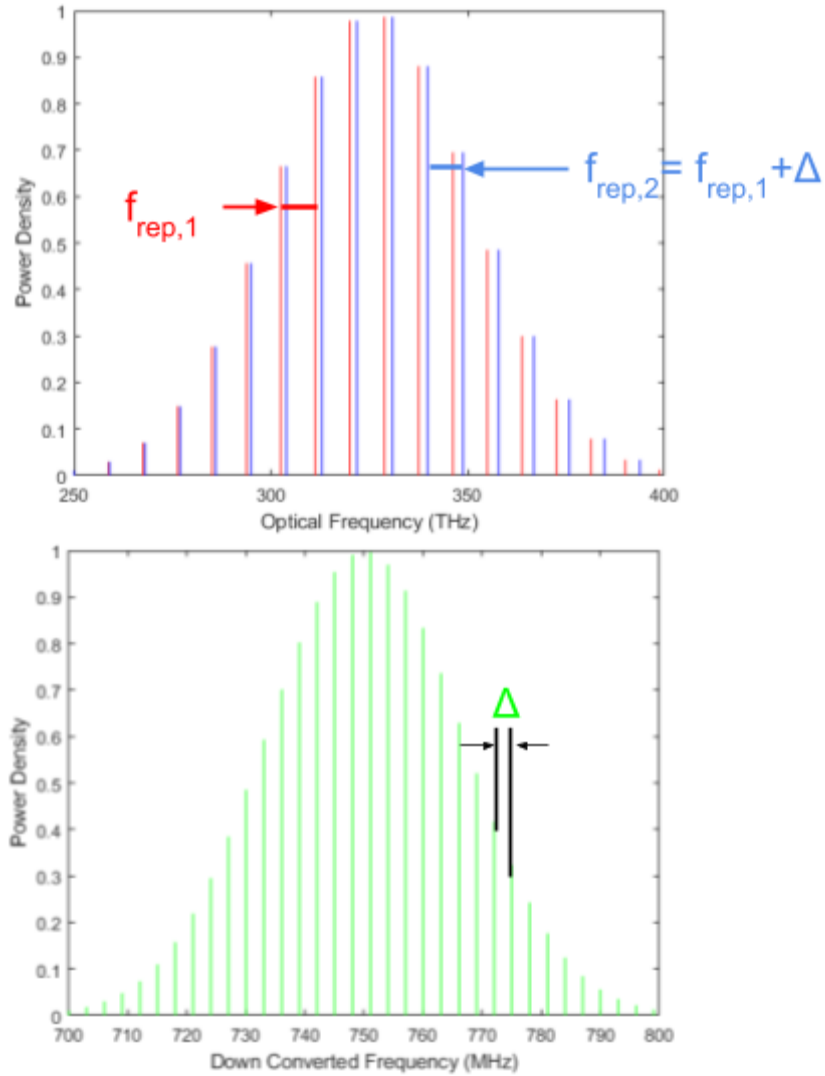


Figure 1.18: Beating pattern in the frequency domain produced from the overlap of two different pulse trains.

Table 1.1: Important Ti:Sapphire crystal and laser characteristics

Feature	Minimum	Mean	Maximum	Units
Cavity Length	380	400	420	mm
Wavelength	770	835	880	nm
Feedback in 1 arm	-	0.081	~0.093	mW/mW
Feedback in both arms(sum)	-	~0.14	0.165	mW/mW
Duration of Modelock	-	-	37 @ 4.3 W	min
Full Width Half Max (FWHM) Bandwidth	25	30	40	nm
Thermal Conductivity	N/A	33 [7]	N/A	W/mK ³
Specific Heat	N/A	0.59 [7]	N/A	J/gK ⁴
Refractive index	N/A	1.77 at 532 nm; 1.76 at 800 nm; 1.75 at 1100 nm [8]	N/A	N/A

1.6 Goals and Objectives

Project description and goals:

The main objective of this project was to build and parameterize a bi-directional dual comb laser. Once assembled the focus became improving the stability of the system and reducing the noise caused by vibration and temperature fluctuations. For temperature, the goal was to implement cooling such that the crystal would exhibit minimal fluctuations in temperature during operation. Thermal expansion of the Ti:Sapphire crystal can cause laser misalignment, and thus temperature had to be controlled to ensure long term stability of the system. We planned to implement a PID controller which uses a piezo-electric stack to provide active stabilization and long term stability. Unfortunately, the group could not complete this task in the time allotted.

Chapter 2 Project Overview

2.1 Recipient Needs

The Physics Department at Santa Clara University, specifically Dr. Lomsadze, is the recipient of this laser. As such, the need is for a single laser assembly as or more capable than the preexisting laser that he put together himself. As future mechanical engineers, we requested some creative freedom to rethink and improve upon the predecessor design. We did this where feasible and free of drawbacks, and addressed his primary issue, a drifting problem noticeable when observing the characteristics of his laser over the course of hours. The primary cause he identified was thermal expansion, which while within only a few degrees or less, had an identifiable impact on his laser that he wished to reduce as best as possible. Apart from this, the central desire presented to the project was the completion and successful alignment, including full functionality, of a bi-directional Dual Comb Mode Locked Laser.

2.2 Core Requirements

The team has set out to build this laser with SCU's Physics department and Dr. Lomsadze in mind and thus, many of the system level requirements have been dedicated towards achieving the goals. SCU Physics is in need of a Bi-directional dual Comb Laser, and this project aims to complete this build with that target in mind.

After conducting a customer needs report, the main systems desired attributes were categorized and can be seen in Appendix C. The team decided that the main desired attributes fit into 4 categories. These categories were performance, safety, appearance, and cost. After discussing with the SCU Physics department, it was clear that reliability and accuracy were of the utmost importance. For instance, the use of a PID loop to fix the cavity from drifting was highly desirable.

The discussion indicated that the system should largely be dust free which was not found in the market research. From the research as well as the interviews, it was clear that the performance criteria for the project should be greatly considered when designing the cavity. Attributes of the project are summarized in Appendix B.1.1. The results of the interview process were summarized into a Weighted Calculation for Performance Criteria. This table can be found in the PDS document in Appendix B.1.2. From the discussion, the evaluation of free running behavior as well as the PID loop improving the stability were given the greatest weight out of all the criteria. Mirror adjustability was also a highly desirable trait for the purpose of cavity alignment; half a thousandth of an inch can have drastic effects on mode locking.

A complete flow down chart of the project is included in Appendix B.1.3. The project revolved around system isolation as well as pristine machinability for the most consistent cavity behavior.

2.3 Conceptual System Layout

The system below, Fig. 2.1, indicates the full conceptual layout of the system. It is important to ensure that the output of the cavity remains mode-locked and thus produces frequency combs.

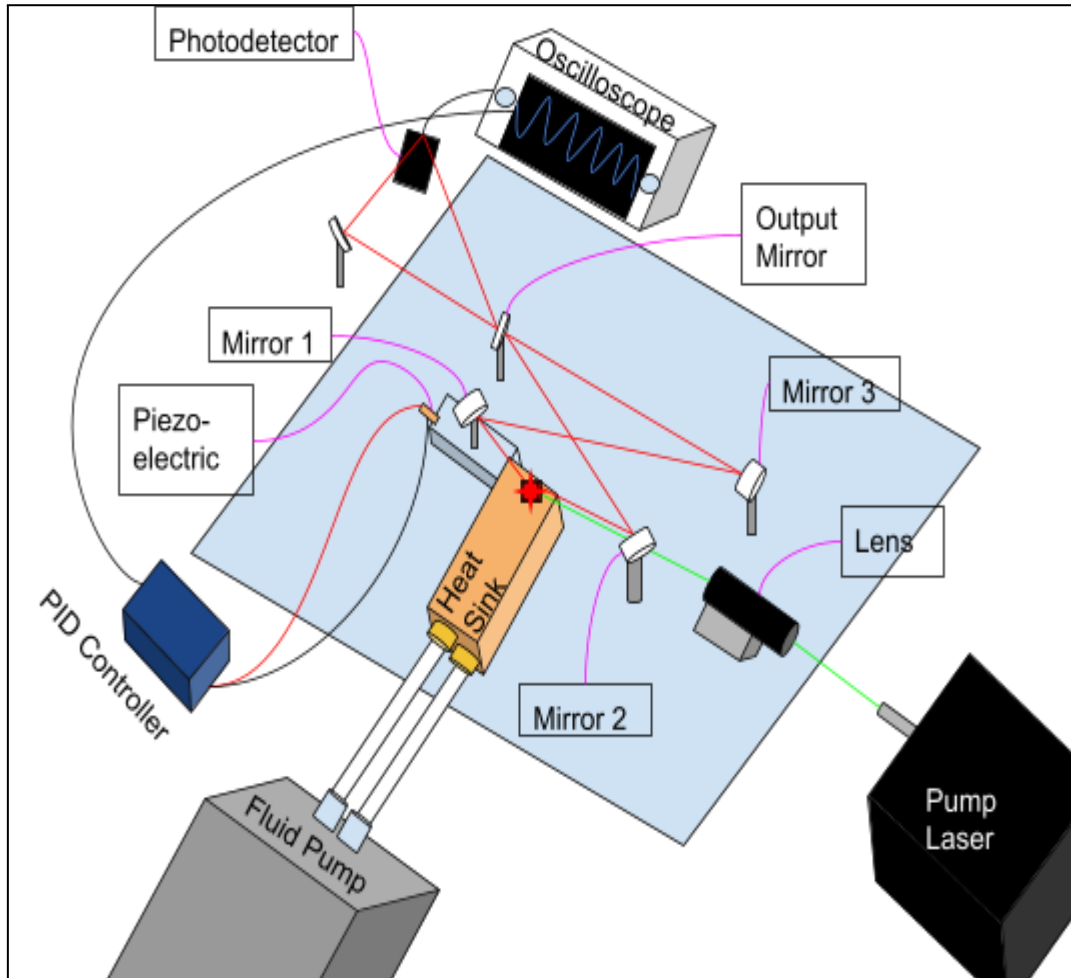


Figure 2.1: Total system overview, simplified for clarity.

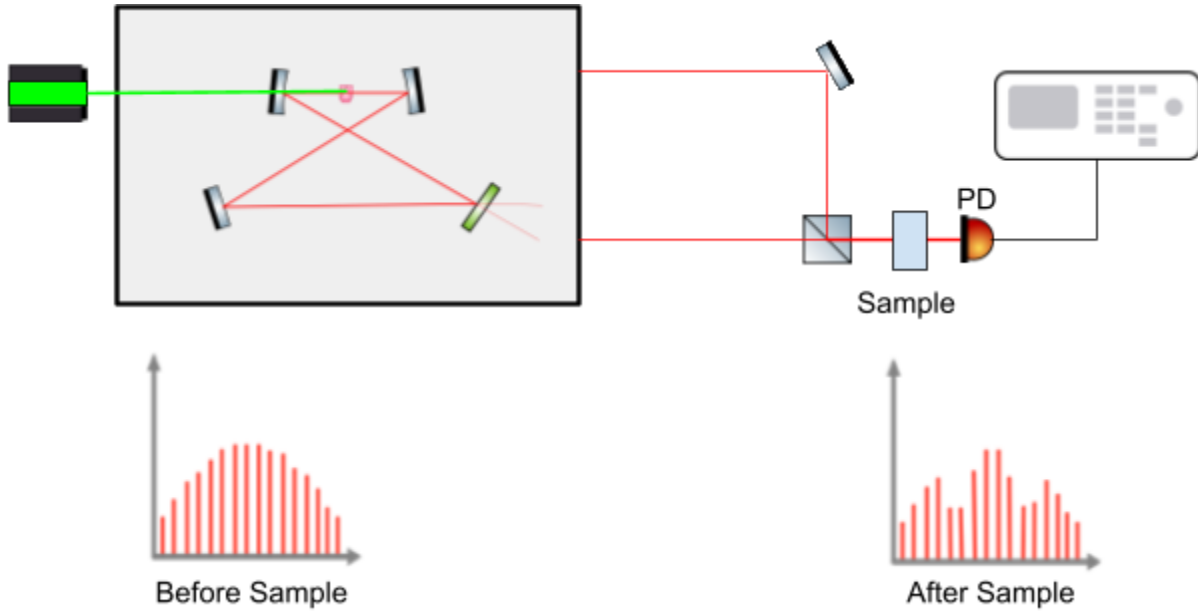


Figure 2.2: System layout for a generic infrared absorption spectroscopy measurement.

A. Franzen, "ComponentLibrary," ComponentLibrary: a free vector graphics library for optics. [Online]. Available: <http://www.gwoptics.org/ComponentLibrary/>. [Accessed: 10-Jun-2021].

Images were made using the optics component library

<https://creativecommons.org/licenses/by-nc/3.0/>

Fig. 2.2 describes a test case scenario where an absorption spectroscopy test on a sample is conducted. The two beam outputs from Fig. 2.1 are overlapped using a beam splitter. The overlapped beam is then shot through a sample and collected by a photodetector (PD). The photodetector is able to rebuild the absorption spectrum of the sample. The absorption spectrum has intensity dips where the sample has absorbed specific frequencies. The intensity dips can be used to identify the elements within the sample.

2.4 Functional Analysis

Fig. 2.3 shows the path of the laser through our completed system. The beam comes in from the right and passes through the focus lens. Once it hits the crystal, the beam transitions from green to near infrared frequency. After leaving the crystal, the beam is split into two paths: one moving right and the other going left. Both beams exit through the output mirror.

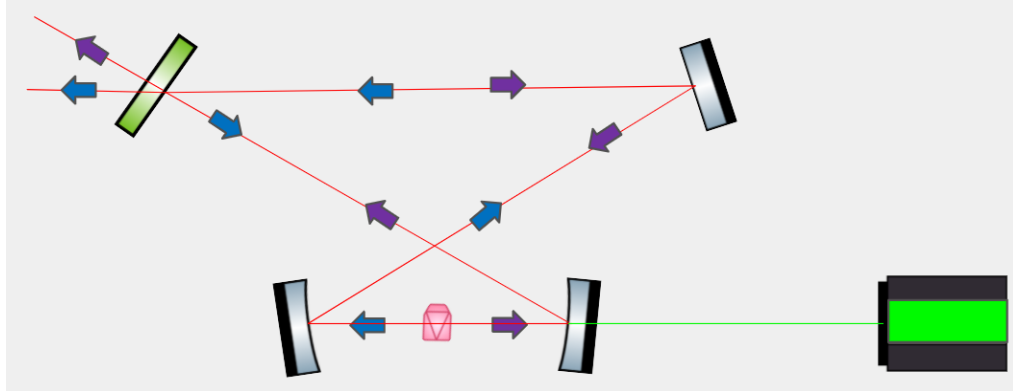


Figure 2.3: Pump beam enters the cavity from the right, hits the crystal, then travels in both directions through the cavity.

A. Franzen, "ComponentLibrary," ComponentLibrary: a free vector graphics library for optics. [Online]. Available: <http://www.gwoptics.org/ComponentLibrary/>. [Accessed: 10-Jun-2021].

Images were made using the optics component library

<https://creativecommons.org/licenses/by-nc/3.0/>

Proper functionality of the laser requires that 2 outputs are produced from a single cavity. Light in the cavity needs to be able to traverse both directions in the cavity. Alignment is thus critical for proper lasing of both arms in the cavity.

The cavity needs to be mode-locked in both directions, i.e. both arms supporting a frequency comb structure. These two pulses when overlapped cause a beating pattern. If the pulses are exactly the same, no beating pattern is produced when mixed.

The pulses will likely have slightly different comb spacing in application. The intensity dependent index of refraction of the crystal causes the opposing pulses to experience different speeds in the crystal and, therefore, different repetition rates. Thus, the intensity profile in the frequency domain will be different for each pulse.

2.6 Key system level issues

The main system challenge that comes with a bowtie design is proper alignment of the laser cavity such that both arms can maintain mode locking. The desire for a single cavity system comes at the expense of precise and fine tuned alignment of both directions in the cavity.

The laser utilizes the intensity-dependent index of refraction of the Ti:Sapphire crystal itself to achieve the dual mode-locked pulses. An unintended consequence of utilizing this method is that subsequent cavity repetition produces a chirp effect where the frequencies within the pulse become unaligned over time. This effect can be counteracted through the use of chirped mirrors.

The cavity is reliant on a constant repetition rate to produce stable mode locked pulses. Thermal drift and vibration can cause unintended variation in the repetition rate of the cavity. It is thus important to design the cavity for the reduction of heat, vibration, air, as well as other external influences.

2.7 Team and project management

Besides the designs, parts, and laser itself, the project consists of a lot more. For the sake of overview, a few are discussed succinctly here, but each is expanded on where appropriate, or in their own dedicated chapters. Critically, the team remained continuously dedicated to completing the project and was able to achieve many project milestones.

2.7.1 Challenges

Throughout this project, we encountered many unforeseen challenges and constraints. The team had to design and manufacture many cavity components in parallel to meet time constraints. As a result, many of the components were manufactured solo, but this greatly increased efficiency.

In contrast, the installation of optical components and beam alignment were more efficient when done in a small group. Overall, the relatively large scope of the project, which also included design machining, thermal control, and active stability, demanded significant total time commitment from everyone involved.

In particular, Covid-19 placed our team under an accelerated schedule due to our postponed access to the laser laboratory and the machine shop. Until we had the ability to manufacture all of our optics mounts, we could not even start the alignment phase of the project, which was the main vehicle for testing our system. Additionally, various setbacks including faulty stages, a warped optical breadboard, and part delivery delays added to the strain on the team. Section 10.1 will go into further detail about this matter.

2.7.2 Budget

The budget that we will go more in depth in Chapter 9 covers everything that would be needed in order to completely replicate the project. Most importantly, our project funding can be broken down into two parts: secured costs covered by an existing NSF research grant belonging to Dr. Bachana Lomsadze, and costs for parts purchased through mechanical engineering department funding.

2.7.3 Safety

While working with any laser system, a person should proceed with caution and mitigate potential hazards in all ways possible. Our pump laser operates at a maximum of 6W, and, therefore, has the potential to cause eye damage, including blindness, in addition to skin damage. This laser system is classified as a Class IV laser system under the OSHA laser safety guidelines which is the highest hazard tier for a laser system. All members took the EHS 0302 Laser safety training course before beginning lab work. Sections 10.2.1-3 provide more detail about the potential hazards we faced in the lab, steps taken by the team to ensure safety, and the in-lab procedures we adopted to

maintain a safe workplace. We are pleased to report that, no safety incidents occurred throughout the course of the project.

2.7.4 Design process

The design process was a crucial step to ensure success of the remainder of the project. Dealing with a laser system requires exact design and manufacturing to the precision of the thousandths of an inch. The exact dimensions of each part fabricated will be examined in the subsystems chapter. For all cases, Solidworks was used to model each part and create dimensioned sketches to be used in the machine shop. The dimensions of each part were defined so that the beam was located 2.275" (5.7785 cm) above the breadboard, a value that ensured that the optical pieces were short enough to ensure stability but tall enough to provide enough space for reasonably comfortable manual control during the alignment phase.

Chapter 3 Pre-Cavity

3.1 Overview and Requirements

The Lighthouse Photonics high power CW 532 nm DPSS Lasers Sprout-G Series was used as the pump laser to produce a 12 W output beam at 532 nm. This wavelength is within the absorption window of our Ti:Sapphire crystal, as required for this application. The pump laser exhibits excellent stability over both power ($\pm 0.25\%$ rms over 24 hour period) and frequency ($>99.9\%$ spectral purity), which helps maintain optical noise to a manageable level. The pump laser beam needs to be precisely focused onto the Ti:Sapphire crystal for the system to operate as intended. In addition, the beam profile should be “level” and “flat” at the location of the crystal.

In this section we describe several key components of the apparatus, including original parts and those we introduced as part of this project.

3.2 Pre-existing Setup

The optics laboratory designated for the new system already contained a wide variety of optics setups and equipment. In the center was an 4' x 12' optical bench that contained a Sprout G pump laser powering the pre-existing DCS laser. To power our DCS laser system, part of Sprout G pump beam's power was diverted in a new direction. The components used to direct the beam to our main laser are referred to as pre-cavity components, and will also be discussed in this chapter. Fig. 3.1 displays the pre-existing setup for the pump beam, and newly added components are labelled.

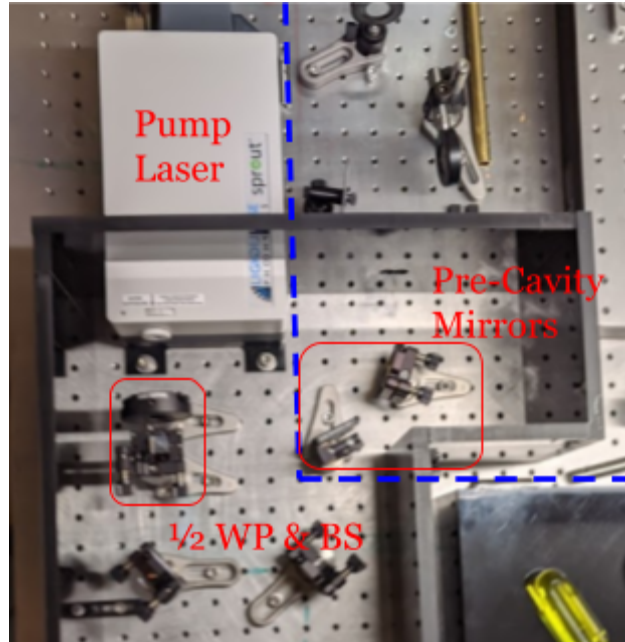


Figure 3.1: Pre-existing pump laser setup is visible left of the dashed line, as well as a half wave plate($1/2$ WP) and polarizing beam splitter (BS). Our new laser needed to operate using the 532 nm pump laser already present in Dr. Lomsadze’s lab. Also visible are the $1/2$ ” thick cell-cast acrylic walls of the pump beam containment box, and first two mirrors(Pre-Cavity Mirrors) used to direct the beam to our laser cavity.

3.2.1 Sprout G Pump Laser

This laser outputs a consistent beam at 532 nm. Although 532 nm is not the optimal absorption wavelength for a Ti:Sapphire crystal, the sprout G provides a very consistent and pure output beam. The spectral quality of the pump laser system exceeds 99.9% as well as having low noise and high long term stability. The DCS system is expected to run for long periods of time and the pump laser provides $< \pm 0.25$ % rms power stability over a 24 hour period. The stability makes the sprout G pump laser desirable for stimulating the Ti:Sapphire crystal.

3.2.2 Half Wave Plate and Beam Splitter

A half wave plate was used in combination with a beam splitter to divert part of the beam to the DCS system. The half waveplate is an adjustable polarization tool that can be used in combination with a beam splitter to get fine control over the power and direction of a beam. The wave plate is a 532 nm wave plate which provides polarization control over the pump beam. The beam path for the pump laser is described in Fig. 3.2 and Fig. 3.3 describes the half wave plate used to divert the beam.

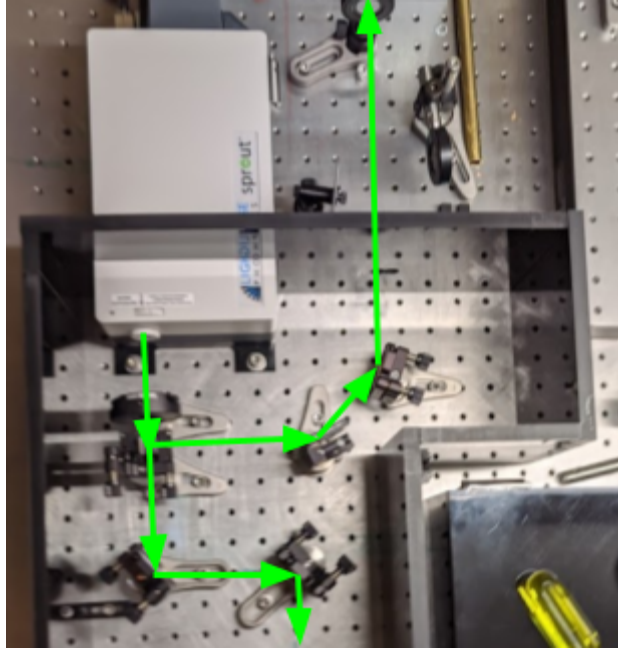


Figure 3.2: (View from above) The existing setup diverts light from the pump laser beam “downward” (as shown) towards the pre-existing laser. The new setup we designed and built introduces a second beam path (deflected “upwards” as shown) originating from the same pump laser, that enables simultaneous and independent operation of a second Ti:Sapphire crystal positioned on a small (18” x 18”) breadboard mounted to the full optics table.

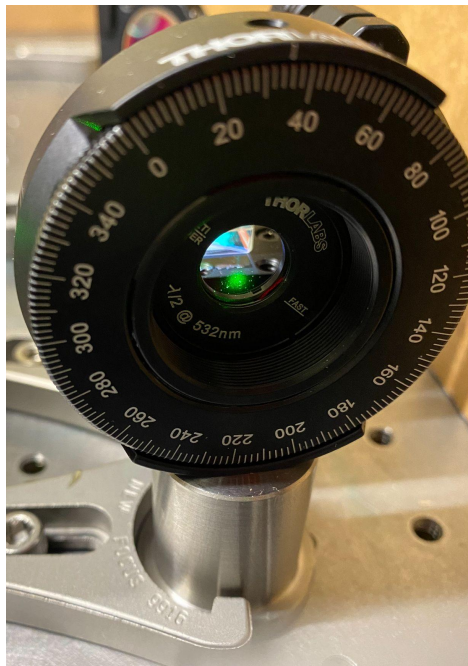


Figure 3.3: Thorlabs WPHSM05-532, 532 nm half-wave plate used to provide fine-scale control over the electric field polarization of the pump beam.

3.3 Redirecting Mirrors

Silver redirecting mirrors are used to direct the beam from the pump beam to the Ti:Sapphire crystal. All mirrors are mounted in mirror mounts which provide fine control over the alignment of the beam. The silver mirrors provide high reflectance over a wide range of wavelengths. More specifically Thorlabs PF10-03-P01 are used to redirect the pump beam. The mirrors are 96.5% to the pump beam output. It is necessary to use as few mirrors as possible when directing the beam to minimize power loss.

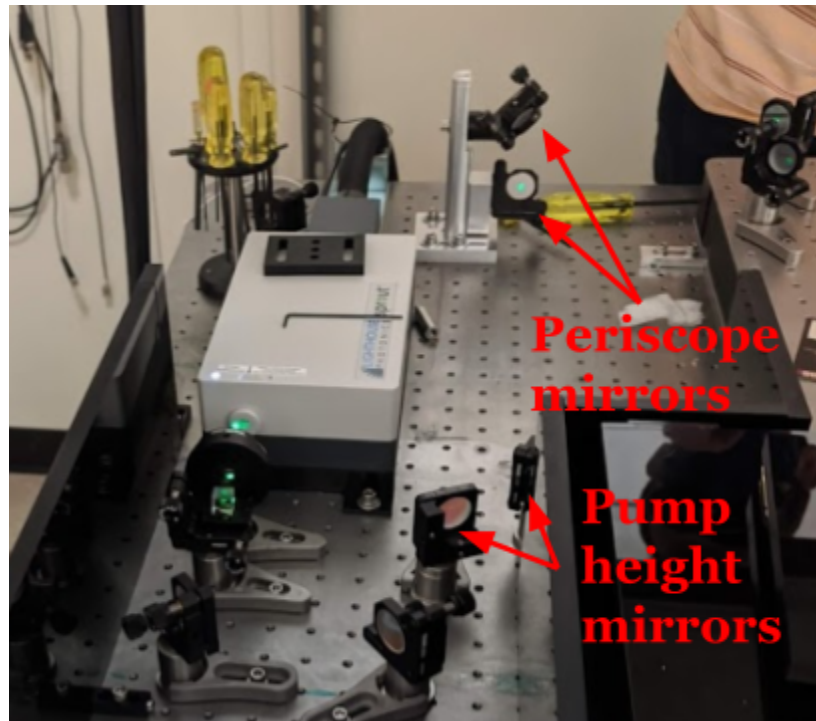


Figure 3.4: Silver mirrors are used to redirect the pump beam to the new Dual Comb system. The pump height mirrors are each angled at 45° .

3.3.1 Pump-Height Mirrors

The pump beam outputs a horizontal beam that is 2.04" above the optical bench. The pump-height mirrors (Fig. 3.4) were mounted with their centers at this height. However, the reflected beams eventually needed to strike a Ti:Sapphire crystal centered 4.637" above the optical bench. A specialized periscope (see next section) was designed and built that could raise the optical axis of the reflected beams to the desired height of the Ti:Sapphire crystal.



Figure 3.5: Mirror configuration in the original pump beam containment box.

3.3.2 Periscope Mirrors

The periscope we designed (see next section) needed to raise the optical axis of our pump beam from 2.04" to the height of the Ti:Sapphire crystal (4.637"). The periscope utilizes two Thorlabs PF10-03-P01 mirrors, each with 96.5% reflectance. The individual mirror mounts each provide additional adjustment for fine control of the beam position. The first mirror is angled upwards at 45° . The second mirror is then used to realign the beam parallel to the optical bench and aim the beam towards the Ti:Sapphire crystal.

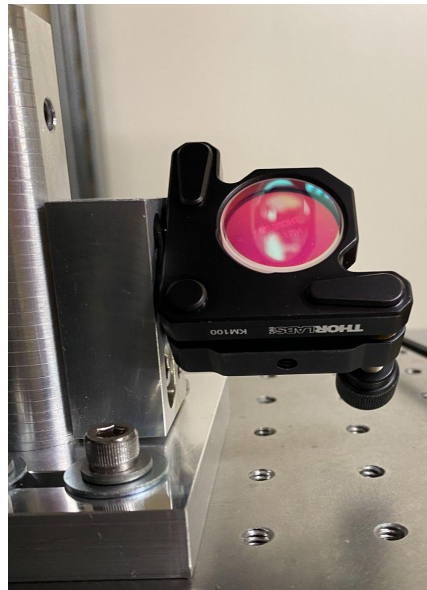


Figure 3.6: Bottom periscope mirror. The mirror is angled at a 45° angle to reflect the beam vertically, where it reflects off the top periscope mirror and is redirected horizontally (top mirror is visible in the reflection).

3.4 Periscope

Our pump laser, which is off of the breadboard and resides on a large optics table (see Fig. 3.1) outputs a beam at a height of 2.04", while the crystal is 4.637" above the optics table. On top of this, existing periscopes were nowhere close to rigid enough. To work around these problems we designed and implemented an adjustable periscope that raises and levels the beam to a height of 2.275" from the breadboard. The choice for 2.275" of beam height was agreed upon because it is short enough to ensure equipment stability but it is tall enough to allow for ease of access to each part.

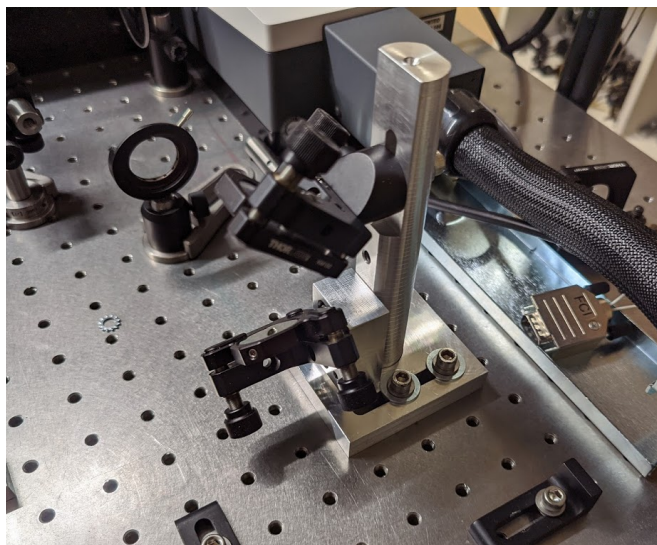


Figure 3.7: Custom built, adjustable periscope used to raise the optical axis of the pump beam to the height of the Si-Sapphire crystal at the heart of our Dual Comb Spectroscopy (DCS) system.

The periscope assembly (Fig. 3.7) consists of 3 individual parts, each of which serve a different purpose. The parts include a periscope tower (Fig. 3.8), to which the adjustable periscope mirror mounts attach, an adjustable mounting plate (Fig 3.10) that allows the periscope to be rigidly connected to the optical breadboard, and a variable mount (Fig 3.11) that provides additional vertical adjustment capability.



Figure 3.8: Left: Machined 6061 Al periscope tower, mounting plate and variable mirror mount. Right: The 6" tall x 1" diameter design model of the periscope tower.

3.4.1 Periscope Tower

The periscope tower consists of three threaded mounting holes for the bottom mirror. These mounting holes are spaced 1" apart and provide a wide range of adjustability for the bottom mirror. More precise alignment can be achieved with the variable mount which will be described later.

The tower also consists of a slotted region for the top mirror. The top mirror is mounted using a screw and washer. For proper alignment of the mirrors, the top mirror needed to be situated further back compared to the bottom mirror. A flat portion was cut out to ensure that the top mirror was located in the correct position compared to the bottom mirror.

The tower has a 1" lip which can be mounted using a standard optical clamp. However, this was deemed insufficient for rigidity. A separate clamp design, the mounting plate, was manufactured to clamp the tower down.

3.4.2 Periscope Mounting Plate

The mounting plate was designed to clamp the periscope tower to the table. It utilizes four 1/4-20 screws with washers to ensure stability and rigidity through its lifetime. The mounting plate consists of a circular cutout for the periscope tower, and two slots which allows the periscope tower some adjustability on the optics table during placement.

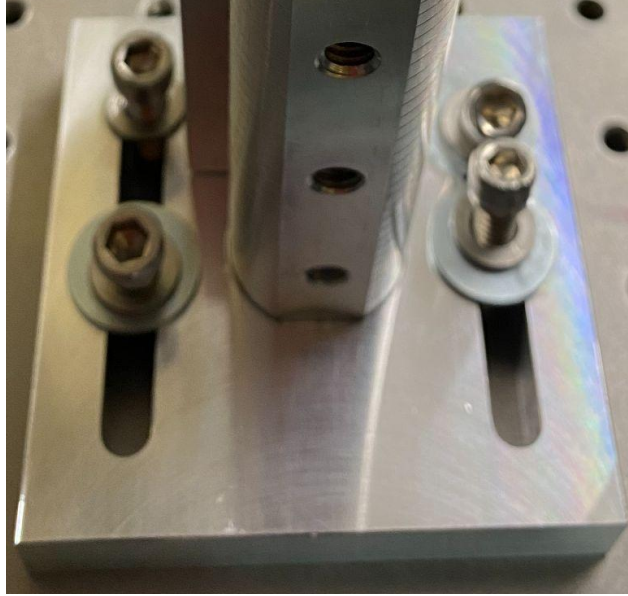


Figure 3.9: Periscope mounting plate used to clamp the periscope tower to the optics table. Visible is the reverse side of the tower, and the four 1/4"-20 screws with their washer sets.

3.4.3 Periscope Variable Mount

The variable mirror mount was designed for the bottom periscope mirror. Since the two mirrors are mounted in different styles, with the top requiring an angle mount, the variable mount was required to keep the mirror centers aligned. It's added features were included to increase the possible configurations the periscope could achieve. The variable mount has two .255"-wide slots which are used to secure the variable mount to the periscope tower. In addition to the slots, five 8-32 threaded holes were tapped into the variable mirror mount to attach the bottom mirror of the periscope. The third was used in the final build.

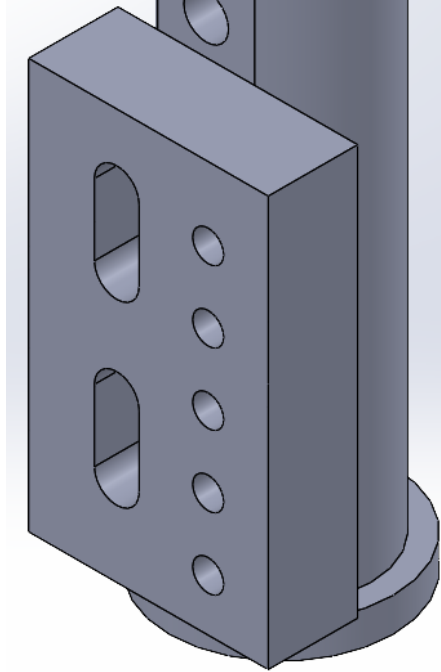


Figure 3.10: Variable mount for the lower mirror of the periscope. The variable mounting plate has two $\frac{3}{8}$ " wide slots that are used to attach the plate to the periscope tower. The five threaded holes shown to the right of the slots are used for mounting the bottom mirror of the periscope.

3.4.2 Periscope Container

An 8" by 9" periscope box (shield) was created to house the periscope. The containment box was implemented to mitigate the potential danger caused by high power pump laser light reflecting off the periscope mirrors and other objects near the beam path. The light-shielding box was constructed using $\frac{1}{2}$ " (12.7 mm) thick black acrylic. It was equipped with $\frac{1}{2}$ " diameter holes for the pump beam to enter and exit. The passage of the pump beam is protected by $\frac{1}{2}$ " brass tubes used to isolate the beam path from possible physical interference. It also serves as a safety precaution, so that the pump beam is completely contained until it enters the cavity box.



Figure 3.11: Top view of the periscope containment (shielding) box, with lid removed. The light-tight box was made using cellcast opaque acrylic and acrylic cement.

The box (with removable lid) was flawlessly effective at containing and catching stray reflections from the periscope throughout the course of the project.

3.5 Optical Analysis

This section is dedicated to specifications and observations as to the impact of these components on the optical performance of the system.

3.5.1 Mount Integrity

Four $\frac{1}{4}$ -20 screws were used to secure the periscope tower base to the optics table. The periscope tower base has a 0.19" high lip used to secure the mounting plate. To ensure proper clamping, the mounting plate was machined for a lip size of 0.188". The mounting plate thus floats on the table when it is on the periscope tower. The periscope tower is always making contact with the optics table, and screwing the mounting plate into the table ensures a proper clamping force on the periscope tower. The remaining two mirrors, on custom manufactured shorter posts, were equivalently stable to similar optics already in use for the pre-existing laser.

3.5.2 Beam Direction

To ensure that the periscope is functioning properly, the team had to test the flatness (leveling) of the beam after it exited the periscope. An iris was placed at the base of the periscope to constrict the beam while we measured the precise beam height. A second iris was then placed in a straight line 10 feet away from the periscope. The

second iris was placed at the same height of the first iris. The periscope was then adjusted until a straight beam could go through each iris without loss. The method ensured that the periscope was outputting a level beam at the desired height above the optical bench.

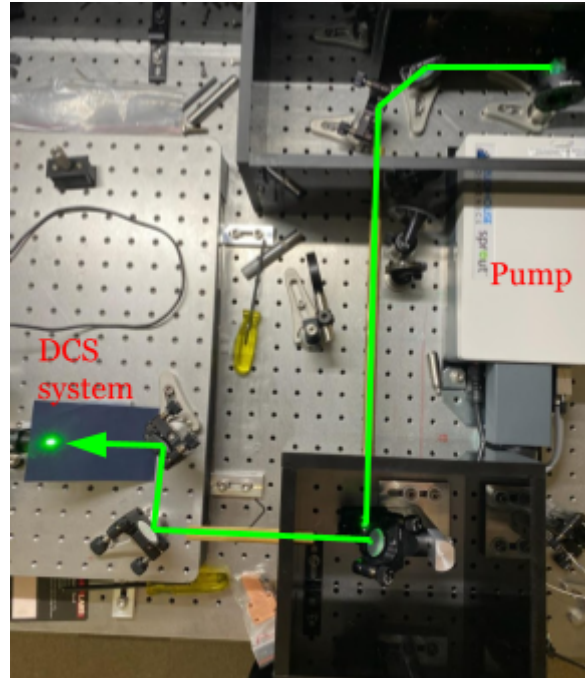


Figure 3.12: Green beam path from pump laser to DCS system.

3.5.3 Optical Power

As mentioned above, silver mirrors (Thorlabs PF10-03-P01), which are each 96.5% reflective at 532 nm, are used to direct the beam to our optical cavity. The beam loss for each mirror is independent of the others and thus an approximate power loss calculation for our system:

$$P_T = P_p(R)^n$$

yields a cavity power of $P_T = 4.84 \text{ W}$ for $P_p = 6 \text{ W}$, $R = 96.5\%$ and $n=6$.

3.6 Problems, Revisions, and Future Changes

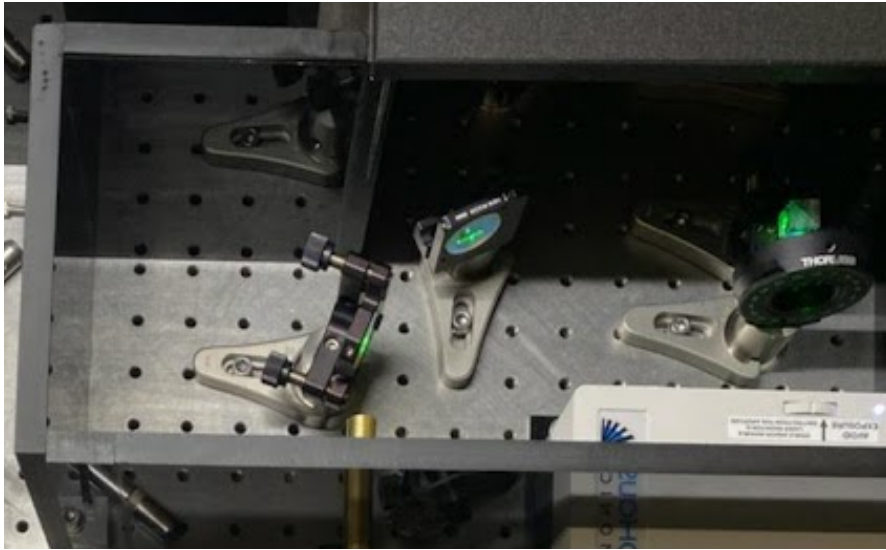


Figure 3.13: Mirror configuration in the pump beam containment box.

The team utilized a two mirror setup (Fig. 3.14) to get the pump beam out of the containment box. In general, a single mirror design would be more desirable since each reflection causes some loss from the silver mirrors. However this was not possible due to the small size of our containment box. To achieve a two mirror design, each mirror had to be oriented at a sharp angle with respect to the incident beam, which is suboptimal for beam alignment and general use of the system. Future revisions that should be considered include replacing the current configuration with a single mirror setup and switching to mirrors whose reflectance values are more optimized for green light.

Chapter 4 Physical Build Components

4.1 Introduction to Physical Build

In this chapter, we describe in more detail how each component of our Dual Comb system was selected, designed and configured. The physical build of the cavity was critical for proper functionality and alignment of the laser beams. Design considerations such as component placement and adjustability were meticulously considered throughout the design process. Simply stated, the cavity needed to be properly aligned in the desired “optical bowtie” design; this required implementing a plethora of sensitive mirror control systems. In total, the eight mounting components on the breadboard alone utilize 12 angle controls, four mechanical stages and more than 30 set screws to determine the full range of positions and orientations of the whole system.

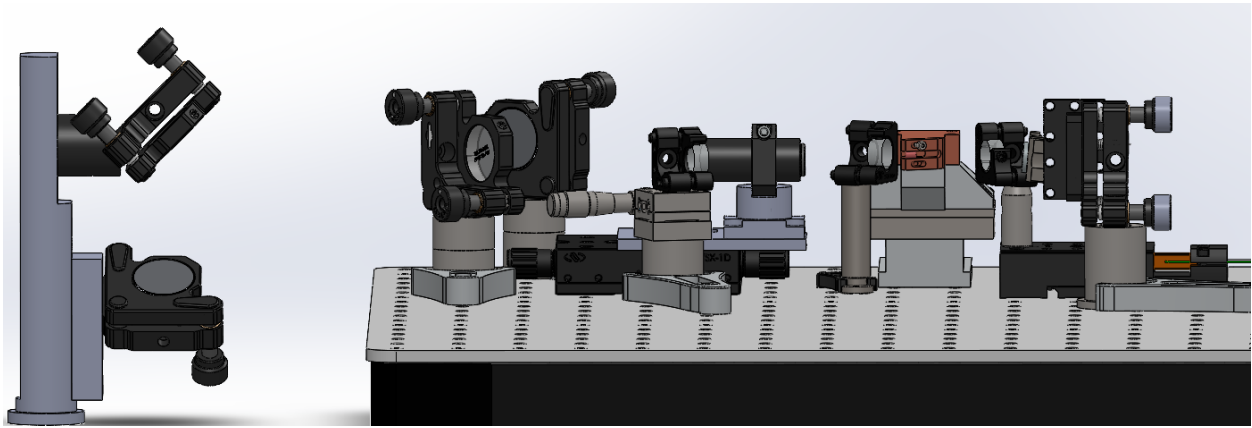


Figure 4.1: SolidWorks model of the completed cavity design. Roughly from left to right: Periscope (with two 1” mirrors), breadboard, two 1” directing mirrors, focusing lens assembly, flat chirped mirror assembly, entry curved mirror, Ti:Sapphire crystal assembly, 2nd curved mirror with linear stage, & output coupler assembly.

4.2 Initial Design Decisions

Individual components such as the four mirrors and the Ti:Sapphire crystal are mounted in dedicated holders. Spacers were designed and manufactured to hold the cavity components at their optimal heights. A height of 2.275” was chosen as the design requirement for all cavity components and spacers to satisfy, and careful consideration was allocated to ensure that all optical components within the cavity hit this target. All of the mounts are adjustable, and some are attached to linear stages that can be adjusted using micrometers. The need for precision adjustability is due to the nature of Dual Comb Spectroscopy experiments that will be performed with this system. Slight shifts in effective cavity length can cause the optical pulses within the cavity to lose their mode-locked configuration.

Ensuring that the crystal face was 2.275” off the table was critical; the crystal has a height of 0.11811” (3.0 mm), and it is essential that successive reflections within the

cavity are able to hit the crystal target. Aluminum spacers were designed and manufactured to keep this tolerance requirement in mind, and a great deal of precision was used when machining the spacers.

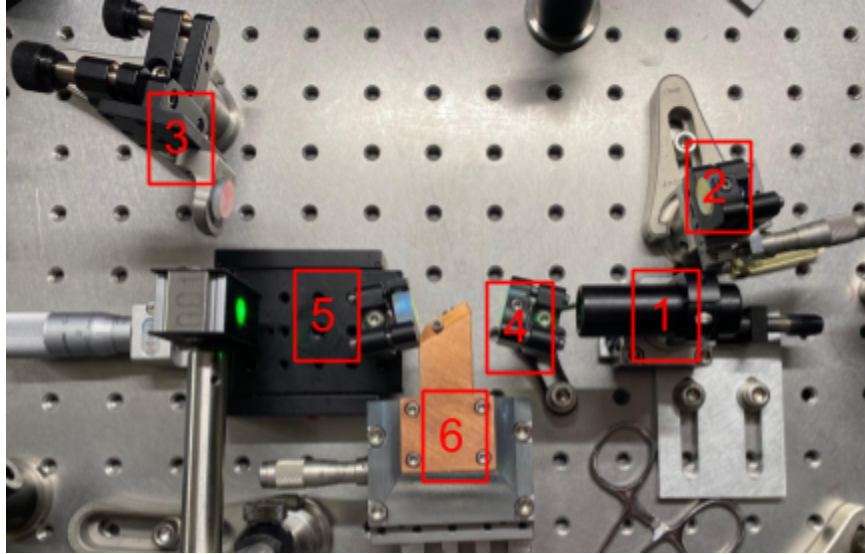


Figure 4.2: Cavity component locations. See Table 4.1 for component names.

Table 4.1: Components in cavity

Key	Part Name
1	Focus lens
2	Flat chirped mirror
3	Output coupler mirror
4	Input Curved mirror right
5	Curved mirror left
6	Heatsink/ crystal mount

Table 4.1 and Fig. 4.2 shows the physical build components we needed to consider when designing and building our cavity. All of the mirrors are situated in dedicated mirror mounts that provide sensitive angle adjustments.

A PID loop system was also part of the initial design. It was intended to address the desire to reduce the drifting behavior which was observable during long term use of the cavity. This affects the repetition rate of the pulses, and is mainly caused by thermal expansion. To counteract this drifting, apart from new breadboard material, a PID system was to be implemented on one of the mirrors to actively alter the length of the cavity. To provide input for the PID to act upon, part of the output of the cavity was to

be used to keep track of the repetition rate of the cavity. This information would have been fed to the PID system, which would have attempted to keep the cavity's f_{rep} at a desired frequency. This reaction would have only occurred once the change reached a threshold amount, which was to be defined by testing. However, the PID system has not been implemented due to time constraints.

4.3 Breadboard

The breadboard serves as the basis of construction of the cavity. It serves to isolate the cavity from the optics table in which the laser system operates on. The breadboard also serves as a distinct boundary in which a container can be placed around the laser cavity system. It is essential that standard optical components can be placed on the breadboard.

A breadboard can also provide different mechanical properties for a laser cavity. If the laser is expected to run into issues due to thermal expansion under normal operating conditions, a breadboard can provide a solution.

4.3.1 Implementation Trade-offs

The standard breadboard design includes $\frac{1}{4}$ - 20 tapped holes spaced 1" apart for the purpose of mounting optical components to the table. The breadboard needs to be chosen such that the cavity can be contained in a box around the breadboard. The breadboard size was ultimately decided based on a targeted cavity repetition rate of 500-1000 MHz. The repetition rate is chosen in correspondence to the type of tests that the system will do. This corresponds to a total targeted cavity length between 30 and 60 cm.

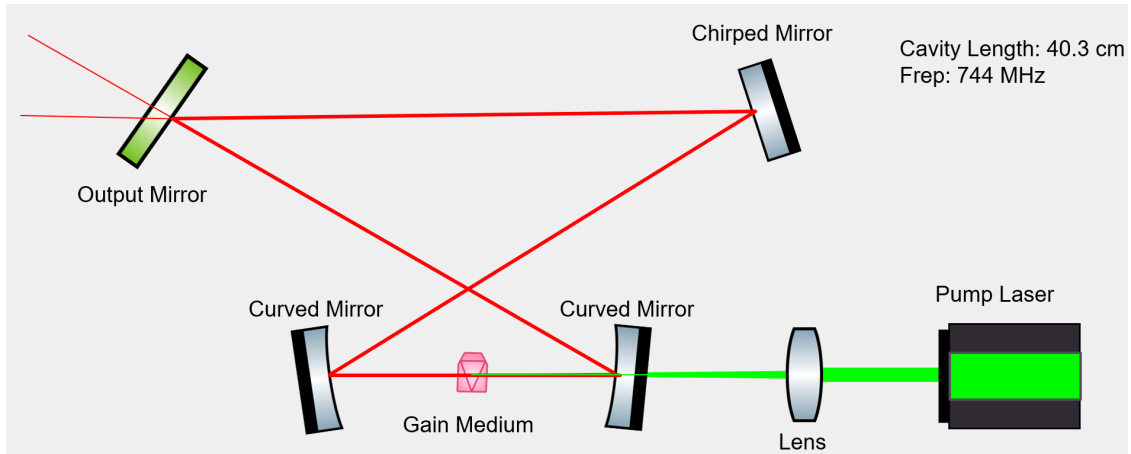


Figure 4.3: Bowtie cavity design. Light from the pump beam is focused into the gain medium through a lens. The gain medium emits light while the left curved mirror directs light to the chirped mirror, the right curved mirror directs light to the output mirror.

A. Franzen, "ComponentLibrary," ComponentLibrary: a free vector graphics library for optics. [Online]. Available: <http://www.gwoptics.org/ComponentLibrary/>. [Accessed: 10-Jun-2021].

Images were made using the optics component library <https://creativecommons.org/licenses/by-nc/3.0/>

Initial cavity design was chosen based on a four mirror bowtie cavity setup. The cavity contains two curved mirrors which are situated on both sides of the crystal. The curved mirrors serve as a method to reflect the light emitted by the crystal and redirect the light to the other mirrors as well as focusing the returning beam back into the crystal. The top right mirror serves as a flat mirror to counteract some of the chirp introduced by the crystal. The top left mirror serves as an output mirror.

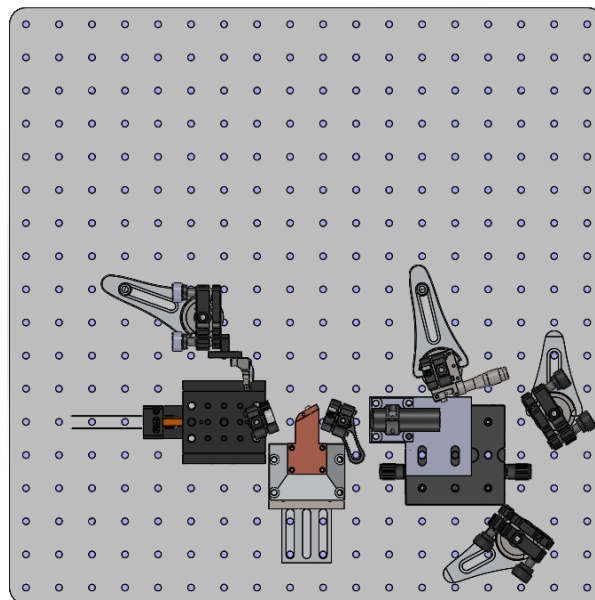


Figure 4.4: Cavity design on a 18"x18" breadboard.

An initial cavity length of 40 cm was chosen for the project, and this correlated to a 9" by 4" (23 by 11 cm) cavity footprint on the breadboard. Once accounting for the mounts, this increased to around 9" by 8", and increased once more to 14" by 9" upon the inclusion of the 2 final directing mirrors that served as the go-between the periscope output, and directing the beam accurately in the direction of the cavity. The alignment that guided the assembly progress can be found in Chapter 8.

An appropriate breadboard size of 18" by 18" (45.7 by 45.7 cm) was chosen such that the cavity and any other pump beam adjustment tools could fit within the breadboard with adequate leeway for unforeseen issues.

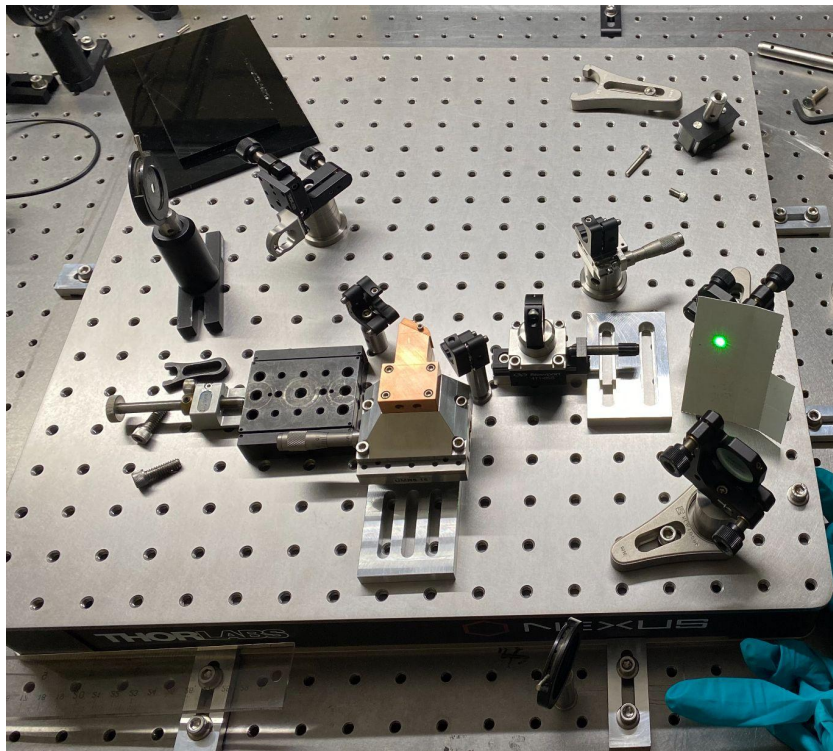


Figure 4.5: Steel optical breadboard. The specific model was chosen for vibrational isolation and reduced thermal expansion. The breadboard is mounted using clamps to an optics table on which the pump laser is situated.

The steel breadboard chosen for the design and implementation of the laser cavity was an 18" by 18" Optical Breadboard with Optimized Damping, and is 60 mm (2.4") thick. Besides being exceptionally flat, the breadboard also provided valuable vibration isolation. The compliance curve included within the breadboard indicates that the breadboard has a resonant frequency at 324 Hz. The full compliance curve for the specific breadboard can be seen in Appendix D.4.

The breadboard's most significant trade off is its height relative to the optics table. The optics table serves as containment for a separate laser system which is the

532nm pump laser which powers the Ti:Sapphire crystal. The breadboard chosen to house the cavity is 2.4” in size which is a significant jump in height from the optics table.

4.3.2 Material

Just as with other cavity mounting equipment, material characteristics were a critical feature when selecting a breadboard. Of the characteristics including density, rigidity, and thermal expansion coefficient, it was the latter that was the most important for addressing the drifting behavior we were asked to address.

Table 4.2: Thermal expansion coefficients for potential breadboard materials.

Material	Coeff. of Thermal Expansion (10^{-6} K^{-1})
2024 Aluminum	22.9 [9]
430 Stainless Steel	11.0 [10]

The integrity of the two pulses is tied to stability so it is important to take significant isolation steps to ensure proper functionality of the cavity. Temperature fluctuations were identified to be the main cause of instability. It is important to note that the specific use case that the product operates in has slight temperature fluctuations that were deemed to be a significant cause of concern. The specific material chosen for the breadboard might have a significant influence on the repetition rate of the cavity.

Breadboards generally used in industry utilize either aluminum or stainless steel. It is expected that the stainless steel breadboards be used in more sensitive applications. An approximate repetition frequency variation calculation was used to justify which breadboard would be adequate. If a cavity design of 42.73 cm is used, it is appropriate to compare the worst case temperature variation between the two materials using the table of thermal expansion coefficients listed above. If we assume that the maximum temperature variance while under operating conditions is 1°C.

Table 4.3: Approximate frequency shift given a 1°C fluctuation in temperature.

Material	Approximate Frequency Shift
2024 Aluminum	16018 Hz
430 Stainless Steel	7694 Hz

The complete calculation can be seen in the Appendix A.1. Overall, the stainless steel breadboard was chosen due to its significant decrease in frequency variation. It was

determined that the increased frequency shift might provide difficulty in achieving a stable mode locked laser cavity.

4.3.3 Breadboard Clamps

The choice to use this breadboard introduced a problem of mounting the breadboard to the optics table. To ensure that the breadboard does not move, clamps were specifically made to clamp onto the bottom lip of the breadboard. For convenience, the clamps were made so that the breadboard's holes lined up with the holes of the optics table. A total of 6 clamps were used to mount the table, 2 sides contained 2 clamps and 2 sides contained 1 clamp.



Figure 4.6: Steel clamps which clamp to the breadboard. Detailed engineering drawings of the breadboard clamps are included in Appendix C.4.

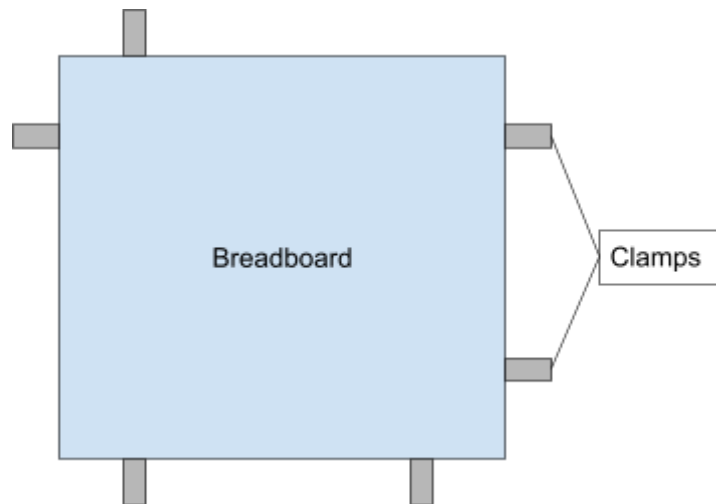


Figure 4.7: Clamp configuration of the board. Configuration was based around exterior optical parts.

4.4 Optical Stages

All optical equipment/stages used within the cavity are summarized in Appendix I. For the left curved mirror, a Newport 9064-X-M with 1.1" (28 mm) travel distance was implemented. The heat sink sits on a Newport UMR5.16 linear stage that can move .63" (16 mm). A Newport TSX-1D linear stage with 1" (25.4 mm) of travel distance is attached to the base of the focus lens mount. A Newport M-SDS25 with 10mm of travel is used beneath the chirped mirror.

4.5 Posts

Posts were designed and manufactured for the output mirror, chirped mirror, and both curved mirrors to ensure that the optical equipment is situated at the desired height. Engineering drawings for all posts are included in Appendix D.3.

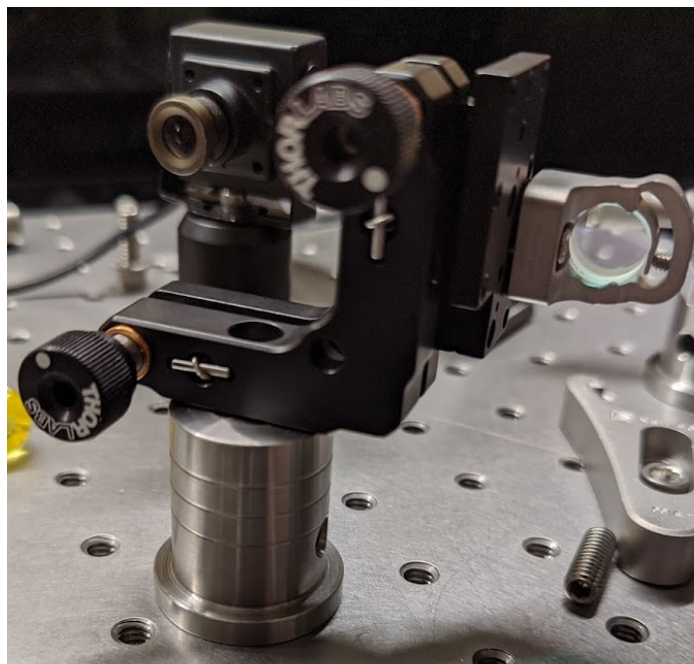


Figure 4.8: Custom manufactured post, standard mount, output mirror at design height.

4.6 Mounting Spacers

4.6.1 Focusing Lens:

Initial design requirements of the lens system indicated that the lens needed adjustability along the optical axis. Spacers were manufactured to the correct design height so that vertical adjustment of optical components was not needed. The design decision to not include vertical adjustment avoided a significant increase in cost.

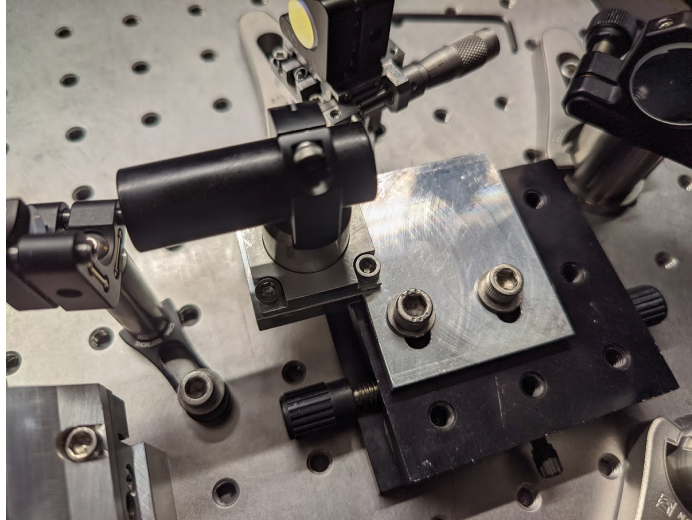


Figure 4.9: Focus lens spacers and linear stage. The linear stage adjusts the focus lens so that the focal point can be moved precisely.

The solution the team came up with is to use 3 spacers. The first spacer is the bottom plate which mounts the focus lens to the linear stage. The second spacer is a steel circular spacer that supports the SM05RC lens mount. The circular shape facilitates angular adjustments. The second spacer also includes a lip so that a clamp can be used to effectively maintain the position of the spacer and fix the position of the focus mirror on the linear stage. The third spacer acts as a clamp and uses 4 screws to secure the second spacer. Detailed engineering drawings of all 3 spacers for the focus lens are included in Appendix D.2. Figure 4.10 demonstrates the adjustability that the stage and spacers provide.

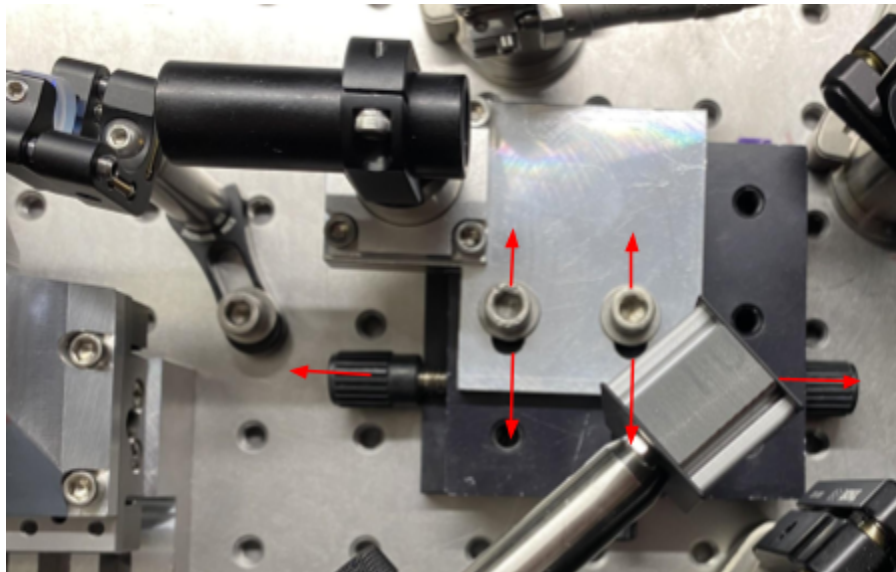


Figure 4.10: Top view of the focusing lens in its 2” long cylindrical mount. Together with the mechanical stage, the spacer enabled full adjustability in the horizontal plane.

4.6.2 Heat sink spacers:

The heat sink for the Ti:Sapphire crystal is mounted to two aluminum spacers coupled to a linear stage that is used for alignment purposes. (See Fig. 4.11) The top spacer underwent the greatest design change when compared to its predecessor in the pre-existing laser. Besides being thicker, the sloped profile reduces user obstruction, and allows for the crystal to protrude further from the base, while the center of mass remains firmly far back for stability. The new neck feature provides support for the neck of the heat sink, and increases copper-aluminum contact, and with the added thermal paste between the surfaces, there is a slight benefit to thermal performance, providing minor protection against overheating if the liquid cooling is not engaged by accident (the risk is minimal regardless). The linear stage, including its manual control knob, is relatively large (~2" by 4") and needs to be far enough from the cavity to ensure enough access to the control knob during beam alignment.

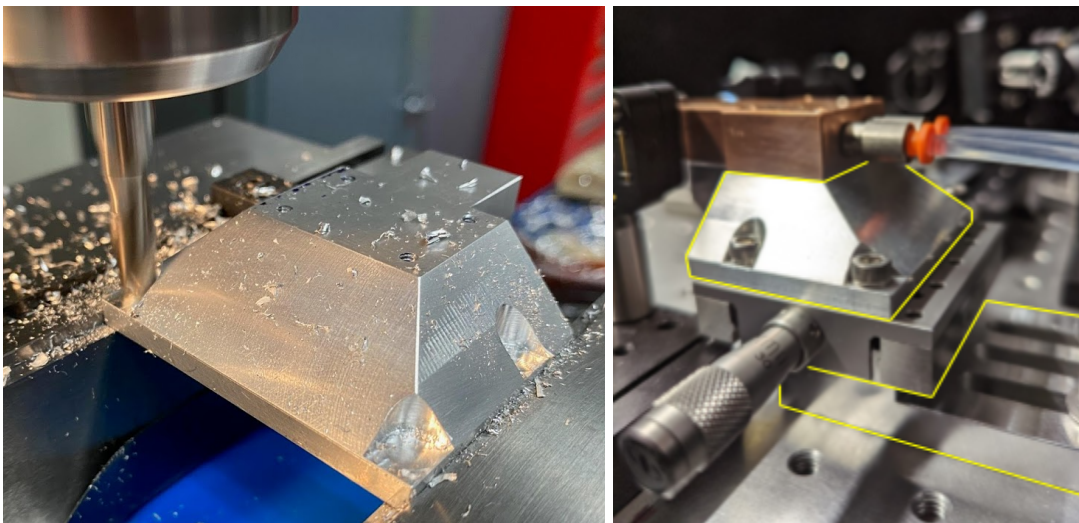


Figure 4.11: Heat sink top spacer during manufacturing (left), top and bottom spacers after full installation (right).

The bottom spacer for the heat sink subassembly provided a height offset, preventing the heat sink linear stage from coming into contact with the 0.75" tall linear stage located nearby. The bottom heat sink spacer is 0.800" tall and includes slots for mounting, which further increase the adjustability of the heatsink on the breadboard. The design provides sufficient stability and adjustability while also not impeding on other cavity components.

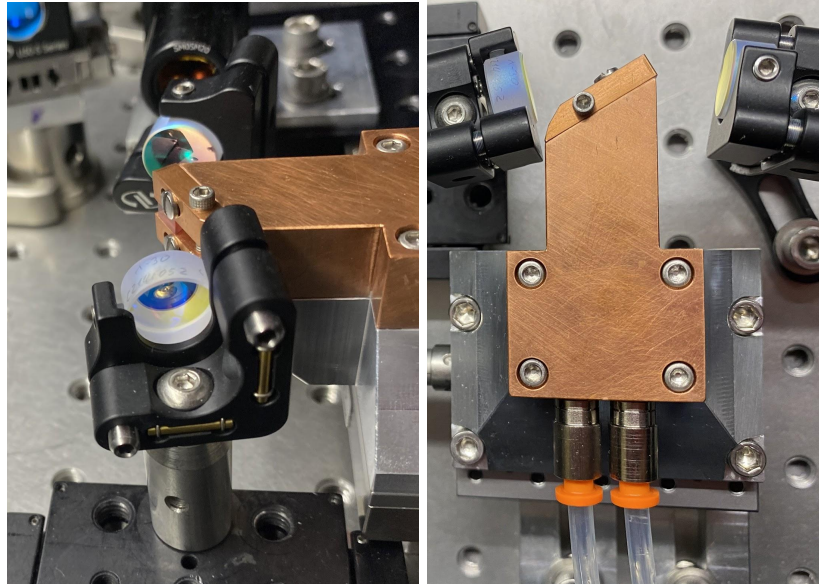


Figure 4.12. *Left:* Bottom heat spacer successfully raises crystal mount above the height of the mirror stage, (visible bottom right). *Right:* Close up of heat sink assembly, showcasing the maximized protrusion of the copper neck, and thereby the crystal.

4.7 Proof of Worth Analysis

As will be discussed at length in Chapter 8, the careful manufacturing of all custom made components in this project led to the first big successes of our new laser system. The group's consistent approach to the manufacturing process was to be as precise as possible to ensure the highest probability for success at each stage, thereby minimizing the time that would be needed later to align the laser in the lab. This approach was justified by the knowledge of how complex and sensitive a good Ti:Sapphire set-up typically is, and how difficult it is to build a functioning Dual Comb Laser system. In the end, the hard work in the manufacturing stages paid-off well; implementation of the finely manufactured parts proceeded smoothly, with few surprises along the way.

4.8 PID Implementation

As stated in 4.2, our initial project plan included developing and implementing PID control of the laser cavity but we did not have time to include this functionality. The PID controller would have been coupled to one of the two linear mechanical stages beneath mirrors in our cavity, and would have operated off a FPGA board. It would respond to μm -scale changes in cavity length experienced over hours of continuous operating time, or to maintain high repetition rates over quick experiments. Unfortunately, this objective became secondary, and thus far has yet to be implemented, due to time constraints.

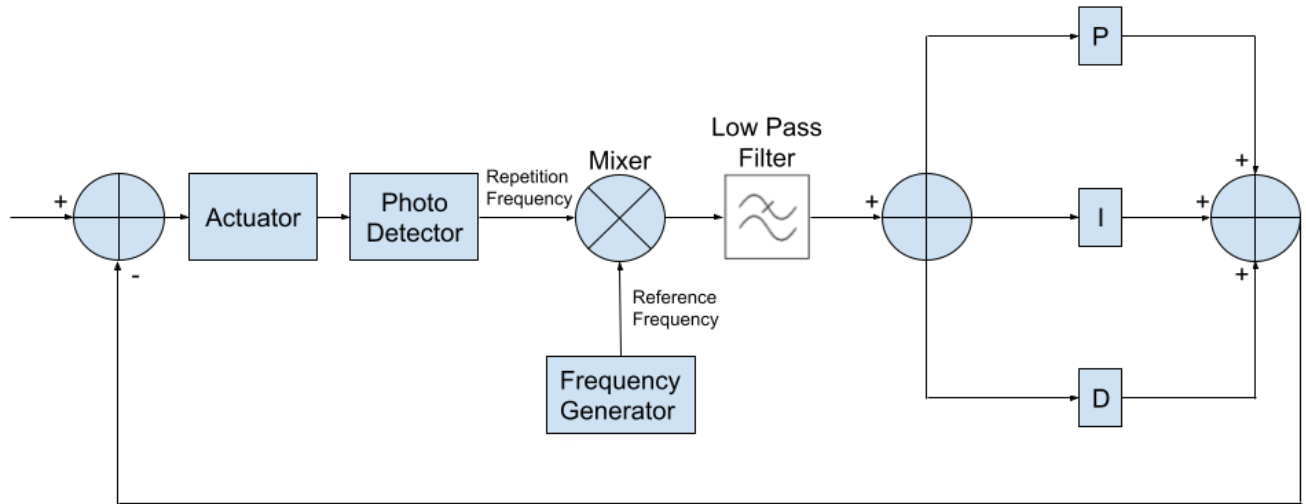


Figure 4.13: Block diagram of PID system.

The plan for implementing a PID controller into our system is shown schematically in Fig 4.13. The position of a mirror actuator would be used to precisely maintain the MHz-scale repetition frequency of the cavity. The repetition frequency is in the MHz region which is difficult for a PID system to track. Instead a reference signal with the desired reference will be mixed and used as the input of the PID system. The PID system will attempt to keep the cavity at the desired reference frequency. This is done by minimizing the error signal where the error is produced by the beating pattern between the reference signal and the repetition rate of the cavity. The beating pattern produces a high frequency signal and a low frequency signal where the high frequency signal is ignored.

4.9 Problems Encountered and Adaptations

Initial cavity designs utilized a smaller linear stage for the focus lens. After construction and alignment with a preliminary linear stage, it was revealed that the stage contained a defect— it was not stable and could be bumped into an offset position. Coincidentally, some of the bumping of the focus mirror provided hints at better alignment, which was used later to controllably increase the power output of the cavity.

Although it was exciting that the cavity could lase better for an instant when bumped, it ultimately indicated that the stage was unstable and could provide potential problems for further alignment. The stage was replaced with the TSX-1D Dovetail linear stage. The TSX-1D was at a different height from the previous stage, which meant that the focus lens spacers were also redesigned. However, because initial cavity alignment was already preliminarily successful with the previous stage, careful design and fabrication of the new spacers was undertaken to maintain the previous alignment progress. This decision was a worthwhile design choice because progress was indeed maintained after replacement.

Chapter 5 Optics

The core elements of our apparatus include four mirrors, one focusing lens, and one Ti:Sapphire crystal. However, six additional mirrors were required to properly direct the incident 12 W source beam into our apparatus.

Each of the five components within the cavity has an impact on which wavelengths can be resonant within the cavity. First and foremost, the emission bandwidth of a Ti:Sapphire crystal determines which frequencies can even be emitted into the cavity. As seen in Fig. 1.4, the crystal can support modes anywhere from 600 to 1100 nm, or 285 to 500 THz. The second most critical parameter for maintaining resonance in the cavity is the combined chirp of the optical components in the cavity. These have a diminished but still broad bandwidth of 770 nm to 880 nm, or 340 to 390 THz. Thirdly, the cavity path length impacts which wavelengths can resonate inside the cavity. In Comb terminology, the first two considerations affect the bandwidth of the frequency comb, while the third one affects how fine-toothed the comb is; smaller cavities space out the teeth further, because of their more rapid repetition frequency.

5.2 Requirements

5.2.1 Assembly Requirements

Building a bi-directional laser requires precision alignment and positioning of all optical components in the system. Here we describe some of the basic characteristics of our optical components and how these properties impacted our design.

5.2.2 Optical Requirements

The components selected need to be able to be aligned properly for lasing and mode-locking while avoiding a significant loss of power, effects of chirp, and astigmatism.

Astigmatism describes how an optical component (e.g. our Ti:Sapphire crystal or the lens of an eye) refracts the light coming into it in non-optimal ways, causing in some cases a double image to form. In our optical system, effects of astigmatism from the geometry and wavelength-dependent index of refraction of our crystal can be negated by mounting one of the curved mirrors near the crystal at an angle with respect to the optical axis. The specific tilt angle needed also depends on astigmatism effects introduced by tilt in the pump lens. In general, knowing how the tilt of the pump beam affects astigmatism allows an experimenter to readily determine the correct angle for negation of the astigmatism (Catalina). In this case, the astigmatism was compensated via an adjustment of the curved mirrors. Without this compensation the output power of our laser cavity drops precipitously.

5.3 Component Selection

The selection of each component was determined by how and to what degree the part fulfills the assembly and optical requirements. We summarize the basic properties of each optical component in Table 5.1.

Table 5.1: Detailed info on each optical part.

Optic	Dimensions	Other Important Values
Redirecting Mirror	25.4 mm diameter	96.5% @ 532 nm
Focus Lens	12.7 mm diameter	40 mm focal distance
Crystal	3x5x5 mm	*see in section 1.3
Curved Mirrors	12.7 mm diameter	9.8° angle wrt crystal 15 mm focal distance Reflects .1% of 532 nm & 99.7% of 720 to 980 nm
Output Mirror	12.7 mm diameter	Reflects 99% of 700 to 900 nm
Chirped Mirror	12.7 mm diameter	~100% reflective -40fs ² of GVD

5.3.1 Redirecting Mirrors

Once the beam enters the plane of the breadboard, coming from the periscope, it could theoretically pass directly through the focusing lens and pass into the crystal. However, this would mean that any fine tuning of the starting position and the vector direction would be controlled by the periscope, which is definitely not optimal. Because directing optics is often done in pairs, two 1” diameter mirrors were used on the breadboard to fine tune the pump beam direction (see Fig. 5.1).

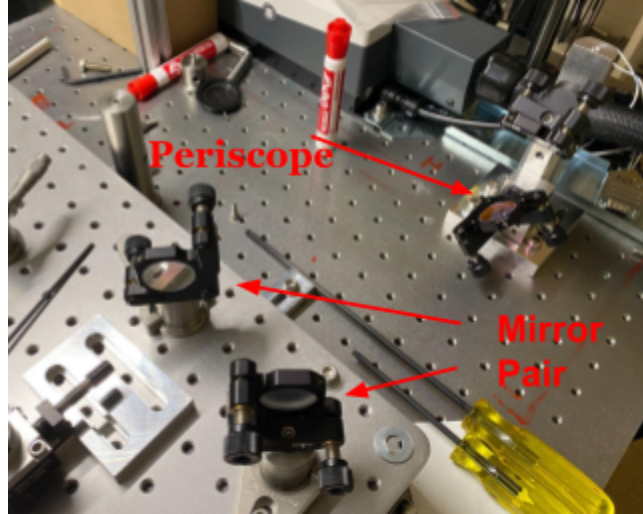


Figure 5.1: The pair of mirrors on the breadboard used to perfect the output from the periscope, as seen during early stages of the build.

5.3.2 Focus Lens

The focus lens is the final optic before the laser cavity, and serves to concentrate the pump beam, greatly increasing its intensity as it reaches its focal point within the Ti:Sapphire crystal. The lens is biconvex and has a focal length of 4 cm, which naturally dictates its placement with respect to the crystal.

5.3.3 Crystal

At the core of the optical cavity is a 3 by 3 by 5 mm Ti:Sapphire crystal with defined entry and exit sides. This crystal is very similar to one used in a laser built by Dr. Lomsadze a few years ago, which had a positive chirp of 170 fs^2 . The crystal essentially serves as a 3-dimensional target at the focal point of our three cavity focusing elements (focus lens and two curved mirrors). Precision alignment of the crystal is required to successfully build a working cavity laser. We achieve this alignment using a precision translational stage (part number).

5.3.4 Curved Mirrors

Two Layertec, Pump Mirror 103469, 12.7 mm diameter, curved mirrors are used to reflect light emitted by the crystal. The mirrors (see Fig. 5.2) have focal lengths of 15 mm and are used to focus light within the cavity back and forth through the crystal. Each of the curved mirrors contributes (-70 fs^2) of negative chirp to offset dispersion effects from the crystal, yielding a total negative chirp of -140 fs^2 .

The curved mirrors reflect $> 99.7 \%$ of light in the 720 - 980 nm near-infrared region, while letting $> 99.9\%$ of the pump beam (532 nm) pass through. This is important because the pump beam needs to pass through the first curved mirror to reach the Ti:Sapphire crystal.

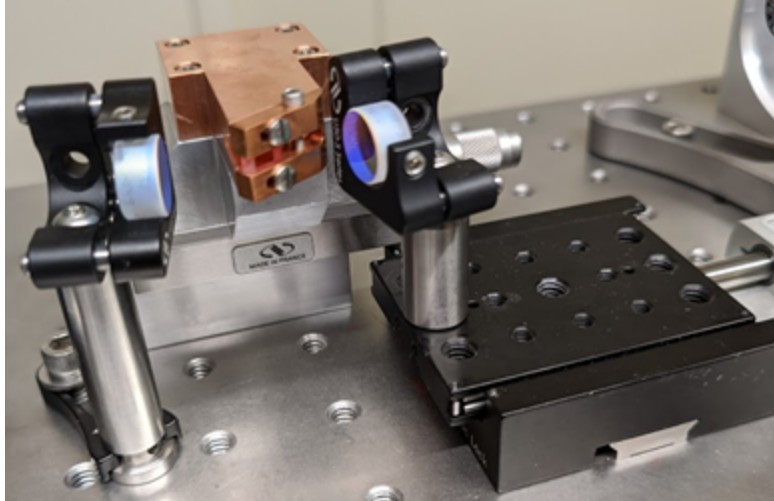


Figure 5.2: Curved mirrors within cavity. Each mirror is placed 15 mm (one focal length) away from the The Ti:Sapphire crystal (shown here in its OFHC copper heat sink mount).

The curved mirrors are aligned at an angle of 9.8° with respect to the optical axis (see Fig. 5.3). This configuration is used to compensate for astigmatism. The method used to calculate the desired angle is called astigmatism compensation and is dependent on the radius of curvature of the mirror, refractive index of the crystal, and the path length inside the crystal [11].

One of the two curved mirrors is mounted on a linear stage that will eventually be controlled using a PID system (not yet implemented). The PID will account for cavity length drifts and will attempt to compensate for repetition frequency changes.

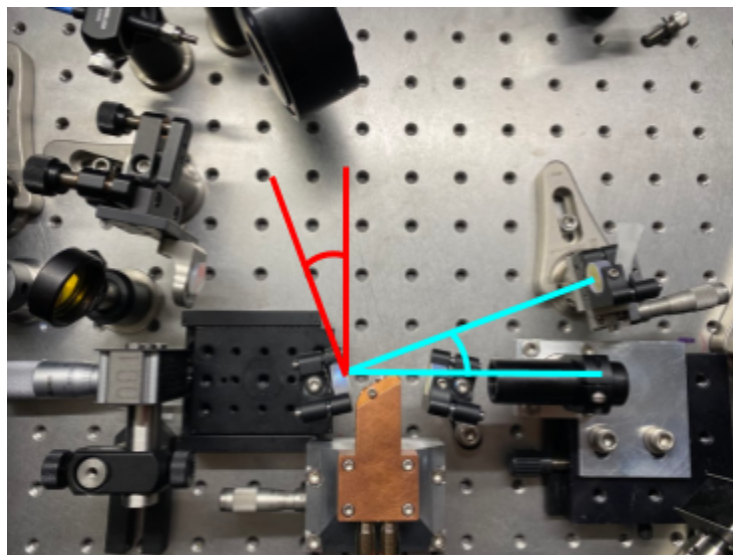


Figure 5.3: The curved mirrors are angled at 9.8° with respect to the optical axis to compensate for astigmatism (half of 19.6° astigmatism compensation angle).

5.3.5 Output Mirror

The output mirror, a Layertec Output Coupler 110371, is a flat mirror that reflects 99 % of infrared/red light between 700 nm and 900 nm. The remaining 1% of light within the cavity passes through the mirror. The mirror is 1/2" (12.7 mm) in diameter.

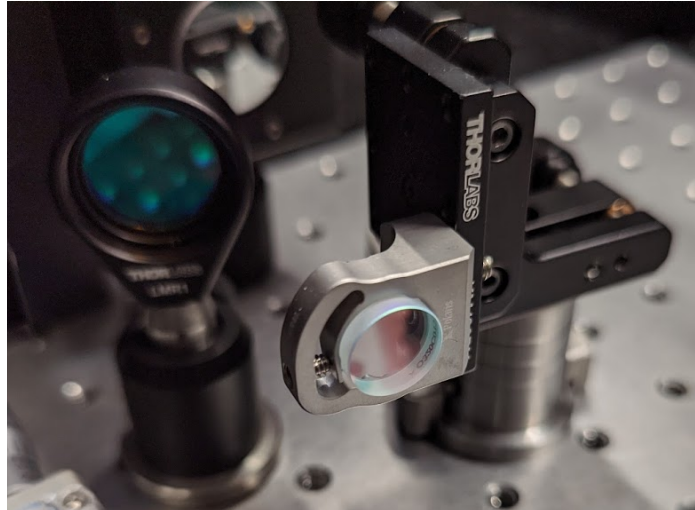


Figure 5.4: Output mirror in mirror mount.

5.3.6 Chirped Mirror

The chirped mirror, a Layertec Laser mirror 141243, is a flat, 1/2" (12.7 mm), >99.9% reflective between 725-875 nm, and provides 40 fs² of negative chirp.

5.4 Cavity

The optical components described above meet all design requirements. Within the cavity, one of the two curved mirrors allows light from the pump laser to enter the cavity and then the two curved mirrors together focus and reflect light from the Ti:Sapphire crystal back into the crystal continuously. A single (flat) output mirror lets ~ 1% of the light within the cavity pass through the mirror and exit the cavity. A final flat chirped mirror is then used to complete the bowtie design.

In total the total positive chirp from the crystal and the output mirror is between +180 & +190 fs². The cavity components have been chosen to compensate for this positive chirp and the combination of the curved mirrors and the flat chirped mirrors provide -180 fs². If the cavity is not properly compensated for the effects of chirp, then mode-locking becomes significantly more difficult. The negative chirp compensation provided by the mirrors is only valid for a specific spectral region (700-900 nm). This value provides an upper limit for maximum bandwidth of the system.

5.5 Post-Cavity Components

Initially, our system was designed such that one of our output beams exited at an angle. This configuration is not ideal for power level testing. To solve this, mirrors were placed after the four-mirror cavity to redirect the beam and allow it to exit in a straight line (see Fig. 5.5).

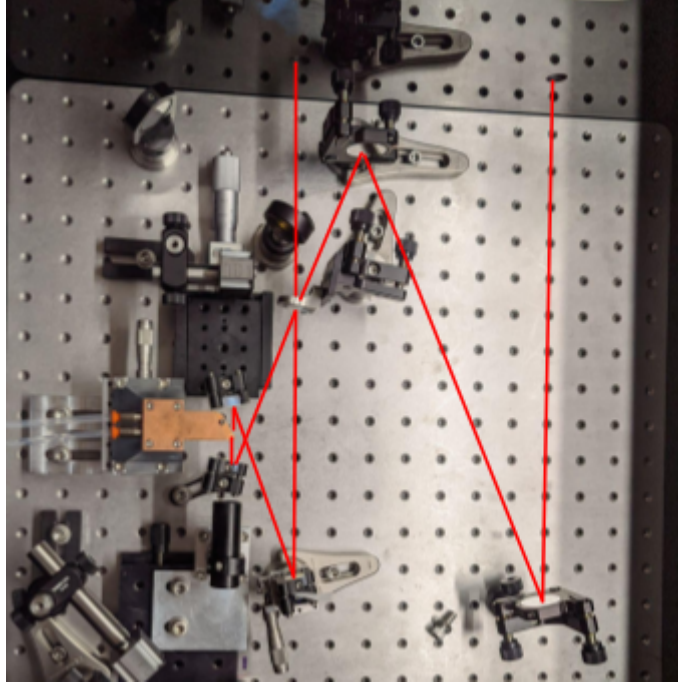


Figure 5.5: Extra pair of mirrors. These were used to redirect the diagonal cavity output beam into a straight line, enabling accurate power level tests of both exit beams from outside the main cavity container.

Chapter 6 Thermal Regulation

6.1 Overview

The thermal control subsystem is required to keep the crystal at a constant temperature. The product is expected to maintain a lasing state over many days, and inconsistency in temperature jeopardizes this by affecting the size and efficiency of the crystal, through thermal expansion and temperature reliant quantum efficiency, respectively. It is important to implement heat removal that ensures constant crystal temperature. Recall that the crystal has an input pump laser power of around 6W. This was used as a limit of input heat power, a vast but satisfactory overestimate of the actual power that needs to be dissipated. Shirakov *et al.* provided experimental fluorescence efficiency values based on Ti:Sapphire crystal temperature. A temperature of 300 K was around 70% efficient while a temperature of 350 K was as low as 50% efficient[12]. The complete fluorescence efficiency chart can be seen in Fig. 6.1. Most of the input beam is converted to fluorescence instead of heat.

It is not desirable to do a fan cooled system on the crystal since this will cause unnecessary vibrations.

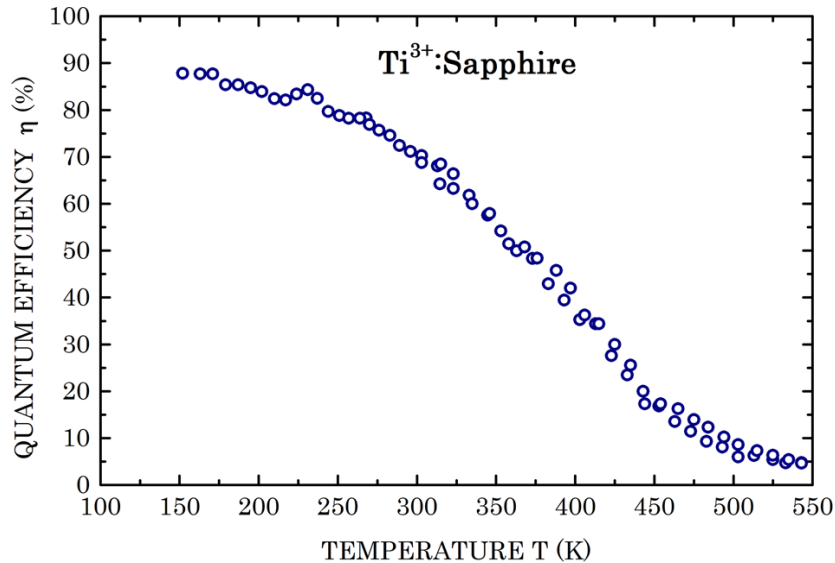


Figure 6.1: Quantum emission efficiency of a Ti:Sapphire crystal.

Shirakov, A., Burshtein, Z., Shimony, Y., Frumker, E., and Ishaaya, A., 2019, “Radiative and non-radiative transitions of excited Ti^{3+} cations in sapphire,” *Scientific Reports*, 9(18810), pp. 1-9.

<https://doi.org/10.1038/s41598-019-55267-8>

<http://creativecommons.org/licenses/by/4.0/>

This image has not been modified.

6.2 Requirements

The major factor at play when considering a cooling system within a laser cavity is for it to be as non intrusive as possible. The crystal needs a clear emission path to its

coupled mirrors. The crystal must also be fixed securely by its mount such that the crystal's position and orientation are not affected by vibration. It is critical that the crystal's position remain constant through all operations of the laser, as any slight adjustments in crystal position will very likely result in the misalignment of the cavity. Metrics for the crystal cooling system are included in Appendix B.1.2 under crystal temperature.

6.3 Design

The heat sink design was specifically designed to be non intrusive within the cavity. An image of the heat sink is included in Fig. 6.2 below. Access to the crystal is provided by a clear area in the form of a horizontal slot. The heat sink tip was manufactured in the shape of a triangle. This was because one of the curved mirrors needed to be relatively close to the heat sink to achieve design requirements for the curved mirror. A triangle cutout was deemed appropriate for making sure that the curved mirror would not hit the heat sink.

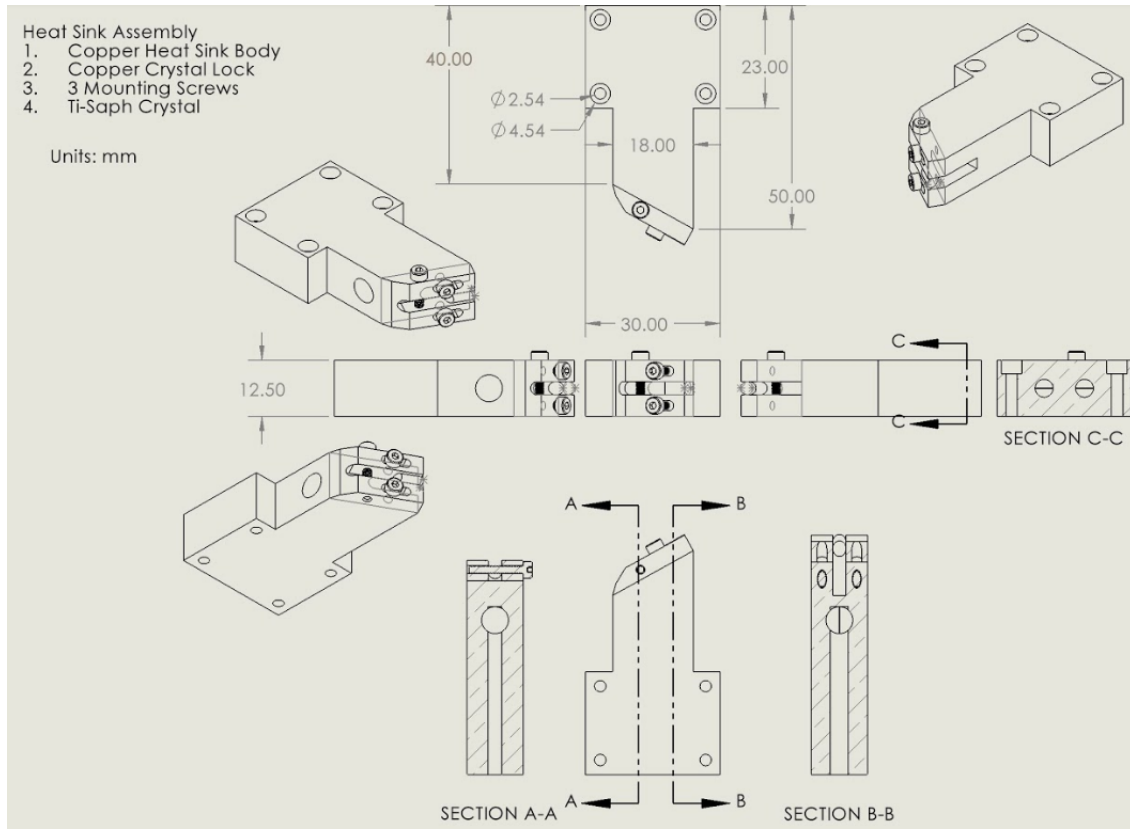


Figure 6.2: Heat sink subassembly drawings. Designed in metric, the various views show the clamping mechanism for the crystal, one vertical screw passing through the custom 29.6° U-clamp, as well as the two screws to fix the mount onto the OFHC copper heat sink, the four through holes for mounting the heat sink, as well as the bored channels for cooling

The material of choice for the heat sink was oxygen free high conductivity (OFHC) copper. The heat sink includes a machined channel to provide chilled-water cooling. Two long semi-tapped holes were first machined into the back of the heat sink. A side channel was then drilled into the heat sink to connect the two channels. A circular plug was then soldered into the side to close off the hole. The design provided a simple, machinable water channel for fluid to be pumped through the heatsink. Four screw holes for mounting were then drilled into the base of the heat sink. A detailed drawing of the heat sink is provided in Appendix D.1.

Figure 6.4: Close up of heat sink cross section. Bored water channels increase heat dissipation.

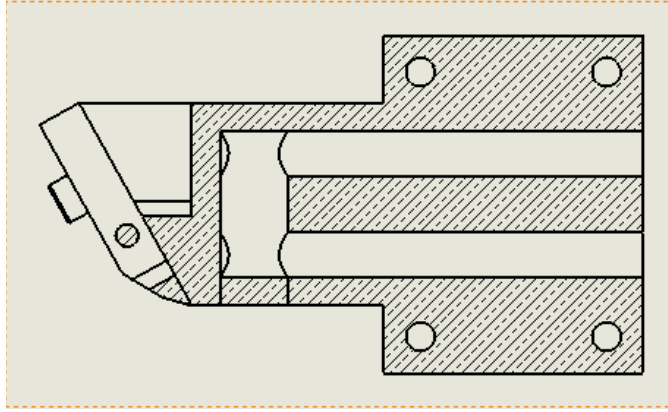
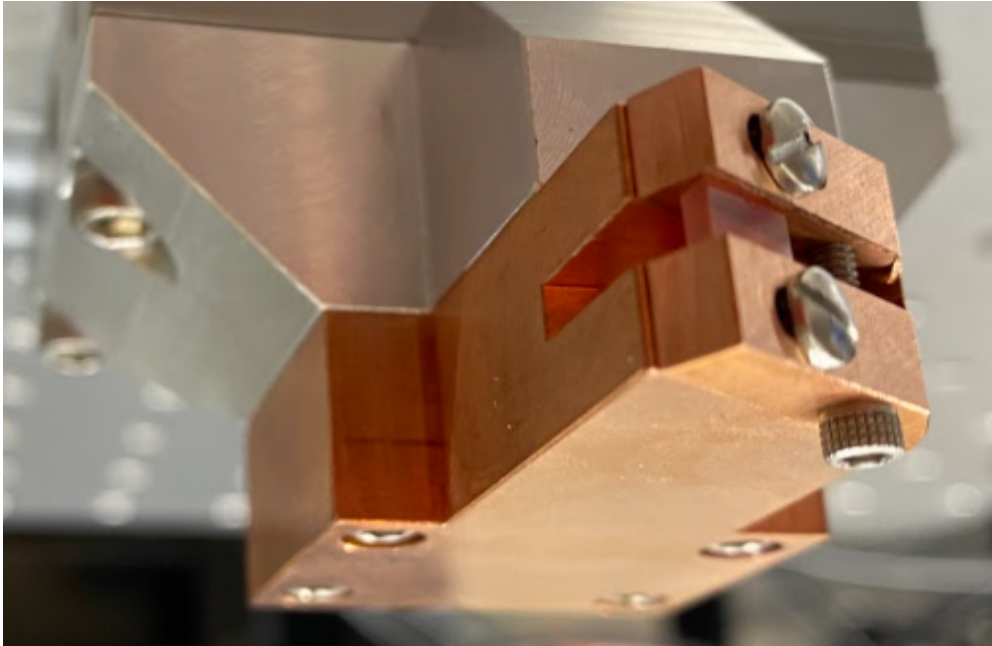


Figure 6.3: Ti:Sapphire crystal mount and heat sink. The top screw provides sufficient clamping force onto the crystal. Further mounting to the sloped spacer and linear stage.



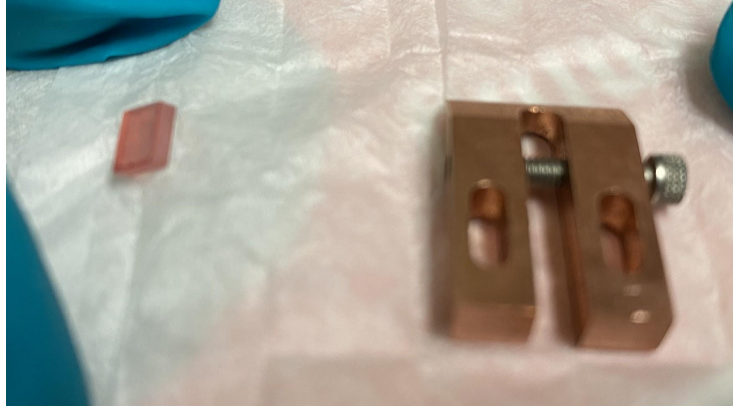


Figure 6.5: Crystal clamp (right) with Ti:Sapphire crystal (left). The crystal clamp includes a tightening mechanism.

The crystal clamp was manufactured from the same OFHC copper as the heat sink and utilizes a U shape design to clamp down on the crystal. A detailed drawing of the crystal clamp is provided in Appendix D.1. A tightening screw is placed on top to ensure that the crystal does not move during the lifetime of the product. Two screws are then tightened to the face of the main heat sink block. Thermal paste was deemed risky, and was only applied at the junction of the copper block and aluminum slanted mount, where it was at no risk of coming into contact with the crystal. The thermal contact conductance in air was taken from the textbook, *Heat and Mass Transfer*, in which the copper-to-copper interface for milled copper is $h_c=55,000 \text{ W/m}^2\text{K}$ [13]. Subsequent thermal paste research found products which list a thermal impedance of $.01 \text{ C-in}^2/\text{W}$ ($155,000 \text{ W/m}^2\text{K}$). The 3x improvement over the already high conductivity of a copper to copper interface was deemed insufficient to warrant the risk.

6.3.1 Tubing Setup

The inlet and outlet ports of the heat sink were tapped so that standard threaded quick-connect adapters could be used to easily connect and disconnect cooling water tubes to the body of the heat sink. Fig. 6.6 and 6.7 shows the finished product with flow control.

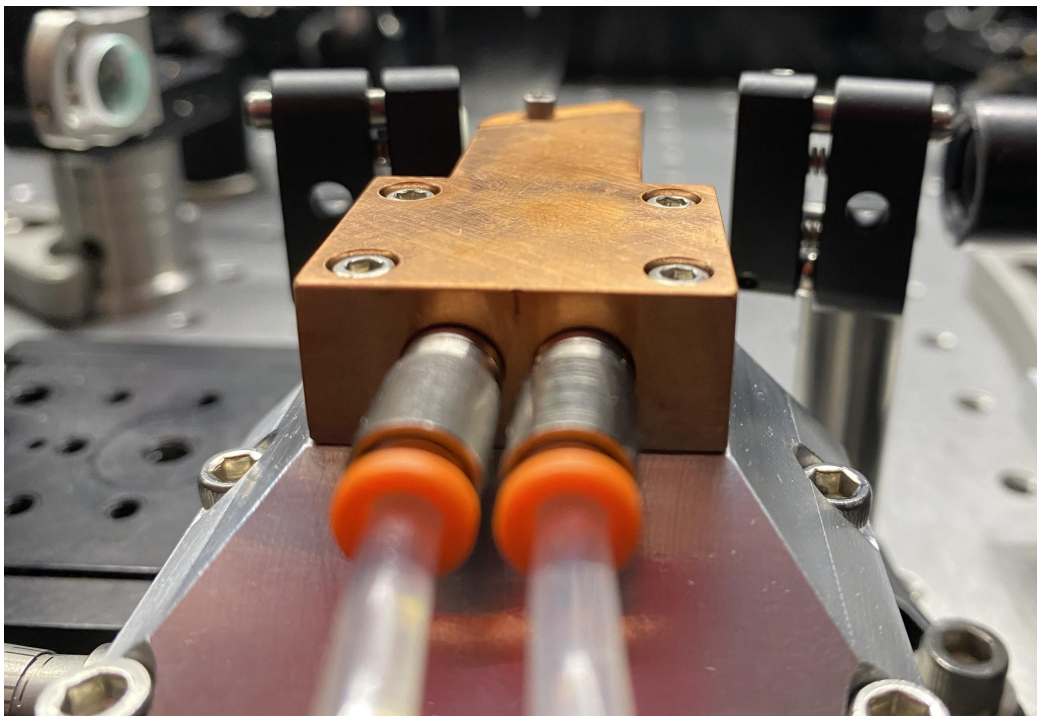


Figure 6.6: Tubing setup for heatsink.



Figure 6.7: Flow regulator which controls the flow to the heat sink.

6.3.2 Flow Source

Cooling water for the heat sink is provided by the pump laser chiller which circulates ambient temperature water at a flow rate of 0.5 L/min. (See Fig. 6.8) In previous systems, the main output of the chiller was used to keep the pump laser at near room temperature, but with the addition of a flow regulator and appropriate tube adapters (see Fig. 6.7), the system can now be used simultaneously with the 12 W pump laser and two small laser cavities (our new one and a similar unit built two years ago). Each apparatus gets $\sim \frac{1}{3}$ of the total flow, or 0.17 L/min of a water isopropyl alcohol

mixture at near ambient temperatures(90% water). The pump laser has a shutoff system that will shut the laser off if the pump laser experiences insufficient cooling. The next section includes a summary of calculations that show our OFHC heatsink receives adequate cooling, given the design choices.



Figure 6.8: Sprout G pump laser power supply and liquid cooling pump (chiller).



Figure 6.9: Junction for fluid pump that directs 0.17 L/min of cooling fluid to the OFHC heatsink of our Ti:Sapphire laser crystal.

6.4 Analytical Solution

The heatsink plays a vital role in mounting and orienting the crystal, but it also must provide adequate heat transfer out of the crystal. The assumed thermal load condition is that the crystal is receiving 6 Watts of thermal power, ignoring the significant portion that in reality gets emitted as light.

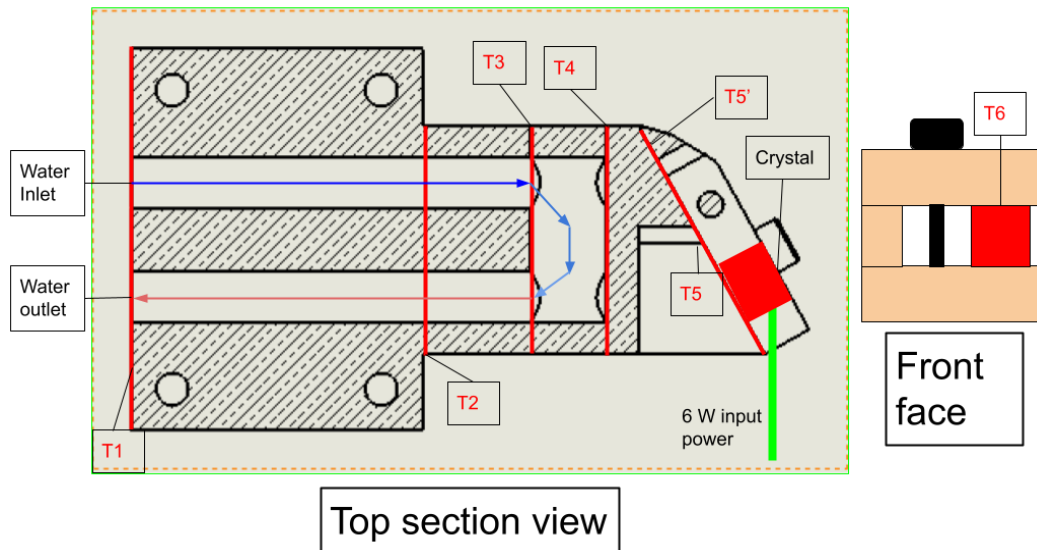


Figure 6.10: Heat sink labeled according to thermal sections based on most significant heat transfer.

The general approach to finding if the heat sink meets the design requirements was to break the problem down into sections of simplified geometry. Elements that are closer to the crystal were expected to have significantly more heat transfer variability and thus were broken down into smaller components. Sections that had complex geometries such as the front of the heat sink were instead estimated to be a rectangular shape of similar size. For this problem, all screws and holes were ignored. It is also expected to operate at a steady state. For this problem, heat transfer from radiation will largely be ignored because it is expected that the temperature difference between the heat sink surface and the ambient surroundings is not significant. Research into the thermal contact resistance between the Ti:Sapphire crystal and copper is not well studied and thus will be ignored for this calculation.

To solve for the temperature of the heat sink, the resistance model was used to calculate the heat transfer from one section to the other. The initial assumption of splitting the heat sink into sections such that a thermal resistance network can be calculated requires that the problem is a one dimensional heat transfer problem [13]. The conditions in which the heat sink operates has little airflow due to the containment box which will close off the cavity. It is expected that the internal flow from the water flowing through the heat sink has a significantly greater amount of heat transfer

compared to the heat transfer from natural convection. The material of choice is OFHC copper which has a thermal conductivity which ranges from 386-394 W/m K [14]. It is believed that the initial assumption of one dimensional heat flow is valid due to the high thermal conductivity and low heat transfer from the external surface. Equations for the thermal resistance model are included in Table 6.1 below.

Table 6.1: Resistance method of analytical heat transfer.

	Heat transfer equation	Thermal Resistance
Conduction	$\dot{Q} = \frac{kA_c(T_1 - T_2)}{L}$	$R_{\text{cond}} = \frac{L}{kA_c}$
Convection	$\dot{Q} = hA_s(T_1 - T_2)$	$R_{\text{conv}} = \frac{1}{hA_s}$
Contact Resistance	$\dot{Q} = h_c A_c(T_1 - T_2)$	$R_{\text{tc}} = \frac{1}{h_{tc} A_c}$

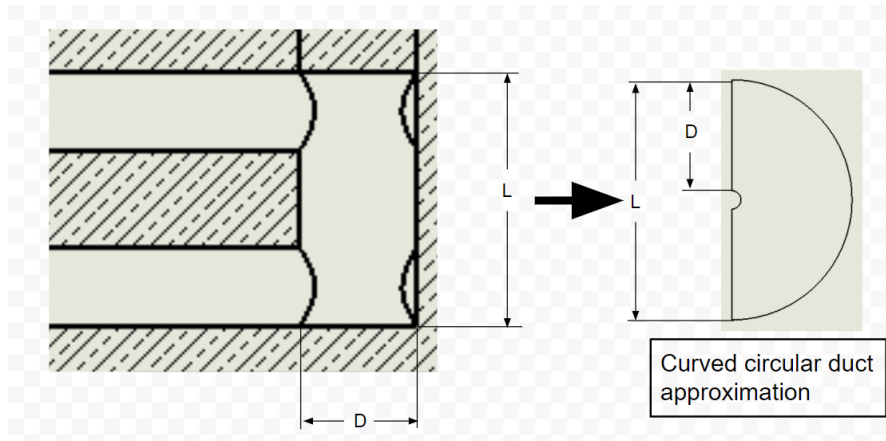


Figure 6.11: Water pipe approximation. The tube was approximated as a curved circular duct for the purpose of a heat transfer calculation.

The final assumption which was done to calculate the heat transfer for the heat sink was a curved circular duct approximation. The heat sink was designed for machinability, and specific flow behavior through the heat sink was not a major consideration in its design. An appropriate model was not found for its particular configuration. However, an analytical solution of laminar flow heat transfer has been explored of a similar heat exchanger in which a curved circular duct is used [15]. This model is not an exact representation of the phenomenon that occurs within the heat sink

and a CFD model will need to be used to confirm the analytical solution discussed below.

The liquid pump that is used in conjunction with the heat sink is expected to pump at a rate of 0.17 kg/min. The pump also includes a chilling system in which water is expected to leave the pump at 20°C or ambient temperature. Initial design requirements indicate that the crystal temperature should reach the ambient temperature for increased fluorescence efficiency as well as more stable mode locking.

The titanium sapphire crystal has a relatively high thermal conductivity but heat is expected to build up within the crystal itself. The supplier of the Ti:sapphire crystal indicated that the crystal has a thermal conductivity of 33 W/m K [16]. It was assumed that the 6 Watts will be evenly distributed as an internal heat generation which is lased in through a pump laser. The dimensions of the crystal are 3 by 5 by 5 mm. The team is interested in the peak temperature within the crystal. It is expected that very little natural convection occurs on the crystal and thus the crystal will be modeled as a one dimensional heat transfer problem in which the crystal is mounted on top and on bottom. It is expected that all of the heat is to transfer through the copper clamp interface which holds the crystal.

Analytical Results:

All calculations can be seen in Appendix A.2. All properties for water/air/copper were found in *Heat and Mass Transfer* [17]. Given that the flow rate through the system is 0.17 kg/min of water, the Reynolds number through the heatsink is 1377 which is less than the cutoff Reynolds number for laminar flow through a tube which is 2300 [18]. The analysis below includes methods for finding the Nusselt number for each section of the heat sink. The Nusselt number was used to find the heat transfer coefficient using the equation below. The heat transfer coefficient can be used to calculate the thermal resistance values for each section as described in Table 6.1 above.

$$Nu = \frac{hL}{k}$$

Section 1:

Natural Convection

When finding the natural convection of an object, the Rayleigh number needs to be calculated. The Rayleigh number equation is included below[19]. The Rayleigh number describes the relationship between buoyancy and thermal diffusivity. The driving force behind natural convection is buoyancy and temperature shifts which causes heat from the surface to transfer to the surrounding air. The hot air then rises which gets replaced with cold air.

$$Ra_L = \frac{g\beta(T_s - T_\infty)L_c^3}{\nu\alpha}$$

The Rayleigh number is dependent on the coefficient of volumetric expansion for an ideal gas which is included below[19].

$$\beta = \frac{1}{T_{avg}}$$

Additionally, the characteristic length must also be used to find the Rayleigh number and Nusselt number. The characteristic length for rectangular plates is included below; An additional table was also used to find characteristic lengths on page 564 [19].

$$L_c = \frac{A_s}{p}$$

The Rayleigh number can be used to calculate the Nusselt number for horizontal and vertical plates as seen by the equations below [19]. The Rayleigh number for many of the horizontal plate sections were below the range for the equation listed in Table 6.2. The team assumed a worse case scenario that conduction was the main source of heat transfer between the horizontal section and the environment.

Table 6.2: Nusselt number formulas for each plate.

Vertical Plate	$Nu = \left\{ .825 + \frac{.387Ra_L^{\frac{1}{4}}}{\left[1 + \left(\frac{.492}{Pr}\right)^{\frac{9}{16}}\right]^{.8/27}} \right\}^2$	For all Ra_L
Horizontal Plate	$Nu = .54Ra_L^{\frac{1}{4}}$	For Ra_L 10^4 - 10^7

Forced Convection

For laminar flow, forced convection through a circular tube with fully developed flow, the Nusselt number is a constant. It is expected that the heatsink has 1-D heat flow through the heatsink. A constant heat flux model was chosen for convection through the tube. The Nusselt number is 4.36 for fully developed laminar fluid flow through a tube with constant heat flux[18].

Conduction

The thermal resistance value was calculated using the contact area of the section, length, and heat transfer coefficient. The equation for the thermal resistance from conduction is included in Table 6.1 above.

Section 2:

Section 2 is similar to section 1 but the geometry of the section has changed. All techniques used in section 2 are described in section 1.

Section 3:

Natural Convection

Methods match those described in section 1.

Forced convection

As mentioned above, a curved circular duct approximation was used to achieve an analytical solution. The equations for the Nusselt number for flow within a curved circular duct is included below[15].

$$Nu_c = \frac{.864}{\zeta} K^{\frac{1}{2}} (1 + 2.35 K^{-\frac{1}{2}}) \quad \begin{array}{l} K > 30 \text{ for } Pr \gg 1 \\ \text{and} \\ K > 60 \text{ for } Pr \approx 1 \end{array}$$

$$\zeta = \frac{2}{11} \left[1 + \sqrt{\left(1 + \frac{7}{47} \frac{1}{Pr^2}\right)} \right] \quad \text{For } Pr \geq 1$$

The Dean's number, or K , in the Nusselt number calculation listed above is a correction value to the Reynolds number for the effects of curvature; the equation is included below [15]. a is the radius of the pipe and R is the radius of curvature for the curved pipe.

$$K = Re \sqrt{\frac{a}{R}}$$

Conduction:

Methods match those described in section 1.

Section 4:

Section 4 was simplified through a change in geometry. A square of similar surface area and volume was used to replace the shape of section 4. The change in geometry can be seen in Fig. 6.12 below. Additionally the calculation for this section is included in Appendix A.2.

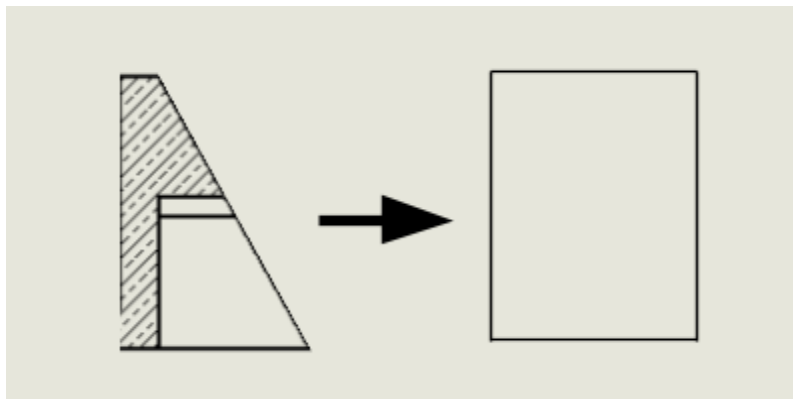


Figure 6.12: Section 4 simplified geometry. The trapezoidal shape was approximated as a rectangle with similar volume/surface area.

Natural Convection

All methods used to find the Nusselt number from natural convection are described in section 1 under natural convection.

Conduction

All methods used to find the thermal resistance from conduction is described in section 1 above under conduction.

Section 5:

Section 5 is similar in technique to section 1.

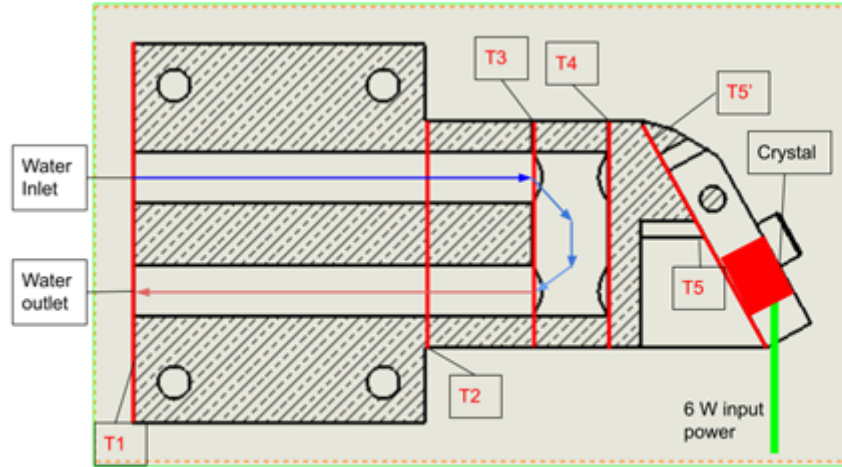


Figure 6.10: Repeated for reference.

Table 6.3: Heatsink resistances values calculated ($Wm^{-1}k^{-1}$).

Section	Resist. Water Conv	Resist. Air Conv	Resist. Cond
1-2	2.678	278.1	.17
2-3	8.99	1240	.089
3-4	1.423	1479	.104
4-5	N/A	1750	.098
5-5'	N/A	N/A	.089
5-6	N/A	456.85	.05

A summary of the heat sink resistance values is included above. All calculations are included in Appendix A.2. The results of the analytical calculations indicate that a significant amount of heat transfer occurs from the water flow due to its low resistance values. As expected, the conduction and contact resistances were significantly less than 1 which indicates that heat transfer through the heatsink is not a bottleneck for the system. Another discovery from this calculation indicates that a significant bottleneck occurs between the surface and the surrounding air. Very little heat is able to be exchanged with the environment through natural convection/conduction due to the high resistance values. The high resistance values for the analytical solution were largely ignored.

The majority of the heat is exchanged through internal forced convection through the water pump system. It thus seems reasonable that the initial assumption of one

dimensional heat transfer is likely valid for section 4 and 5. Significant heat transfer occurs in section 3 due to the high surface area as well as the change in flow conditions in which a full turn is achieved within the heat sink. A CFD model was used to confirm the interaction in section 3.

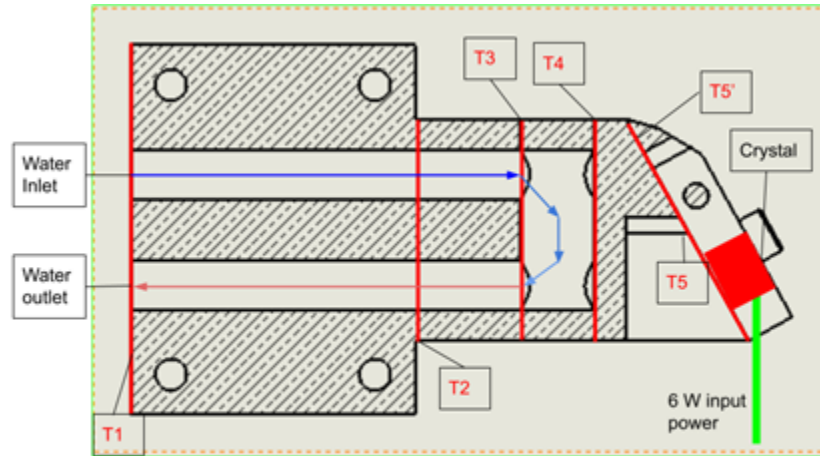


Figure 6.10: Repeated for reference.

Table 6.4: Temperature change at each location in heat sink assembly.

T1:	T2:	T3:	T4:	T5:	T6:	Center of crystal
4.7°C	5°C	5.2°C	5.8°C	6.9°C	7.2°C	11.7°C

Using the network resistance model, the surface temperature of the crystal can be easily computed using the resistance values found earlier. A system of equations can be created from each section and the initial heat transfer rate of 6 Watts is the total heat transfer that occurs in the system. Solving the system of equations indicates that the surface temperature of the crystal should reach a temperature of 7.2°C above room temperature. Using the one dimensional internal heat generation model indicates the crystal's maximum temperature difference is expected to be 11.7°C, directly in the center of the crystal. This indicates that the heat sink satisfies the design requirements.

This calculation is a significant overestimate of what occurs in operation of the cavity. Overall, the analytical solution indicates that the heat sink is able to achieve its design requirements with a significantly large factor of safety for expected operating conditions due to the 70% fluorescence efficiency.

6.5 CFD analysis

A CFD model was also created in conjunction with the analytical calculations to ensure that the heat sink configuration reached the desired design criteria, and was created in Simcenter Star CCM+ using Siemens PLM software. The version number

used was 2020.2(15.04.008-R8). The CFD model serves as a comparison between the two models.

The model was generated with two meshes, one mesh for the fluid flow and another for the rest of the heat sink. The internal flow mesh contained 90,000 cells and the rest of the heat sink had 260,000 cells. As mentioned above in the analytical calculations, the Reynolds number for the flow through the pipe was calculated to be 1377. A laminar flow simulation was done on the heat sink. Additionally, the physics models used for the simulations were coupled energy, steady, constant density, and three dimensional liquid flow. The liquid is water at 293 K or ambient temperature.

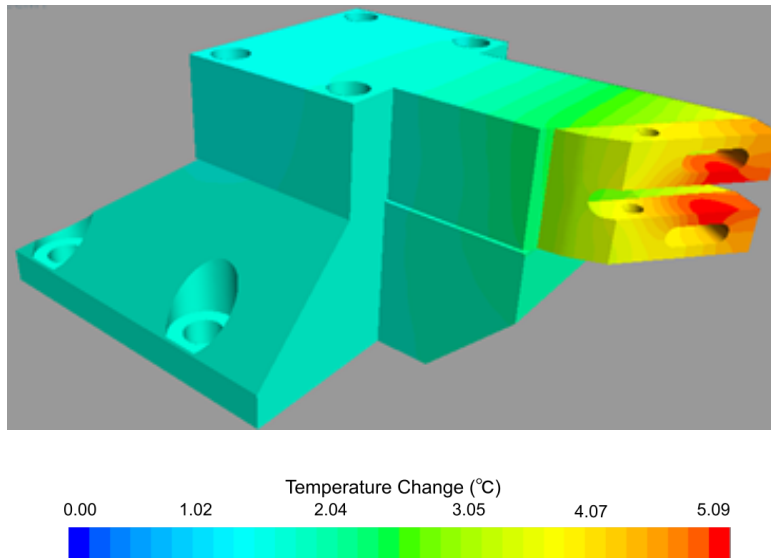


Figure 6.13: CFD temperature gradient graph solution of heat sink model. OFHC copper heat sink & mount, and slanted aluminium mount are shown.

The maximum surface temperature of the model occurs where the crystal is clamped to the heat sink. The maximum temperature indicated by the model is 5.09°C which is a 2°C decrease from the analytical calculations.

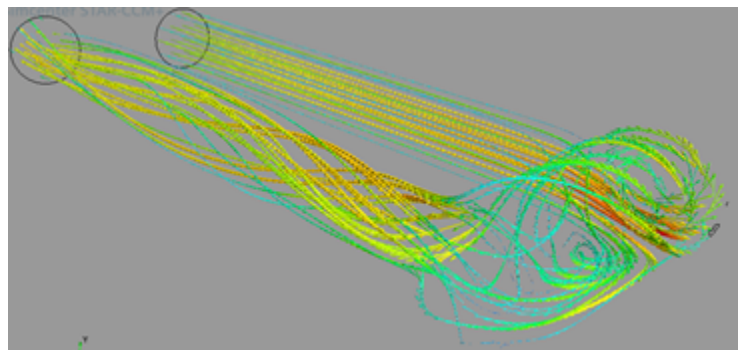


Figure 6.14: CFD solution streamlines for internal flow within the heat sink.

The analytical calculations likely underestimated the heat transfer which occurs in section 3. The transition from section 2 to section 3 is likely more complex than the proposed curved circular duct approximation which was used in the analytical solution. Complex behavior occurs within region 3 which can be seen in Fig. 9 in which streamlines are shown. Flow congestion occurs in which the fluid speed is slowed to 0.1 m/s as the flow exits region 3. This is significantly slower than the initial speed of 0.225 m/s from the fluid that enters the heat sink. The CFD model serves as an indication that the initial assumptions were likely not correct for the problem at hand. Residuals and stabilization of the CFD model are included in Appendix A.3.

6.6 Thermal Performance Verification

Test plans for confirming the analytical and CFD model were planned, but have proven unnecessary. The plan was to confirm these calculations by using an infrared thermometer. It was not desirable to attach a thermocouple to the heatsink since the heat sink will need to be damaged to adequately attach the thermocouple lead into the heat sink.

Instead, the team plans to paint the heat sink black so that an adequate thermal test can be conducted using the infrared thermometer. The black paint will allow the heat sink to act close to a black body. The team will then run the laser for 10 minutes at max power (6 W). The 10 minute wait period is for ensuring that the heatsink has reached thermal equilibrium. The team will then shut off the laser and conduct the test immediately. The readings will allow the team to back calculate the temperature at the measured point. The team will conduct the test at the points of interests which are highlighted in the analytical solution of the heat sink in section 6.4.

The team cannot conduct the test while the laser is running due to the large amount of infrared light which is generated by the Ti:Sapphire crystal while in operation.

6.7 Problems and Revisions

A key system issue that is related to using a liquid controlled heat sink is that it is likely causing mild, unnecessary vibrations distinctly close to the crystal. Although no calculations have been made to justify this issue, future plans to quantify and fix this issue are being considered.

A peltier cooling system would likely be used to replace the fluid cooling system if deemed necessary. The peltier cooling system would provide high efficiency and low vibrational problems given that it can adequately dissipate heat with natural convection. Forced convection can provide unnecessary sources of vibrations which is not ideal for a sensitive system.

Chapter 7 Manufacturing and Preliminary Assembly

7.1 Overview and Requirements

All of the parts described in this section were designed by our team, and manufactured throughout the project in the SCU machine shop in collaboration with University machinists. The material and manufacturing costs were therefore disregarded.

7.2 Materials Selection

Materials selection was driven by application and manufacturability, as well as referencing materials typically used in this application. Additionally, the relative rigidity and thermal performance of each of the materials was used to decide which material would be used for each part. Due to the importance of optic height, vertical components such as posts were made out of Stainless steel, while shorter ones like spacers and mounts were manufactured out of aluminum.

7.3 Stainless Steel

7.3.1 Posts

303 stainless steel rods were the number one choice in optimizing components in the vertical dimension. Besides the good thermal performance, the relative hardness ensured that the components mounted to them would remain stable. In total, seven 303 stainless steel posts were manufactured, all within one thousandth of an inch of desired height, in addition to obtaining optimum finish on bottom, top, and flange surfaces to ensure ideal mounting behavior.

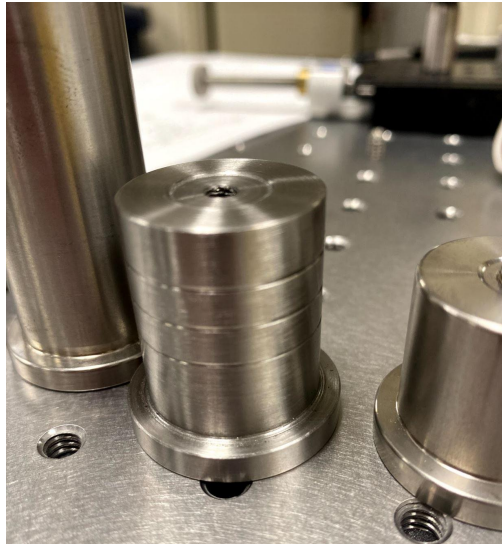


Figure 7.1: Custom machined post for output coupler mirror. Finish difference is minimally noticeable, and it includes a replicated counterbore to standard mounts, which help prevent rocking

7.4 Aluminum

The aluminum grade used for this project was mostly 6061 aluminum because of its availability and ease of manufacture. Through concerted efforts, and careful methodology, guided with the use of Mitutoyo Micrometers, even the bowing behavior (when mounted in a mill vice) of rolled aluminum was minimized, sometimes under an impact of 1.5 thousandths across 2-3" of material.



Figure 7.2: Aluminum during manufacturing, which was used to make all the breadboard clamps.

7.4.1 Spacers

Spacers were essential to mounting many of the linear mechanical stages, as the standardized 1" grid of the breadboard would not directly interface with the various types of components that made up the central cavity. In other cases, spacers were required to mount components with different size screws, or to produce a fixed displacement between components in the assembly. Manufacturing consisted of mostly end mill work.

7.4.2 Periscope

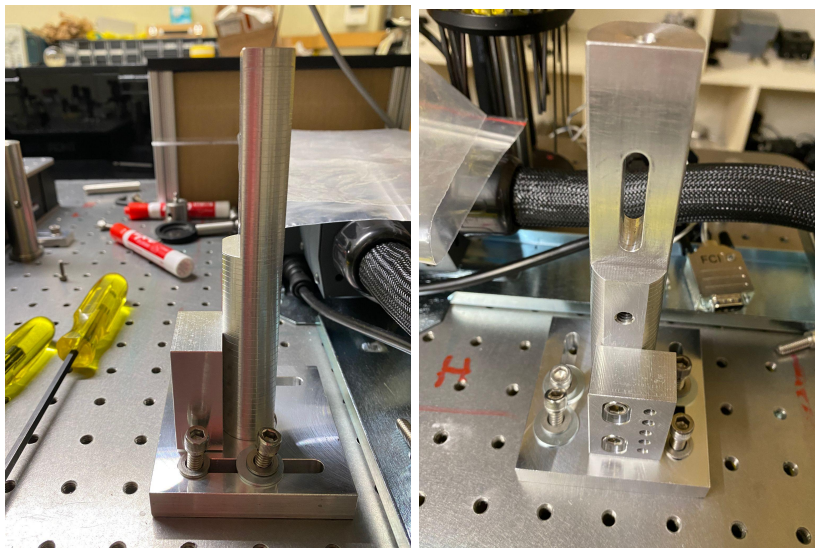


Figure 7.3: Periscope (side and front view).

The Periscope became necessary when it was realized that the standard periscopes available in the equipment section of the laser laboratory were nowhere near rigid enough, nor sized appropriately for the important role they had to play in ensuring the pump beam rises to the level of the crystal. The new periscope's structure is completely immunized from accidental and even strong purposeful tampering.

7.5 Acrylic

$\frac{1}{2}$ " thick, fully opaque acrylic was chosen as our containment material of choice, because a device within the lab was already using it, and it proved substantially rigid, and though difficult to work with, could be precision machined and hold strong at the joints upon applying plastic cementing fluid.

7.5.1 Cavity Containment

As can be seen in Fig. 7.4, the aforementioned material now forms a 19" by 19" by 10.5" (48.26 cm by 48.26 cm by 26.67 cm), one-half inch thick stay-hinge-lid container for operation, manipulation, but maximum safety when operating the main laser cavity.

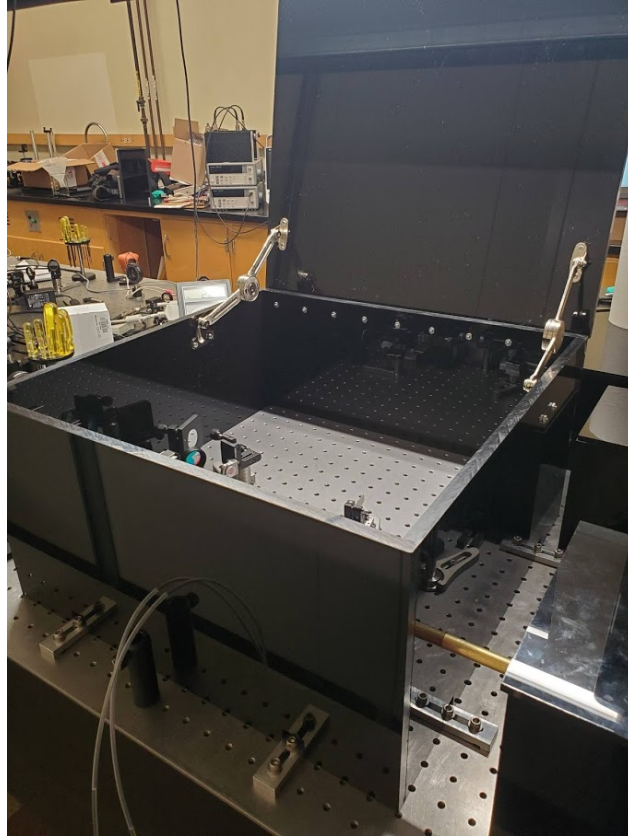


Figure 7.4: Stay-hinge-lid container.

7.5.2 Periscope Containment

Made of the same fully opaque acrylic, the periscope connects the two major acrylic safety containers, with precision bored holes for the brass tubes that encase the beam as it passes through the path from the pump laser to the Ti:Sapphire cavity.

7.5.3 Other Improvements

Because of a technical error, we ended up with an excess of acrylic, and found an excellent use for it. It not only supplied the material used for the periscope, but the additional acrylic enabled us to upgrade the containment of the pump beam from a rough cardboard construction to a rigid and much more stable, airtight acrylic containment, that also unified the appearance and containment method of the laser sources on the optics table.

7.6 Screws

Besides using standardized screws, the project also used various machine tools to shorten screws to ideal lengths needed for the various components that had non-standard thread depths. This was done by grinding and sanding the tips of screws until the desired length was achieved.

7.7 Timeline considerations

The accelerated manufacturing timeline became a necessity with the late access to the machine shop, and a vast majority of the weeks consisted of machining every weekday. Alongside this intense demand for progress, implementation of parts was often done same-day, or on weekends, to provide adequate time to verify successful components, plan further components, or continue laser assembly and alignment progress. .

Chapter 8 Laser Alignment and Results

8.1 Overview

Throughout this report, mentions and specific comments on alignment are interspersed. The purpose of these is to provide context when appropriate to clarify as best as possible the ‘big picture’ of this project. In this chapter, the various stages of aligning, including further detail and interconnectedness, are included in the order that they were relevant to successfully completing the DCS Laser, including Dual Comb Mode Locking.

Upon completion of the assembly, alignment procedure was outlined as: align the final two 1” silver mirrors in the order in which the beam strikes them, align the 4 cm focusing lens, place the crystal in an approximately correct position, install the 4 mirrors in starting positions, and work on the laser cavity itself; this final step will be broken down further.

8.2 Challenges & Solutions

Achieving mode locking is in general a much more rigorous process than any other mirror aligning undertaken throughout this project. In the long run, meticulously aligning optics along the pump path greatly benefitted the rate of success during the more challenging lasing and mode-locking phases, and began with directing the pump beam on the optics bench. Besides reflecting as close to the center of mirrors as possible, the critical area of alignment consideration at this stage was the periscope(see fig 8.1). Specifically, any imperfections in the horizontal direction before the periscope, which were relatively simple to deal with, became imperfections in the vertical direction after the periscope, which were much more difficult to correct. Eliminating this imperfection was the final critical factor in careful alignment of the 4 initial mirrors, after which the laser was considered “on the breadboard”(see Fig. 3.12).

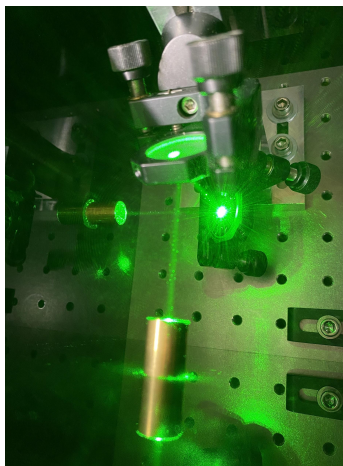


Figure 8.1: Pump beam passing through the periscope.

The final two of the six 1” mirrors that direct the pump beam to the focusing lens are located on the breadboard with the laser cavity. These final two are mounted on the breadboard using the custom posts, such that their mirror centers at the predetermined height of our laser cavity, 2.275”, the centerline of the crystal within. While the beam could have been directed from the final periscope mirror, a slight discrepancy in angle between table and breadboard planes, as well as the simpler fine tuning process and beam safety, all contributed to committing these two final mirrors into the pre-cavity design. Once the beam was determined to be travelling parallel to the crystal from the desired angle and height, the aligning process continues by adding the focusing lens. This ½” (12.7 mm) diameter, 40 mm focal distance lens is central to the success of the infrared laser's functionality. The path of the focused pump beam through the cavity and Ti:Sapphire crystal was the critical feature to align the fluorescence of the infrared photons during lasing in the cavity.

For all initial aligning procedures, and the beginning of the next phase, the power level of the pump beam remained at its minimum of 10mW. This amount was already considered medium eye injury risk, rated Class IIIB. To reiterate, any operation of the pump or the main laser required use of protective goggles. However, at this junction, the beam was about to be powered up further, increasing eye risk, as well as eventually posing a material and skin burn risk(noted when appropriate). The procedure continued by placing the full crystal assembly onto the breadboard and into position.

8.3 Component Placement

Now that we have successfully passed the pump beam into the crystal, it is time to install the four mirrors which complete our laser cavity. Initial placement of these five components roughly determines the eventual repetition rate of the dual comb signal that can be achieved with it. For our cavity, there’s a slight design influence, which suggests that we have a total cavity length of around 40.1 ± 0.3 cm, as well as the angles related to astigmatism prevention, as mentioned in Chapter 5.

8.4 Initial Alignment

The bottom right mirror is the first one to direct attention to, as once fastened, the mirror and post cannot change translationally, and will hardly change rotationally. This is because altering this mirror is incredibly difficult due to its proximity to other components, leaving its Allen screws fairly inaccessible. On top of this its impact on the system is significant if moved, so placing it in a workable position and then not moving it is preferable. As a result, the astigmatism compensation angle and the base position are critical. Because the mirror is in the focal length of the focusing lens, it is best to do this with the pump beam blocked intermittently or completely off for this step, since the concentrating beam can be dangerous. The mirror may change the alignment of the beam into the crystal, but likely to a negligible amount. Once complete it is possible to

continue with the pump laser on once again. The second curved mirror is then mounted in the bottom left position atop the mechanical stage, such that the astigmatism angle is within a few degrees, the distance of between the curved mirrors is around 30 mm, and the green beam passes through the crystal, and strikes near the center of this curved mirror. The final two mirrors are placed as symmetrically as possible from the crystal and curved mirrors, and the green reflecting off the bottom left should strike the top right 'chirped' mirror. This reflection is then directed at the top left 'output coupler' and then from there to the bottom right mirror.

8.4.1 Hazard Awareness

It is important to mention that this is the stage at which the optical risk is about to increase substantially, as more intense, and possibly pulsed, infrared light will begin to be emitted from the cavity. As such, it is not visible to the eye, but still poses a risk of permanent eye damage and blindness. Appropriate safety measures were verified by the team before continuing further alignment.

8.5 Feedback Alignment

Alignment at this time and relatively low power level is directed by optical viewing cards and optical viewing paper. Once satisfied with these rough reflections around the cavity, it is time to direct the alignment actions with output power, and thus the input power is increased. If done properly, the beams should strike all optics on center, and given the careful manufacturing of the posts, all of the optics mounts should be as close to center position as possible. To optimize for power at this stage, the power meter is placed in the path of the diagonal exiting beam (purple arrows), as this one allows for three of four mirrors to be changed without altering the direction of the output, as well as the fact that the green should not be exiting in this direction(it contaminates the power measurement). The goal is to alter the position and orientation of mirrors one control at a time, maximizing the detected power continuously, and moving from control to control in a reasoned order once a maximum has been achieved on a control. At 10 mW, we began with a few dozen microwatts, and with some direction, were able to achieve 103 μW in a half hour. This quantity meant the beginning of feedback had occurred, a precursor to lasing. The goal was to continue increasing this, and it was estimated that improving the alignment until 150 μW was experienced would likely lead to lasing, whereupon the power would jump significantly.

From the theory point of view, the power meter is placed to detect one arm, and then the controls that impact only the non-detected arm are altered. This may seem counterintuitive at first, but it is the methodology because the beam-detector interaction must not change, and if this were not followed, the beam would change how exactly it contacts the power meter, falsely changing the detected power level. So, the process holds that manipulating the non-detected beam improves its alignment with the crystal focal point, where it increases the power available for fluorescence, increasing both

beams, including the one which is detected. Once this has been optimized in one arm, it can be repeated on the other by moving the power meter, and manipulating different mirrors, until it too is optimized, at which point this cycle is repeated, back and forth until the power level no longer increases at all. An image of the power meter used to read the feedback of the beams can be found below(fig 8.2).



Figure 8.2: Power meter and sample reading.

In practice, beginning at the measurement of $103 \mu\text{W}$, progress was slow. In the first half hour, the detected power had only risen to $106 \mu\text{W}$, $1 \mu\text{W}$ at a time. Then, something odd happened. While applying light pressure to the focusing lens, the power detected jumped significantly, to well over $600 \mu\text{W}$. It was the result of slightly altering the focus lens orientation, but was also a sign of a significant problem: that the lens mount was not stable enough. It required replacement, as discussed previously. Fortunately, following the replacement, the next alignment attempts resulted in lasing.

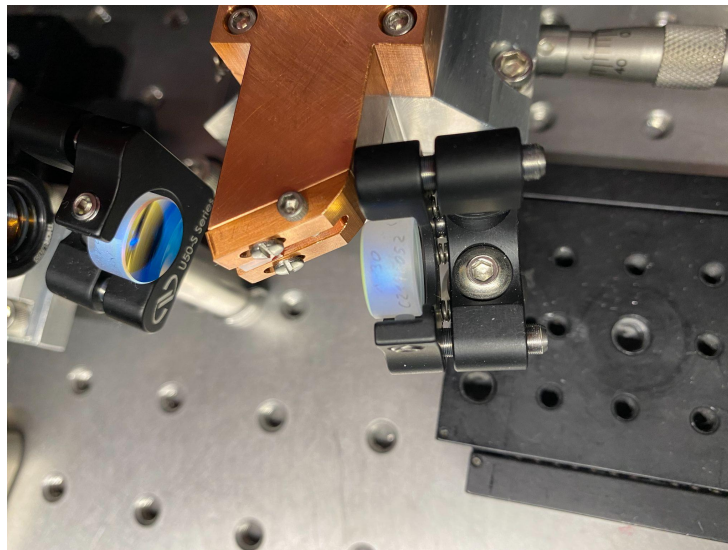


Figure 8.3: Close-up of the two curved mirrors angled at half the astigmatism angle, 9.8° .

8.6 Lasing Alignment

Once the focusing lens mount issue was corrected, alignment continued swiftly, and the feedback alignment became optimized enough to cause lasing. The jump in output power was significant, from a pump to output ratio of 0.00035 to 0.046. At the input power of 500 mW to 1000 mW, the procedure continued, continuously optimizing for power until the ratio approached 0.146. It is important to mention that the numbers specifically were not critical, but rather their relative magnitudes. The critical operator controls are shown in the partially blacked out image below. Besides the actual positions of each optical via their respective mount, the following changes can be made: two dials on each of the 1" mirrors, stage movement for the focusing lens, vertical and horizontal angle adjustment of each of the four cavity mirrors, as well as stages for the bottom left, top right mirrors and the crystal stage, as seen in the figure below.

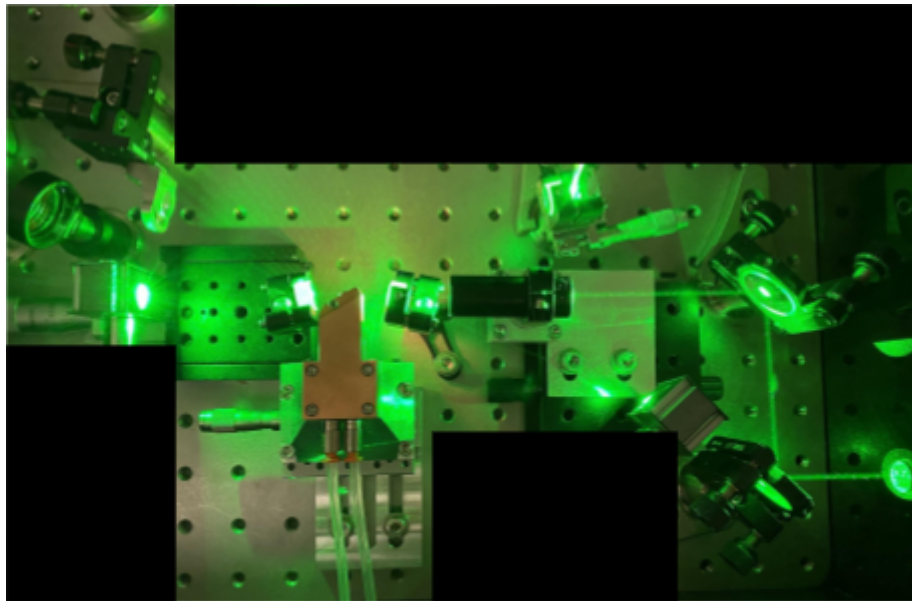


Figure 8.4: Cavity with micrometers for optical components. These pieces are not reflective of all of the methods of adjustment for alignment. Sections blocked out for clarity

8.7 Mode Locking Alignment

Mode locking alignment involves much of the same procedure as lasing alignment, only more gently making changes. This helps in identifying the very fine alignment ranges that may support mode locking, and then testing the alignment by perturbing the system to check for single and hopefully Dual Comb Mode Locking. When mode locking is active, depending on the noise and presence of CW waves, and operator experience with the cavity, it is possible to change the alignment of components during mode locking. This change is noticeable on the power meter, spectrum graph, and sometimes even visible to the user (while wearing the safety goggles) through changing brightness in the cavity. Optimization is a process of careful trial and error, and keeping a record of changes is not necessary, but recommended.

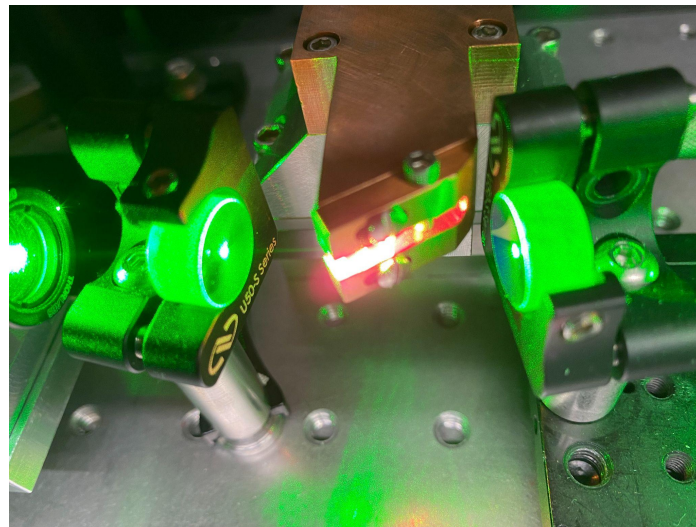
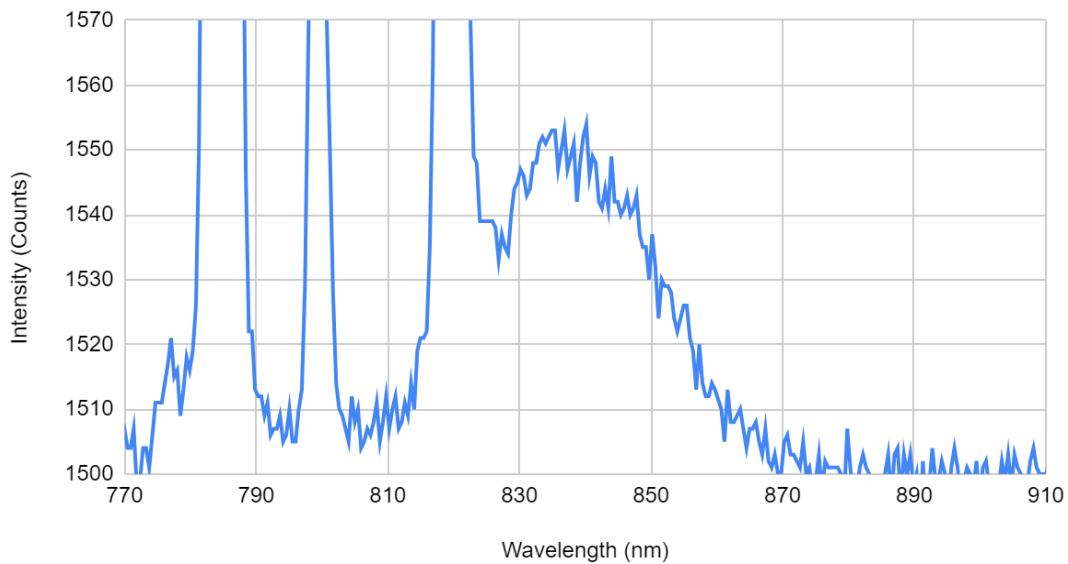


Figure 8.5: First evidence of mode locking, solely in one arm, and with static and CW noise. FWHM bandwidth appears to be around 30 nm. Also shown is the appearance of the curved mirrors and crystal around 4.5 W pump power.

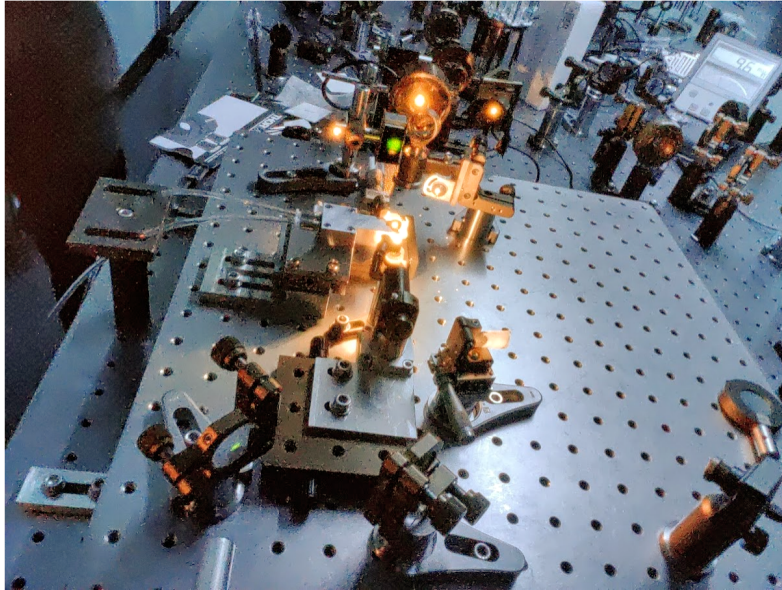


Figure 8.6: Mode locked cavity, seen here with the power meter just visible in the top right corner.

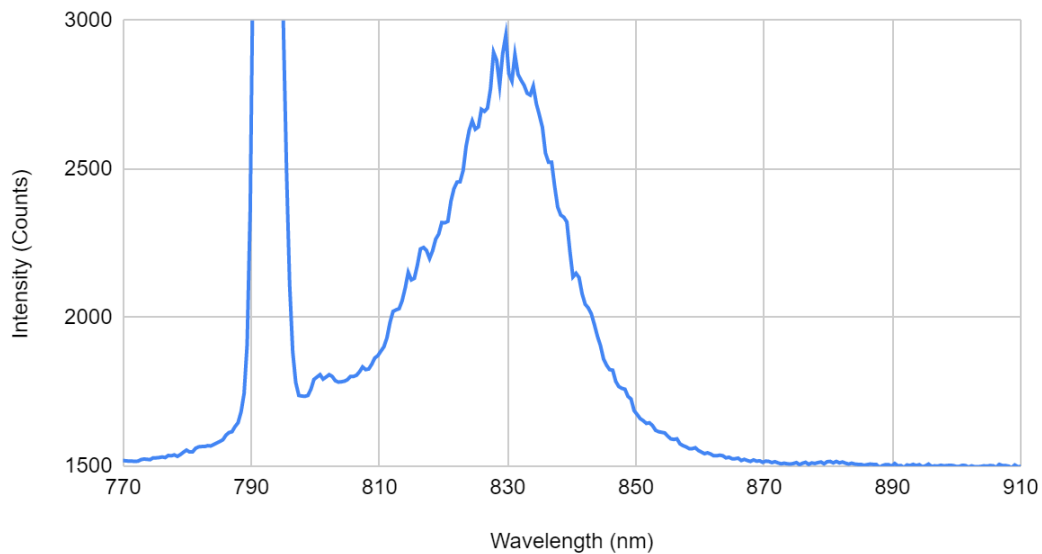


Figure 8.7: Mode locking progress in a single arm, improving signal to noise ratio and eliminating some CW waves within the cavity.

For our project, we were able to produce and record evidence of the cavity in Dual Comb operation, included in section 8.9. It was possible to achieve this at a few different pump power levels, but output power started to hit a limit, and produced diminishing returns above a pump power setting of around 5 Watts.

8.8 Iterations, Power, Appearance

This section serves as a summary of some of the raw values achieved during the acquisition and improvement of lasing, including mode locking, displayed in the following table.

Table 8.1: Output power values for different power settings, in the order they occurred during aligning and optimization tests. Recall that because the pump beam loses power during reflections off mirrors on its way to the cavity, input energy is lower than pump output power.

Notes	Pump Laser Power (mW)	Ti:Sapphire Output, One Arm (mW)	Ti:Sapphire Output, Both Arms sum (mW)
	500	.103-.106	0.179
*	500	12.3	N/A
	500	0.086	0.161
	500	14	23
**	500	8	15
	500	28	51
	1000	68	122
	1000	74	146
***	3220	~230	~400
+	4530	363	445
+	4300	410	712
+	5940	~360	723

*Power output revealed during the discovery of the faulty stage, which was then replaced, causing a slight rest.

** Laser turned off for the day. When turned back on it began at a lower output power. This can happen and is normal.

***Lowest power level that supported mode locking in at least one arm.

+ Each of these were found to support dual comb mode locking, and the associated values represent one of the power levels recorded at that pump power.

8.8.1 Green

The laser cavity with an all green beam running straight through the focus lens and both curved mirrors and eventually to a beam block can be seen in Fig. 8.8 below.

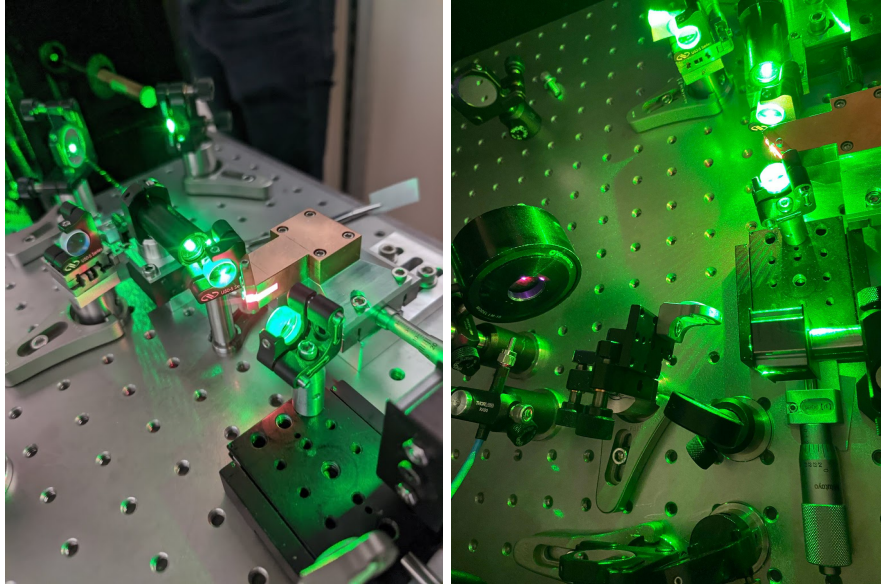


Figure 8.8: Green beam. To the naked eye, the laser would appear like this, as the emittance of the crystal is mostly in the infrared

8.8.2 Red/Near Infrared

Below is an image of the laser cavity aligned such that red and near infrared beams are propagating throughout the bowtie configuration.

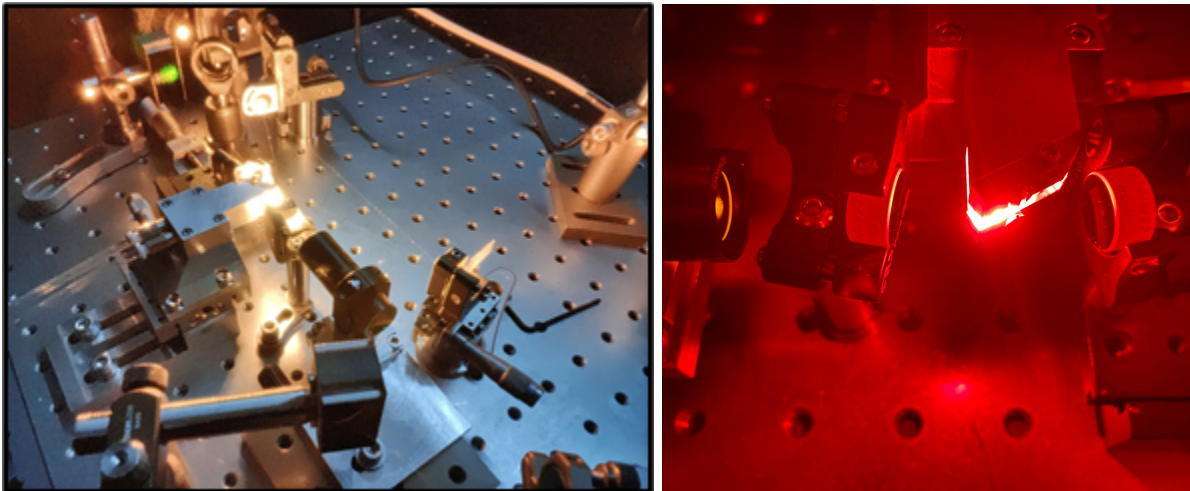


Figure 8.9: Red/Near Infrared appearance. With the exception of the beam block in the back, the brightness in the infrared now clearly overpowers the green. The green dot visible on the beamblock helps confirm the transparency of the curved mirrors to 532 nm light, as most unabsorbed green should exit the cavity straight through the farthest curved mirror.

8.9 Laser Qualitative Analysis

8.9.1 Mode Locking Quality

By the end of the project, the successful acquisition of stable Dual Comb Mode Locking is the marker for Quality, as it is significantly more difficult than achieving mode locking in a single arm. However, the laser does not always remain there, and ideally, it holds the mode locking indefinitely. The 37 minutes we were able to achieve is a good start, as is the 40 nm Bandwidth we were able to achieve, and the nearly 'CW-noiseless' spectrum. However, hypothetically the Bandwidth could approach or even surpass 70nm, and the laser could last at least a day when left undisturbed. The system in place though should be able to achieve these given enough time with further alignment and testing.

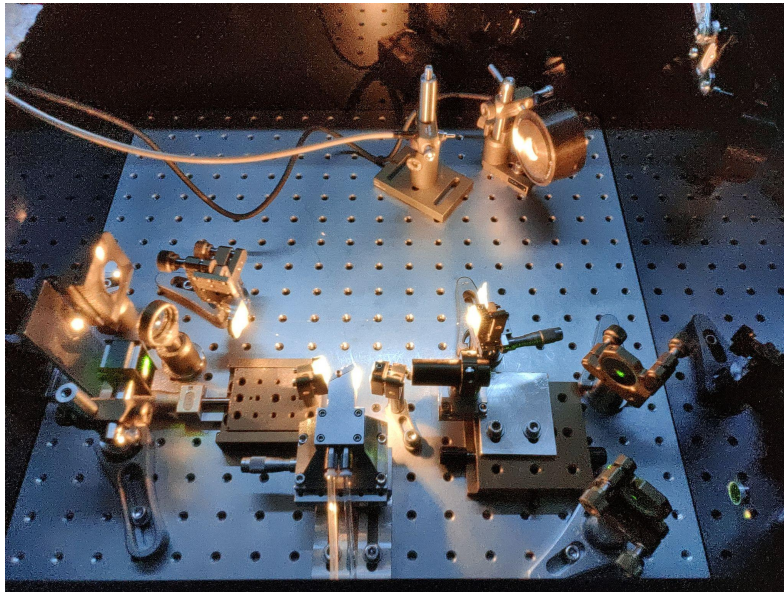


Figure 8.10: Mode locked cavity under testing. The infrared beams can be seen striking the power meter located in the top right, as well as the spectrum analyzer directed at the point of contact.

8.9.2 Pulse Repetition Rates

After achieving mode locking in at least one arm, we were able to successfully verify it's repetition rate, which was done by shooting the output beam into a thin piece of glass. The ~4% reflection of the beam was directed through a focusing lens into a detector, and displayed with the frequency counter shown in Fig. 8.11.

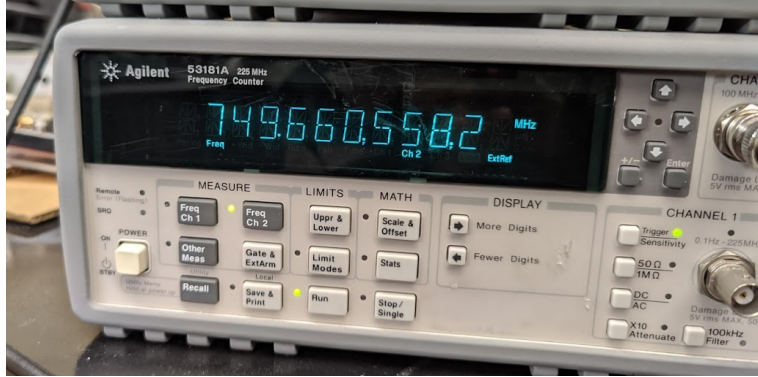


Figure 8.11: Repetition rate testing equipment, Agilent Frequency Counter 5-3181A, showing the f_{rep} from one arm of the mode locked laser. This number indicates a cavity length of around 40.02 cm.

8.9.3 Dual Comb Status

Through a careful period of experimentation with different cavity alignments, power levels, and repetition, we were able to successfully get dual comb mode locking to function with some initial stability. While it was not verified to be stable for a significantly long time, we were able to achieve it for a minimum of 40 minutes (see fig 8.9). Due to time constraints we continued working on other optics during these mode locked periods, which expectedly led to occasional loss of dual comb mode locking. The comb information was collected using SpectraSuite from Sun Microsystems in combination with an Ocean Optics spectrometer.

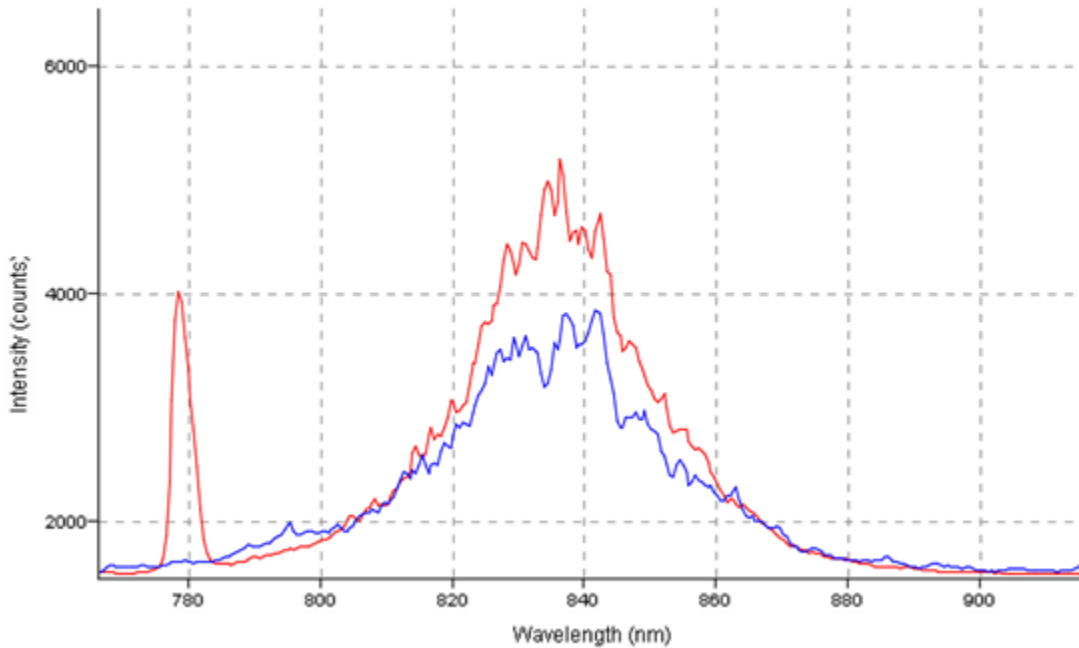


Figure 8.12: Spectrum overlay graph, as shown in SpectraSuite. Visible are both combs, now with greatly reduced CW noise, with FWHM bandwidths of around 40 nm.

8.9.4 Absorption Spectroscopy Test

No test of absorption spectroscopy was performed, though it will likely happen shortly after the conclusion of this project

8.9.5 Frequency Combs

Unfortunately, despite promising results and good lasing, the process of overlapping the combs to extract the frequency comb information was not completed. A number of hours were dedicated towards achieving this goal, but the project needed to be compiled and concluded before it was possible to collect the necessary data. It as well will likely happen shortly after the conclusion of this project.

8.10 Aligning Summary

Overall, the laser now aligns quite quickly, relative to our expectations. Achieving mode locking can still be a challenge, but in reality, we were able to return to single comb mode locking with some predictability even when replacing the focusing lens mounts repeatedly. However, simultaneous Dual Comb is still very challenging, and it is more difficult to say if it is “easier” to achieve it with our laser system, though we do believe that precision manufacturing has helped. If further improvements were made on top of those implemented here, facilitating Dual Comb Mode locking is certainly an expected byproduct, though we are not sure to what extent. Four significant improvements to this build are likely: increased number of mechanical stages (stacking stages in parallel might help with perfecting the coincidence of the focal points), replacing silver mirrors with 532 nm optimized mirrors (as is planned for this laser), refining crystal mount design without compromising thermal control, and PID implementation.

8.11 Future Plans

Looking past the official end of the senior design project, we aim to continue to fine tune our laser to an even better degree. We will be able to then obtain results that have the potential to be used in an published academic paper. Furthermore, our laser will soon be integrated with the preexisting laser cavity that Dr. Lomsadze built so that different experiments can be run with the integrated systems.

Chapter 9 Budget Analysis

Our budget is mainly focused on the performance of our system. Having performed AHP Weight calculations, we determined that performance should control 57% of our total attention given to this project while other categories such as cost, appearance, and safety hold less high importance. After taking this into consideration, here is a breakdown of the parts needed for the project.

9.1 Presecured Components

A number of parts for this project were acquired previous to the beginning of our senior design project. These were purchased by Dr. Bachana Lomsadze through a grant given to him for his research. The following is a list of these items. Not included are costs for the pump laser, optics bench, or other optical equipment that was used but is not limited to applications specifically with our laser.

Table 9.1: Pre secured covered costs.

Secured Covered	
Part	Total Cost
M-SDS25 stage	\$536
UMR5.16 stage	\$289
TSX-1D stage	\$194
curved mirror	\$817
curved mirror	\$817
chirped mirror	\$373
1/2" Waveplate	\$1,040
Titanium Sapphire Crystal	\$1,600
Output coupler	\$320
Piezoelectric Actuator	\$310
∅25.4mm Mirror	\$295
Beamsplitter	\$210
Long pass filter	\$160
Prism mount	\$80
1/2" Beam splitter mount	\$80
Convex lens	\$70
km100pm	\$80
Km100 x 8	\$320
U50-s mirror mounts x 3	\$210
Lens mounting ring	\$32
Miscellaneous additional parts	\$103
Grand Total (incl tax):	\$7,936

9.2 Directly Funded Components

9.2.1 Funding

Here is a breakdown of the funding that we proposed and was later granted by the mechanical engineering department for our project. This was an initial idea of how we would spend the money.

Table 9.2: Mechanical engineering department funding.

Mechanical Engineering Department Funding	
Part	Total Cost
Stainless Steel Breadboard 18x18x2.4 in	\$800
1/2" Mirror mounts w/ Micrometers	\$800
Grand Total Requested:	\$1,600

9.2.2 Budget Dedication

We were able to spread our \$1600 of funding very well between a multitude of parts which are included below.

Table 9.3: Purchased parts costs.

Purchased Parts	Total Cost
Plastic Clear Tubing	\$10.50
Polycarbonate Round Tube	\$3.36
Universal-Thread Push-to-Connect Tube Fitting for Air and Water	\$22.64
Pipe Fitting Straight Connector with Hex	\$27.92
Brass Ball Valve with Lever Handle Female	\$13.03
Optical Rail	\$35.00
Brass Round Tube	\$11.56
Tube Fitting for Water - Straight Adapter with HexMale	\$2.76
Universal-Thread Push-to-Connect Tube Fittings	\$19.04
Tube Fitting for Air and Water - Adapter Female(2)	\$7.14
Tube Fitting for Air and Water - Straight Adapter with HexMale	\$2.76
Lid Stays, Folding Lid Support Hinges	\$23.98
Cast Acrylic - Opaque Black 19x19 in	\$78.10
Cast Acrylic - Opaque Black 10x18 in	\$74.00
Cast Acrylic - Opaque Black 10x19 in	\$74.20
Mirror Mount (2) 100-TPI Allen-Keys	\$201.00
Thorlabs LB1 Beam Block	\$107.12
ARN-2-M AILERON STAY	\$82.50
Honeycomb Breadboard	\$761.00
Grand Total (incl tax):	\$1,557.61

9.2.3 Retrospective

Given the extent of the project, its success would not have been possible without some of the resources that covered the gaps where our budget could not reach. Given that we were unable to access the build location until much later than the budget

requests were due, it was very difficult to properly gauge all the small things that would be required to complete the project. However, our estimate did leave some wiggle room, and we carefully allocated whatever remaining portions we could. In addition, by sheer luck we ended up with twice the amount of acrylic that we had ordered, so rather than just the acrylic main cavity containment, we designed and constructed both the periscope and pump laser containers, thereby improving the safety of the laser optics table on the whole.

9.3 Other Components

All other parts that were implemented in our project are those that we machined or cut ourselves. Using the resources that the school provided through the machine shop allowed us to cut down on potential costs. These resources included acrylic glue, custom screws, and significant amounts of aluminum and stainless steel. Also, the time and effort put in by the team as well as the long term help from the school's professional machinists, allowed for no extra funding to be spent on labor.

Chapter 10 Team and Project Management

10.1 Project Challenges

The immense reach of this project has not come without serious challenges, sacrifices, and consistent dedication. Especially considering the year of this project, massive delays outside of the group's control prevented progress by a total of 3-4 months. The most significant milestone, the beginning of manufacturing the custom parts, and the ordering of the honeycomb breadboard to mount the cavity, were delayed until only 3 months before the completion of the project. The process from there on was incredibly fast paced and demanding. Between the three project members, easily 1100 hours have been spent on completing the project, and pushing a minimum of 25 hours each for 13 weeks straight is definitely the defining challenge of this project.

On at least four different occasions, monumental project problems have arisen, and required rapid and yet perfectly precise solutions, with little to no room for error or second chances. From designing and prototyping the periscope within 4 hours of discovering the precise parameters necessary, to revamping the entire pre cavity lens assembly because the linear stage was not rigid enough, to taking apart the heatsink, inverting it, removing and replacing the thermal paste, and carefully repositioning the tiny titanium sapphire because the cavity was unable to reach any aligned position.

All custom made aluminum and stainless steel designs were original concepts, and pushing these to manufacturing within one to three thousandths of inches increased production times, and certainly raised a few eyebrows from skeptics. With such a complicated end goal, it was completely infeasible to ever properly convince some of the importance of these precision decisions.

In addition, the complexity also made some options in system construction not even appear on our broadest radar until far late into the project. This compounded with the limited budget, which was sufficient, but did not leave room for purchasing alternatives, given the expense of optical and mechanical stage components in the hundreds of dollars.

10.2 Laser Protocol

10.2.1 Hazards

Due to the laser cavity's function, which converts a continuous wave pump laser into a pulse train laser, the power level in the pulses can reach substantial power peaks of over 1 Megawatt. While the laser operates at the near infrared range, meaning the pulses appear invisible to the human eye, the pulses exceed a high output power quantified by a Class IV laser system, and can cause damage even if the beam is not seen. The beam may have random reflections within the cavity, as well as having reflections off of mirrors during realignment. More about laser safety and agreements is included in chapter 12.7.3.

10.2.2 Mitigations

Besides the mandatory laser safety course and guidance from advisors on laser safety, training and experience in the lab were the number one assurance of safety within the lab. Given this, one primary member of the group with previous experience in the laser lab was selected and approved by both the Mechanical Engineering and the Physics department to ensure avoidance of the potentially serious risks. Besides this, Dr. Lomsadze purchased additional LG 12 goggles that protected against all possible wavelengths in the project, as opposed to specialized goggles that are typically swapped at the different stages of the laser's development.

Many engineering control systems have already been implemented into the laser lab room. The following systems were utilized to help minimize the danger associated with working on a Class IV laser. The room has curtains/blinds that block any windows. The lab room also has a laser interlock system that indicates that the laser is in operation at the entrance of the door, and prevents unauthorized entry, and prolonged opening of the entryway. The laser cavity remained confined in a box when in use. The box was taken off during cavity adjustment.

The team wore personal protective equipment while within the lab area. These include correct wavelength eye protection with optical density (od) grade 7+. All participants shall also be wearing protective arm and leg gear that are reasonably tightly fitting(long sleeve shirts, pants, closed toe shoes).

10.2.3 In Lab Procedure

On top of the mitigations, lab procedure was a significant part of the team's process, and helped ensure the continued comfort and safety of all individuals involved. Primarily, consistent verbal communication, dedicated use of the Nominal Hazard zone to limit the individuals exposed to the laser, and careful methodology of laser alignment ensured the healthy completion of the various laser stages. As the project moved from certain laser power levels and alignment qualities, and the risks increased, procedure was thoroughly maintained and led the pace to ensure redundant safety protocol. More about in lab procedure is included in chapter 12.7.3.

10.3 Timeline

Once the first full set of laser cavity components were completed, the green pump laser could begin being aligned. This corresponded with a CW laser power of ≤ 10 mW, already over the minimum for Class III lasers. In parallel with these first laser alignment components, in the pre-cavity, was the machining of the periscope and custom 303 SS posts, as well as the laser containers for the periscope and the pump laser. Through various stages, including installation of the breadboard clamps and the directing mirrors on the breadboard, three weeks passed, but the build height of the components was confirmed with the first striking of the Titanium Sapphire Crystal within the mount. For

this stage, laser goggles blocking 532 nm were worn, and the remaining group members were able to get first access to the laser laboratory, though capacity was still limited to two people at a time.

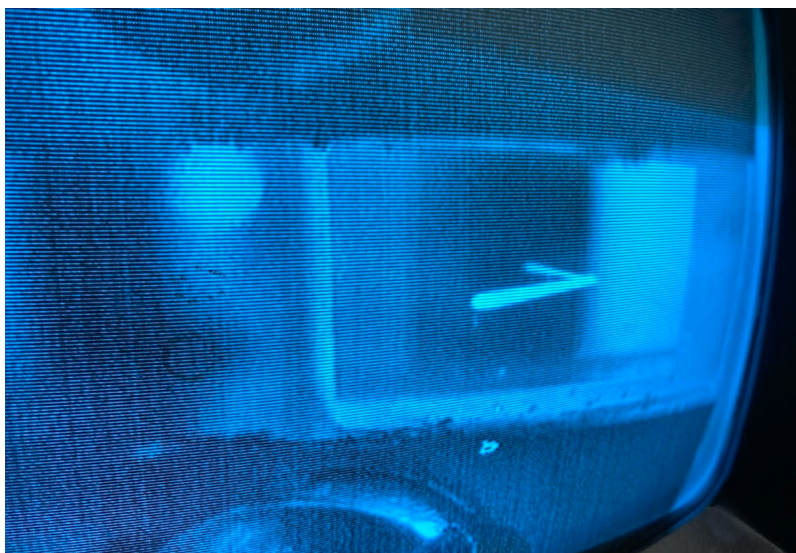


Figure 10.1: The image shows, as accurate as was possible, the focal point of the pump beam in the center of the crystal. The pump beam passes through a focus lens and is adjusted until the focal point is within the crystal. The image is of a CRT monitor that was connected to the infrared camera, and the main beam is visible in the center, as well as a reflection slightly above it which was also picked up by the camera. The two crystal mount screws can be seen at the top and bottom of the image.

Following the installation of the 5 remaining optics, the pump beam could be focused into the crystal, beginning the true red and infrared fluorescence of the crystal. At lowest power and with some filtering, some of the most team bonding moments were captured in images of the fine line passing through the crystal, at long last. See Fig. 10.1. From this stage, after various big changes previously discussed, requiring another 2 weeks, the power was finally pushed to the 500 mW level, and the first feedback of the laser let us change from visual alignment (the use of Iris's) to power output optimization based alignment (using power meters). Final stages of the project included improving this further to achieve lasing, increasing the pump power, and iteratively testing alignment which eventually resulted in single and then Dual Comb Mode Locking. Following that week was one final week of acquiring a repetition rate, trying to optimize mode locking, and some work to attempt to overlap the outputs, which will hopefully be achieved soon after this project concludes.

10.4 Design Process

The main focus of this project was determined to be the performance of the laser, and thus the design process had this in mind. It was determined through research that

the system was expected to be highly sensitive to external factors [20]. General material decisions were chosen such that vibrational and thermal expansion would theoretically have less influence on the system. The design of the cavity was also significantly impacted by the cost of the anti chirp mirrors. Although more mirrors could theoretically have better anti chirp performance, it was determined that the cost to performance ratio was significantly reduced if more mirrors were included. Overall, the design process was heavily skewed towards reaching maximum performance of the system.

10.5 Major Breakthroughs and Successes

Within 24 hours of achieving first feedback, we achieved lasing! What a rush, after eight weeks of the pump laser being in use, the jump from feedback to laser happened lightning quick. But it didn't end there. 24 hours later, without much warning, after pushing output power to greater and greater heights, and ramping input power up to 4530 mW, the first Mode locking was achieved! Granted, it wasn't that great, we only had evidence of it in 1 arm. However, the output power of 360 mW was far higher than we had anticipated, and the noisy CW waves were only fractionally within the mode locked range. It really breathed new life into the project. These two days were the proof we needed that all the meticulous work, and the fine tuned precision of the manufacturing, was worth it, assisting in this awesome 48 hour speed-run of mode locking from first ramping up the power to beyond the thresholds required to achieve the phenomenon that weeks earlier we had some doubts of ever achieving. And yet, it wasn't done there. In the next two days, single arm mode locking became significantly better, and after discovering the aforementioned serious issue with the lens linear stage, and making not one, but two precision redesigns, we managed to reestablish mode locking within five additional days(Laser week 9). Each of these, and the other successes, including the achievement of >37 minute stable Dual Comb Mode locking, have been team efforts, and would not have been possible without the commitment to safety and care with the consistency that we have managed.

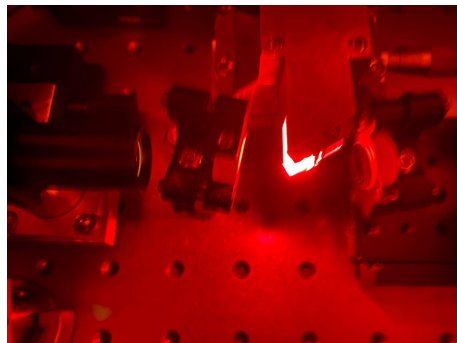


Figure 10.2: Fluorescence in the red/infrared range from the crystal. Green light has been filtered.

Chapter 11 Patent Search

11.1 Invention Overview

The heat sink is the main topic of the patent search. The heat sink is composed of Oxygen-Free high Conductivity copper (OFHC copper) machined into an inverted T shape. Running through the heat sink are two bored channels serving as an inlet and outlet for fluid. The purpose of this heat sink is to dissipate the heat generated by a Ti:Sapphire crystal that is being hit with a green pump laser away from the crystal itself. The heat sink design has improvements over similar products due to the complex geometry of our idea that enables high efficiency in dissipating heat while still maintaining a low profile. In addition to the interesting geometry of our heat exchanger, another unique property of it is that it also serves as the primary mount for the crystal, the heat source. So on top of the heat sink's role in dissipating thermal loads, this application requires it to play a vital role in maintaining the integrity of the laser alignment. It accomplishes this at the tip, where a small clip made of the OFHC copper holds the crystal, and is face mounted to the remaining heat sink via two screws which firmly clamp the copper together and thereby secure the crystal in place.

11.2 Summary of Patent Classifications

For our heat sink, the patent classification that would be most applicable would be a D type patent. Many heat sinks, whether in computers, lasers, or industrial machines, already use a fluid propelled and recycled by a separate component. Additionally, our heat sink design is based on how the crystal is arranged in the system. The shape and size of the heat sink channel is based on creating the best possible conditions with regards to a very specific type of laser. Therefore, a patent that describes shape and form, instead of functionality, would be the most sensible categorization.

11.3 Sketch

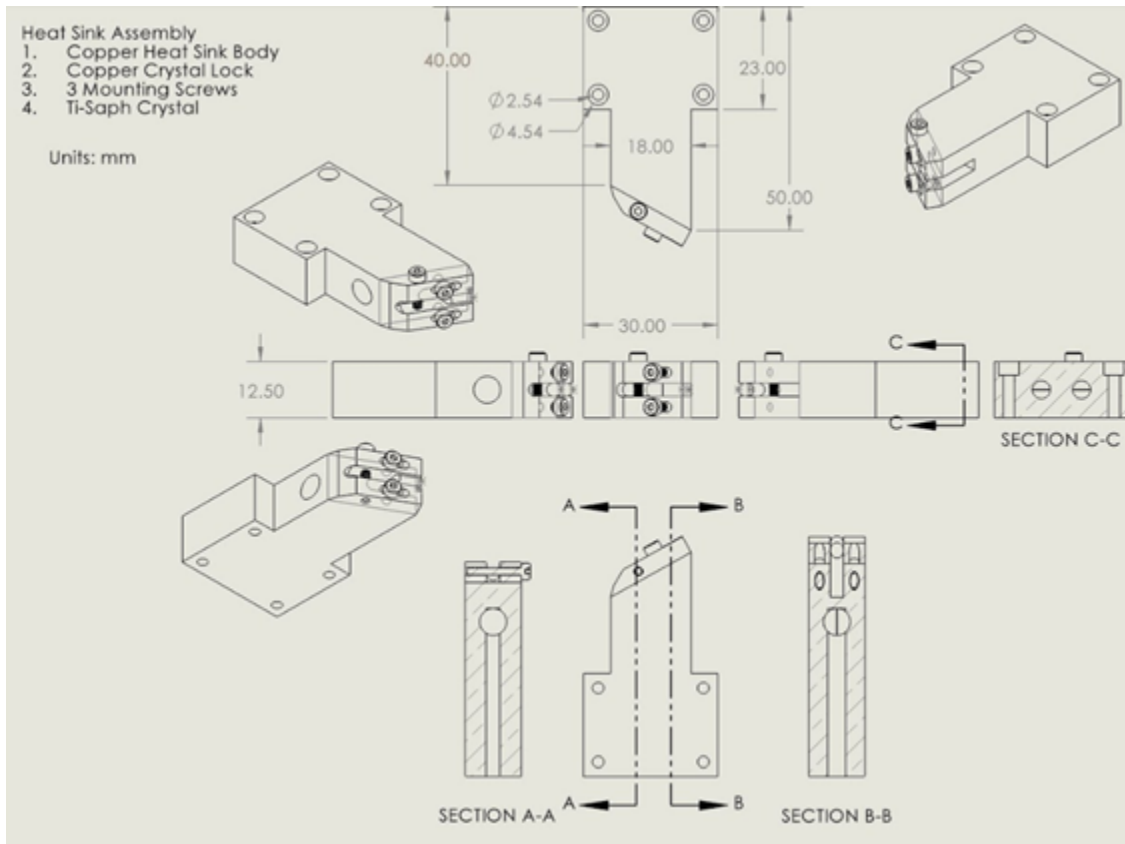


Figure 11.1: Sketch of heat sink. (See also Fig. 6.2)

11.4 Review of Prior “Art”

Our patent differs from many but not all ideas in terms of functionality, but is unique in form and shape. Patent number US20060227827A1 describes using a similar idea of a heat sink than ours. It has chambered liquid flowing in multiple channels. This invention uses a system of layered channels that are stacked vertically within a square system. Our idea implements a much simpler path for fluid to cross while having a more complex shape of the actual heat sink block. Patent number US4901324A contains differences compared to our heat sink when relating to its setup. This system uses one close ended pipe with two parts. The first part is in a heat exchange relationship with the laser medium, while the second part is in a heat exchange similar relationship with the heat sink. This is at odds with our designed piping system that has one uniform part that is only in contact with the heat sink. The third patent that is relevant to the application of a heat sink is patent number US20060215715A1. In this invention, two radiating plates are joined around a laser medium. The first plate has grooves cut into it to make space for the laser and the second plate is flat. When joined together, they make a container that is smooth and flat on the outside but complex and intricate on the inside. There is no use of any fluid to dissipate the heat in this system, unlike in our idea. The

invention of a “Heat dissipating device for laser diodes,” patent number US5029335A, is composed of two parts: a solid state device and a heat sink. The heat sink is connected to the solid state device and has a base with many attaching elongated heat conducting elements. The last patent researched, number US8199787B2, has an interesting approach to dissipating heat. Surrounding a laser is a cylindrical container of fusible solid metal. When the laser is turned on, this metal heats up and undergoes a phase change into liquid form. The heat that is taken in by the metal is the main method of heat transfer. Once the laser is off, the metal will turn back into its original solid form.

11.5 Preliminary Patent Search Choice: Heat Sink

Below are the important details regarding the prior searches we performed for the prior “art” that we compared to our proposed patent of the heat sink.

Table 11.1: Descriptions of preliminary patent searches.

Title	Patent Number	Important Dates
Semiconductor laser device and heat sink used therein	US20060227827A1	Filed 2006-04-11 Published 2006-10-12
Heat transfer device for cooling and transferring heat from a laser diode device and associated heat generating elements	US4901324A	Filed 1988-12-19 Granted 1990-02-13 Published 1990-02-13
Heat sink, laser module, laser device, and laser-processing device	US20060215715A1	Filed 2004-02-18 Published 2006-09-28
Heat dissipating device for laser diodes	US5029335A	Filed 1989-02-21 Granted 1991-07-02 Published 1991-07-02
Laser diode package with enhanced cooling	US8199787B2	Filed 2011-08-04 Granted 2012-06-12 Published 2012-06-12

11.6 Conclusion

In regards to patentability, the idea of a heat sink for a Ti:Sapphire Laser does have a specific utility being heat dissipation in a certain lasing system process. The heat sink is different in form and shape than the other patents discussed but not in regards to functionality in some cases. A person in the field of laser operation would have a general

idea of a heat sink used in the process. However, the specific design of a heat sink that is machined for high efficiency in a Ti:Sapphire setting would be unknown to them for the most part. If the shape and size of the heat sink as well as the system it operates within, i.e. a bi-directional Kerr-lens mode locked titanium sapphire laser system, are emphasized within the patent, it is believed that there is a possibility for patent approval.

Chapter 12 Realistic Constraints & Engineering Standards

12.1 Manufacturability

Throughout the design and manufacture process of each of the components, maintaining comprehensibility was implicit. This benefitted both our production of the components directly, but also benefits any attempts to reproduce our components using identical or entirely different methods. Though this does likely require heavy machining, this is very likely not outside the expected range of projects with the aim of building lasers.

12.1.1 Project Unique Components

All manufactured parts for the project are manufacturable with basic heavy machining training. The three main materials, 6061 aluminum, 303 stainless steel, and acrylic, are fairly accessible, and all designs were carefully considered to ensure reasonable and replicable manufacturing, despite their unique applications. Designs found in the appendices should aid in direct reproduction of these unique components or can serve as inspiration for similar ones.

12.1.2 Component Assembly

Assembly of all components did not require many specialized tools, and can be done completely by hand. An exhaustive list of the tools used by the team can be found in Table 12.1 below, and those required for assembly are italicized.

Table 12.1: List of tools used, italicized if required for assembly process specifically.

Carpenter Square	Vise and Clamps	Adjustable Wrench	<i>Imperial Allen Wrench Set</i>
Caliper	Power Drill	Hand File	<i>Metric Allen Wrench Set</i>
Painters Tape	Hand-Saw	End Mill	<i>Powder Free Nitrile Gloves</i>
Pliers	Lathe	Face Mill	<i>Screwdriver set</i>

12.1.3 Laser Alignment Skills

This is the most exclusive part of the manufacturability process, because it is almost certainly necessary that laser alignment training has been given to at least one member of the project, and the greater the number of experience hours, the better it ensures the success of the alignment phase. This stage of the manufacturing process also

requires a lot of patience and intentional action, to ensure that no components or persons are damaged or worse, throughout the process.

12.2 Economic Impact

Directly, this project produced a laboratory use device, not a consumer product. Thus, its economic impact is limited, and the full cost of such a device would likely fall under a research budget, rather than a consumer or business expense. The approximate total cost of everything needed to enable this device to function within standard protocol depends on scope. This is simplified if it is assumed that a purpose built laser laboratory exists, along with an optics table equipped with a pump laser and sufficient “standard” optics mounting equipment. These excluded, the costs are within \$7,936. Alternatively, designs of a six mirror cavity setup instead of the four mirror setup would provide more control over variables such as chirp but would also increase the cost of the project by an additional \$800.

Additional economic costs come into play when associated with material choice for which the optical equipment sits on. 303 stainless steel provides low thermal expansion coefficients when compared to aluminum and thus was chosen for many of the manufactured spacers.

12.3 Environmental Impact

The environmental impact of this project is minimal, excluding the impact of the acquisition of raw materials in the various optical components, and the impact of their manufacturing. Applications of this type of product include long range identification of volatile organic compounds (VOCs) in the air. Dual comb spectroscopy is able to identify concentrations of VOCs in the air. A team has demonstrated that dual comb spectroscopy is able to identify VOCs over a 500m distance with sensitivities of 15 ppb for ethane and 25 ppb of butane over a two minute time period [21]. Optical measurement of atmospheric monitoring over a wide range is a highly applicable use of dual comb spectroscopy because it is non destructive and has a fast acquisition rate and high resolution.

12.4 Sustainability

Our project does not require the use of any external exhaustible resources, but does require a source of electricity. In terms of product viability, the absence of moving parts of a single cavity dual comb laser extends the product lifetime indefinitely. The cavity itself needs minimal electronic equipment to operate but needs a wide range of measurement equipment to properly quantify its operation. Proper setup has been done such that typical measurement equipment seen in an optics lab can be used on the laser. Additionally, proper use and maintenance of the mirror surfaces would only be necessary if dust could build up, which will be negligible due to the fully enclosed

containment system. The lasing medium, the Ti:Sapphire crystal, does not undergo damage unless the thermal control system were to fail, which should not occur if water supply is replenished under standard conditions. Additionally, the team has designed the cavity such that realignment was an easy and achievable task which greatly increases the reusability of the cavity.

12.5 Health and Safety

This project involves a Class IV level laser as defined by OSHA, which can cause serious eye and skin damage if the necessary precautions are not taken. However, our team has taken a laser safety course that describes the potential dangers as well as how to properly use the laser. Additionally, there exists a laser interlock system that shuts the laser off if the door was forced open. The team ensured the use of laser protective eyewear around the laser and a procedure to either turn the laser off or stay outside the Nominal Hazard Zone (NHZ) when without eyewear. On the wall of the NHZ, and outside the lab, signs light up when the laser is on so that everyone in the lab or outside the entrance is aware. Finally, the laser containers that we manufactured further protect against stray beams. Proper beam paths were manufactured into the system to provide protection to those operating the laser.

12.6 Ethical Considerations

Table 12.2: Team based ethical considerations.

Problem	Consequence	Solution
Avoid internal team conflict.	Breakdown of team communication and chemistry.	Open discussions and welcomed all creative criticism as a necessity for progress. Never demeaned or talked down to others.
Avoid plagiarism and copyright.	Investigation into academic dishonesty even if unintentionally done.	Creative copyright images only, labelling them appropriately. Properly cited text when needed in the thesis body.
Avoid copying previous senior design projects.	Consequences range as a previous team would lodge a formal complaint of varying degrees of accusations.	Have no knowledge of any previous project that was close to the subject matter of the team's laser.

Table 12.3: Design based ethical considerations.

Problem	Consequence	Solution
Reduce all possibilities of danger to the individual.	Create an unsafe environment for individuals to be in.	Followed all safety protocols including OSHA when designing cavity, designed sufficient beam containments, and passed laser safety course.
Avoid all remaining danger from system	Temporary or permanent eye and skin damage.	Followed proper laser procedure, wore correct PPE, used laser interlock system, used NHZ correctly, and only kept laser on when needed.

12.7 Engineering Standards

12.7.1: Introduction

The team has identified that specific manufactured parts are needed before initial laser parts are created. This includes spacers for optical cavity components, safety equipment such as containers and tubes along the laser path, and optical components such as a beam block or mirror stand. Many of these components have tight tolerances which ensure the operation of the laser cavity. It is thus important that the communication of design pieces followed a standard for which correct manufacturing of the parts was done.

Once initial assembly and alignment was complete, the laser needed to be active to make further improvements. This meant beaming a pump laser into the cavity, where it enters the Ti:Sapphire crystal, which by design radiates electromagnetic waves (i.e. photon emissions). In addition, even when carefully controlled, the laser's spectral and diffuse reflections are capable of causing eye damage and skin damage; it is of utmost importance to follow laser safety standards and procedures while in the vicinity of the laser. The lab where the laser system will be operated and maintained follows specific protocols which are in line with many many voluntary standards to ensure the safety of all parties involved throughout the assembly, alignment, and operation.

12.7.2 Drawing standards

The team identified that engineering drawings are communicated using the ASME Y14.5 for dimensioning and tolerance of engineering drawings. Manufacturing of these components was of utmost importance and thus specifications of the parts were communicated using this standard for engineering drawings.

12.7.3 Safety Standards

Two standards have been identified to ensure that correct laser safety standards were followed within the lab. The first standard is OSHA Technical Manual (OTM) Section III: Chapter 6 which identifies occupational standards for the use of lasers [22]. The second laser safety standard includes the EHS 0302 Laser safety training course. The course outlines correct procedures for operating and building a laser system.

12.7.3.1 Identification

While working with a laser system, it is important to identify the wavelength operation and output power of the laser system. Two laser systems were in operation in the project. The pump laser is a continuous wave laser that provides the energy to the second laser by “pumping” 532 nm light into it, at a power of up to 6 W. The pump laser is a Lighthouse Photonics Sprout-G laser system, which includes a cooling mechanism as well as an enclosed power supply. The second laser system originates in the Ti:Sapphire crystal medium within an enclosed four mirror cavity. One of the greatest risks posed by this cavity occurred during the alignment phase of the project, when the reaction within the crystal was unenclosed. The Ti:Sapphire crystal was struck by the lens-focused 532 nm pump laser beam and outputted a gaussian distribution centered at 800 nm which was identified to be near infrared. At completion, the Ti:Sapphire laser also poses a safety risk because it becomes a pulsed laser system in which pulses can achieve power levels of Megawatts due to the femtosecond long pulses if an input power of 6 watts is considered. This behavior is achieved when the cavity is mode locked and is significantly more dangerous than the constant power level constituting the pump beam, while also being invisible to the human eye. It was important to identify the class of both of these laser beams so that correct PPE as well as correct engineering controls and administrative controls were used while in operation of both laser systems.

12.7.3.2 Classification

OSHA identifies a Class IV laser system as:

Class IV: High power lasers (cw: 500 mW, pulsed: 10 J/cm² or the diffuse reflection limit) are hazardous to view under any condition (directly or diffusely scattered) and are a potential fire hazard and a skin hazard. Significant controls are required of Class IV laser facilities[22].

Both laser systems during operation are identified as Class IV laser systems which required significant controls to ensure the safety for all parties involved. OSHA identified that Photochemical and thermal retinal injury can occur within the eye if hit by the visible light pump laser and skin effects include thermal burns and photochemical effects [22]. OSHA has also identified that eye effects such as cataract and retinal burns can occur if hit by an infrared A(0.780-1.400 μm) as well as skin

effects such as burns. It is important to note that Class IV is the highest categorization for lasers.

12.7.3.3 Hazard Zone

OSHA has also identified that a NHZ(nominal hazard zone) is important to identify before operation of the laser. MPE(Maximum Permissible Exposure limit) is an important factor when identifying the NHZ. The MPE for a pulsed laser is different from that of a cw (continuous wave) laser. Pulsed lasers concentrate their power in short packets and, therefore, have the potential to damage the eye more than that of a cw laser with the same power rating. This forces the threshold level for pulsed lasers to be less than that of cw lasers in order to account for the additional danger. The MPE has been identified as near instantaneous for the infrared A laser system. Expected pulse length varies between 10-200 femtoseconds and direct or diffuse contact with a pulse causes burning of the skin and blindness. The visible light laser system has been identified to cause burning of the skin and serious eye damage if direct or diffuse contact with the beam. OSHA has identified that the NHZ definition is:

The Nominal Hazard Zone (NHZ) describes the space within which the level of direct, reflected, or scattered radiation during normal operation exceeds the MPE. The NHZ associated with open-beam Class IIIB and Class IV laser installations can be useful in assessing area hazards and implementing controls [22]

The team has identified that the room of operation of the laser lab exceeds the MPE within the operating table and a curtain has been put in place to block the hazardous area from the entrance of the room. Significant control systems which included PPE, engineering controls, and administrative controls were needed within the hazardous area given the current class of laser in operation.

The room has implemented the OSHA control measures for the given class of laser in operation. Control measures are included in Appendix G.1: OSHA Control Measures. These control measures are broken down when they should be applied depending on the class of laser as well as certain situations regarding MPE . A complete list of hazard assessment as well as PPE, engineering controls, and administrative controls is included below. The team adhered to the outlined rules to ensure the safety and health of all parties involved. PPE includes protective goggles for specific applications. Specifications for PPE while in the laser lab are included in Appendix G.2.

12.7.3.4 Summary/ Safety Agreement

Hazard Assessment and control systems for laser safety operation

<p>Hazardous Activity, Process, Condition, or Agent : Non-Ionizing Radiation</p>	<p>Danger Level: Very High</p>
<p>Summary of Procedure or Tasks: Once initial assembly and alignment is complete, the laser will need to be active to make further improvements. This means beaming a pump laser into the cavity, where it enters the Ti:Sapphire Crystal, which by design radiates electromagnetic waves (i.e. photon emissions). In addition, even when carefully controlled, the laser's spectral and diffuse reflections are capable of causing eye damage.</p>	
<p>Hazard Description: Due to the laser cavity's function, which converts a constant wave pump laser into a pulse train laser, the power level in the pulses can reach substantial power peaks of over 1 Megawatt over around 10 femtosecond (10^{-14} seconds). While the laser operates at the near infrared range, meaning the pulses appear invisible to the human eye, the pulses exceed a high output power quantified by a Class IV laser system, and can cause damage even if the beam is not seen. The beam may have random reflections within the cavity, as well as having reflections off of mirrors during realignment.</p>	
<p>Hazard Control Measures: PPE: All participants within the lab shall wear the correct wavelength eye protection with optical density (od) grade 7+. Specifically, Lg9 goggles from ThorLabs are worn when aligning the laser. If the crystal is not in the laser setup, Lg3 goggles may be used when applicable. Lg12 googles are also included which provide protection from both the 532nm pump laser as well as the near infrared pulse laser. All participants shall also wear protective arm and leg gear that are reasonably tightly fitting(long sleeve shirts, pants, closed toe shoes). Summary of PPE gear specifications can be found in appendix G.2 Engineering Controls: The room has curtains/blinds that block any windows. The lab room also has a laser interlock system that indicates that the laser is in operation at the entrance of the door, and prevents unauthorized entry, and prolonged opening of the entryway. The interlock system is able to shut down the laaser if the entryway into the room is opened. The laser cavity will remain confined in a box when in use but not needing adjustments. The team has also manufactured beam block tubes which confine the laser beam along its path restricting diffuse reflections.</p>	

Administrative Controls: All participants within the lab shall receive proper laser training from EHS 0302 Laser Safety Training course. Before operation, a checklist of proper safety conditions shall be conducted.

CheckList:

1. Ensure that all participants within the lab are wearing proper eye protection as well as proper attire before proceeding past the curtain.
2. Curtain should be closed before operation
3. Outside laser interlock system should be turned on
4. Lock the entrance to the laser room(automatic)
5. Check to ensure that mirrors are correctly aligned
6. Announce that the laser will be turned on

The following actions and conditions must be accomplished/reached given the following situations:

Physical harm to eye or skin due to specular or diffuse reflections: Contact 911 as soon as possible. If this option is not readily available, seek help from whatever peers and qualified faculty and staff that are nearby.

If physical harm to eye or skin due to specular or diffuse reflections are merely thought to have occurred with the slightest probability (even if no harm is felt): Visit a local doctor as soon as possible, and contact Dr. Lomsadze and faculty advisors. Do not wait; temporary or permanent damage may take a few days to be noticed.

Dangerous conditions in the lab brought about by equipment breaking: Exit the area and turn off the laser (permitted danger levels not immediately health threatening). Contact Dr. Lomsadze. If not available, contact whatever peers and qualified faculty and staff are on hand.

Fire in the lab: Exit the area and pull the fire alarm as quickly as possible. If it is determined that the fire can be contained, use of a fire extinguisher is highly recommended. Immediately contact the fire department.

**given current covid restrictions, three members are allowed to be within the lab at once. The team must adhere to covid guidelines such as social distancing and wearing a mask at all times.

**Stratos, Ricky, and Dylan are only allowed to work alone (individually) and without faculty in the lab if:

- A. They are performing calculations or measurements in the preparation room with the curtain closed or the laser switched off. Or:

B. Have completed the laser safety course, received sufficient instruction for the given task, had sufficient hours of experience performing the given task under supervision(~20 hours), and Dr. Lomsadze is in the building(Daly Science 300)

**If students are interacting with the laser and/or aligning the laser in any way new to the student, Dr. Lomsadze will be present in the room to ensure safe procedures. Before the first full operation of the laser in infrared lasing, they will perform a walkthrough, go through an assembly review, and be signed off by Dr. Lomsadze in order to ensure that all students are fully knowledgeable about the procedures and safety of general and site specific laser use. Also, each time the laser is to be turned on, the students will perform an initial safety check with Dr. Lomsadze in the room.

**If students are taking measurements (while the laser is on) or performing calculations alone, Dr. Bacha Lomsadze will be nearby in the building or on campus in case of the need for consultation or help.

Chapter 13 Conclusion

13.1 Summary

In summary, we have successfully built and aligned a dual comb spectroscopy laser which maintains two combs, has a 750 MHz repetition rate, and a bandwidth of 30-40 nm centered at 835 nm using a Titanium Sapphire. In addition, we have designed and manufactured many components for proper functionality of the cavity. Finally, we designed a heat transfer system for the crystal so that it has optimal performance. Unfortunately we were not able to implement the active control PID system but the design and research that was done during the project will help with implementation in the future.

13.2 Focus on the Future

Our laser system still has potential to be further developed for more than just the application that was the focus in this report. The technology in this field is always advancing and our Ti:Sapphire laser is able to function to these ends with continued refining and changes to the setup.

13.2.1 Spectroscopy

In general, the cavity that we have completed in this project will immediately go into use in Spectroscopy, and aid in work in the Santa Clara University's Physics Department aimed at completing research and publishing academic papers. We're thrilled that our academic work at the junction of two fields of study will continue to provide academic momentum at the University.

13.2.2 Two Unidirectional Cavities

One of the best assurances as to the applicability of our laser are its secondary uses, which will not require any additional parts. The first of these would change only the alignment of the mirrors, into a configuration designed to produce a single comb. This arrangement, when carefully matched to that of the other laser in the optics laboratory, would allow for the use of Dual comb spectroscopy of two separate lasers, allowing for some up and coming research which benefits from this particular setup.

13.2.3 Quad Comb

On the more ambitious side of optics, our laser represents the next step in attempting to achieve Quad Comb Spectroscopy. We cannot speak to the nature of this science and its capabilities, but it most certainly holds promise for even greater applications of frequency comb laser technology.

13.3 Reproducibility

Through detailed descriptions of all of the subsystems, CAD drawings, manufacturing specifications, component assembly, calculations, alignment processes, testing, and results, our team has provided a pathway that walks any undergraduate wishing to pursue a similar system systematically through each step necessary to accomplish their goals. Despite the novel nature of our project's subject matter, the unforeseen constraints of COVID-19, the incredible results that our team has achieved prove that it can be reproduced, given significant effort, even under the most stringent of conditions.

13.5 Reflections

Dylan:

This senior design project has tested and pushed my abilities to apply what I have learned in mechanical engineering and combine it with new knowledge of laser physics. Our team embarked on what we knew would be a tough project. Our progress and results are reflective of great team communication and hard work ethics. As we come to the end of our official time on the project, I recognize my growth as not just an engineer, but also as a member of a team aiming to create what many have noted is a difficult task not just for undergraduates but also for multidisciplinary individuals. I am greatly appreciative of all of the hard work from my team members as well as the incredible help that we have received from our faculty advisors and the machine shop instructors.

Ricky:

This project is by far the biggest responsibility I have ever undertaken. It is the culmination of multiple years of experience with Lasers, and nearly a year from conception to completion. I could not have asked for more from my team from the moment we were finally granted better access to the physical workspaces necessary for the build. The nature of lasers has really shaped this project on so many levels, from manpower to our main order of operations, which differed quite a bit from what is typically found in SCU's Senior Design Projects. The help from faculty was invaluable, and I only wish the project could have started earlier. My advice: start every step as early as possible. We got very lucky with how quickly we were able to hit our targets when it came to laser aligning; that portion, which was only 3 weeks, definitely could have been 3 months instead. Perhaps we were just very prepared.

Stratos:

This project was the most complicated project I've undertaken. It forced me to learn new skill sets such as machining and CFD modeling as well as reinforcing skills I've learned previously. The project has taught me that nothing is out of reach, I had no

previous experience in optics but this project has forced me to learn quickly and research the minute details that are involved in constructing a precision laser system. I've been able to apply what I've learned in classes to this project and I believe that this project shows my growth as an engineer. Even though it was a stressful last three months, from Covid delays, the project was exciting and demonstrates all of our abilities to push and persevere through a project.

Bibliography

- [1] Jones, D., Diddams, S., Ranka, J., Stentz, A., Windeler, R., Hall, J., and Cundiff, S., 2000, "Carrier-Envelope Phase Control of Femtosecond Mode-Locked Lasers and Direct Optical Frequency Synthesis." *Science*, 288(5466), pp. 635–639.
- [2] Moulton, P. F., "Spectroscopic and laser characteristics of Ti:Al₂O₃," *Journal of the Optical Society of America B*, vol. 3, no. 1, pp. 125–133, Jan. 1986.
- [3] Liu, A., "Ti:Sapphire Lasers - University of Michigan." [Online]. Available: <http://www-personal.umich.edu/~alberliu/writing/lasers/TiSapphireLasers.pdf>. [Accessed: 01-Jun-2021].
- [4] I. Coddington, N. Newbury, and W. Swann, "Dual-comb spectroscopy," *Optica*, vol. 3, no. 4, pp. 414–426, 2016.
- [5] G. C. Kerber, K. F. Lee, G. Zhou, M. Cassinerio, J. Jiang, M. E. Fermann, and S. T. Cundiff, "High-Power Broadband Dual Comb Spectroscopy in the Mid Infrared," *2020 Conference on Lasers and Electro-Optics (CLEO)*, pp. 1–2, May 2020.
- [6] K. Yang, X. Chen, H. Li, D. Hu, R. Huo, Q. Hao, M. Yan, K. Huang, and H. Zeng, "Temperature Measurement of Water Vapor by Adaptive Dual Comb Spectroscopy," *14th Pacific Rim Conference on Lasers and Electro-Optics (CLEO PR 2020)*, Aug. 2020.
- [7] Paschotta, R., "Titanium–sapphire Lasers," *RP Photonics Encyclopedia - Titanium-sapphire lasers, Ti:sapphire laser, femtosecond, regenerative amplifiers*, 28-May-2021. [Online]. Available: https://www.rp-photonics.com/titanium_sapphire_lasers.html. [Accessed: 01-Jun-2021].
- [8] "Ti:Sapphire Laser Crystal," *The Roditi International Corporation Ltd.* [Online]. Available: http://www.roditi.com/Laser/Ti_Sapphire.html. [Accessed: 01-Jun-2021].
- [9] Figliola, R. S., and Donald E. B., 2015 "Appendix A." *Theory and Design for Mechanical Measurements* 6th ed., Wiley, pp. 585–585.
- [10] "430 Stainless Steel," Penn Stainless, October 24, 2018, www.pennstainless.com/resources/product-information/stainless-grades/400-series/430-stainless-steel.
- [11] Penzkofer, A., Wittmann, M., Lorenz, M., Siegert, E., and Macnamara, S., 1996, "Kerr lens effects in a folded-cavity four-mirror linear resonator," *Optical and Quantum Electronics*, 28(4), pp. 423-442.
- [12] Shirakov, A., Burshtein, Z., Shimony, Y., Frumker, E., and Ishaaya, A., 2019, "Radiative and non-radiative transitions of excited Ti³⁺ cations in sapphire," *Scientific Reports*, 9(18810), pp. 1-9.
- [13] Çengel, Y. A., and Afshin, G.J., 2020, "Steady Heat Conduction," *Heat and Mass Transfer: Fundamentals & Applications* 6th ed., McGraw-Hill Education, NY, pp. 151-249.

- [14] “Oxygen-Free High Conductivity Copper,” European Copper Institute, Copper Development Association, 2018,
<https://copperalliance.org.uk/about-copper/conductivity-materials/oxygen-free-high-conductivity-copper/>.
- [15] Shah, R K., and London, A. L., 1971, “laminar Flow Forced Convection Heat Transfer and Flow Friction in Straight and Curved Ducts A Summary of Analytical Solutions, “ 75th ed., Office of Naval Research, pp. 212–217.
- [16] “Ti:Sapphire Crystals.” *4Lasers*, Optogama,
<https://4lasers.com/components/crystals/laser-crystals/ti-sapphire-crystals>.
- [17] Çengel, Y. A., and Afshin, G.J., 2020, “Appendix,” Heat and Mass Transfer: Fundamentals & Applications 6th ed., McGraw-Hill Education, NY, pp. 945-973.
- [18] Çengel, Y. A., and Afshin, G.J., 2020, “Internal Forced Convection,” Heat and Mass Transfer: Fundamentals & Applications 6th ed., McGraw-Hill Education, NY, pp. 491-555.
- [19] Çengel, Y. A., and Afshin, G.J., 2020, “Natural Convection,” Heat and Mass Transfer: Fundamentals & Applications 6th ed., McGraw-Hill Education, NY, pp. 555-623.
- [20] D. E. Spence, P. N. Kean, and W. Sibbett, “60-fsec pulse generation from a self-mode-locked Ti:sapphire laser,” *Optics Letters*, vol. 16, no. 1, pp. 42-44, 1991.
- [21] Cossel, K. C., Waxman, E. M., Giorgetta, F. R., Baumann, E., Yeas, G., Herman, D. I., Friedlein, J. T., Bon, D., Coddington, I., and Newbury, N. R., 2020, “Field deployment of a mid-infrared dual-comb spectrometer for measurement of volatile organic compounds,” in Conference on Lasers and Electro-Optics, OSA Technical Digest (Optical Society of America, 2020), paper SF1N.4.
- [22] “OSHA Technical Manual (OTM) Section III: Chapter 6” U.S. Department of Labor, Occupational Safety and Health Administration, OSHA,
<https://www.osha.gov/otm/section-3-health-hazards/chapter-6>.
- [23] Bao, Hua, and Xiulin Ruan. “Absorption Spectra and Electron-Vibration Coupling of Ti:Sapphire From First Principles.” *Journal of Heat Transfer*, vol. 138, no. 4, 2016, doi:10.1115/1.4032177.
- [24] Paschotta, R., “Doping Concentration,” *RP Photonics Encyclopedia - doping concentration, number density, laser-active ions, molar, atomic percent, ppm, weight*, 28-May-2021. [Online]. Available: https://www.rp-photonics.com/doping_concentration.html. [Accessed: 02-Jun-2021].
- [25] Paschotta, R., “Brewster's Angle,” *RP Photonics Encyclopedia - Brewster's angle, polarizing angle, p-polarized incident light, reflectivity, Fresnel equations*, 19-May-2021. [Online]. Available: https://www.rp-photonics.com/brewsters_angle.html. [Accessed: 10-Jun-2021].

[26] Paschotta, R., "Astigmatism," *RP Photonics Encyclopedia - astigmatism, aberrations, human eye, laser beams, focus position, dioptric power*, 13-May-2021. [Online]. Available: <https://www.rp-photonics.com/astigmatism.html#:~:text=Astigmatism%20as%20a%20Kind%20of,angle%20against%20the%20optical%20axis>. [Accessed: 10-Jun-2021].

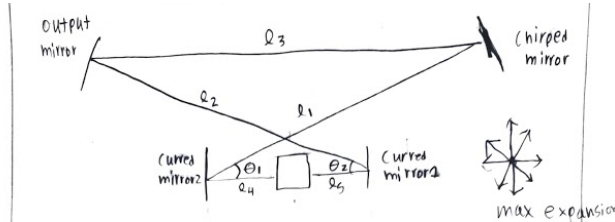
[27] Siegman, A. E., *Lasers*. Mill Valley, CA: Univ. Science Books, 1986.

[28] Yamakawa, K., Aoyama, M., Matsuoka, S., Akahane, Y., Kase, T., Nakano, F., and Sagisaka, A., "Ultrafast, Ultrahigh-Peak Power Ti:sapphire Laser System," Jan. 2001.

Appendices

Appendix A : Detailed Calculations

A.1: cavity expansion



$$r_1 \approx 11 \text{ cm} \quad \theta_1 = 14.6^\circ \quad r_3 = 17.73 \text{ cm}$$

$$r_2 \approx 11 \text{ cm} \quad \theta_2 = 14.6^\circ$$

$$r_4 \approx 1.5 \text{ cm} \quad r_5 \approx 1.5 \text{ cm}$$

$$r_{\text{total}} = r_3 + r_2 + r_1 + 1.5 + 1.5 = 42.73 \text{ cm}$$

$$c = 299,792,458 \text{ M/s}$$

$$n_{\text{air}} = 1.0003$$

$$c_{\text{air}} = \frac{c}{n_{\text{air}}} = 298,895,771 \text{ M/s}$$

$$f_{\text{rep}} = \frac{298895771}{.4273} = 699448645 \text{ Hz}$$

Stainless Steel

$$\alpha_s = 11.0 \cdot 10^{-6} \text{ m/mK} \quad @ \Delta T = 1^\circ \text{C}$$

$$r_1' = r_2' = \sqrt{[r_1 \cos(\theta) (1 + \alpha_s)]^2 + [r_1 \sin(\theta) (1 + \alpha_s)]^2} = .1100121 \text{ m}$$

$$r_3' = r_3 (1 + \alpha_s) = .17730149 \text{ m}$$

$$\Delta f_{\text{rep}} = |f_{\text{rep}}' - f_{\text{rep}}|$$

$$r_4' = r_5' = r_4 (1 + \alpha_s) = .015000165 \text{ m}$$

$$\Delta f_{\text{rep}} = 7694 \text{ Hz}$$

$$r_{\text{total}}' = .4273047 \quad f_{\text{rep}}' = \frac{298895771}{.4273047} = 699490451 \text{ Hz}$$

Aluminum

$$\alpha_A = 22.9 \cdot 10^{-6} \text{ m/mK} \quad @ \Delta T = 1^\circ \text{C}$$

$$r_1' = r_2' = \sqrt{[r_1 \cos(\theta) (1 + \alpha_A)]^2 + [r_1 \sin(\theta) (1 + \alpha_A)]^2}$$

$$r_1' = r_2' = .11002519 \text{ m}$$

$$r_3' = r_3 (1 + \alpha_A) = .17730406017 \text{ m}$$

$$r_4' = r_5' = r_4 (1 + \alpha_A) = .0150003435 \text{ m}$$

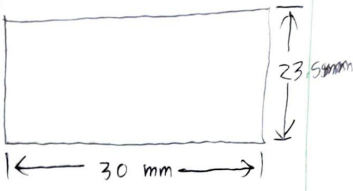
$$r_{\text{total}}' = .42730978517 \text{ m}$$

$$f_{\text{rep}}' = \frac{298895771}{.42730978517} = 699482627$$

$$\Delta f_{\text{rep}} = 16,018 \text{ Hz}$$

A.2: heat sink calculation

Section 1:
Air convection:
horizontal plate



$$Ra_L = \frac{g \beta (T_s - T_\infty) L_c^3}{\nu^2}$$

$$L_c = \frac{A_s}{P} = \frac{(0.03 \times 0.0235)}{(2 \times 0.03) + (2 \times 0.0235)} = 0.0066 \text{ m}$$

$$\beta = \frac{1}{293 + 298} = 0.0034$$

$$Ra_h = 151.68$$

no relationship exists for horizontal plate with low Ra. Assume similar relation to vertical plates

$$Nu_h = 2.48$$

$$h_{\text{horizontal}} = 9.46$$

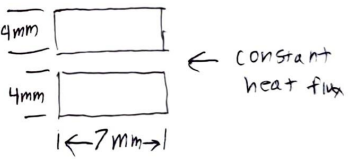
$$h_{\text{vertical}} = 6.95$$

$$S_{A_h} = 0.030 \times 0.0235$$

$$S_{A_v} = (0.03 + 0.0235 + 0.0235 + 0.006 + 0.006) \times 0.0125$$

$$R_{\text{air}} = \frac{1}{h_h \cdot S_{A_h}} + \frac{1}{h_v \cdot S_{A_v}} = 278.1$$

Section 2:
Water convection:
initial conditions



← constant heat flux

$$T_{\text{water}} = 10^\circ\text{C}$$

$$\rho = 999.7 \frac{\text{kg}}{\text{m}^3}$$

$$\nu = 1.31 \times 10^{-6} \text{ m}^2/\text{sec}$$

$$Pr = 9.45$$

$$K = 0.58 \text{ W/mK}$$

$$\dot{Q} = 0.17 \text{ kg/m}^3$$

$$V = 0.225 \text{ m/s}$$

$$Re = 688.6$$

laminar flow fully developed

$$Nu = 4.36 \text{ (cengel, 508)}$$

$$h = \frac{Nu \cdot K}{D} = 632.2$$

$$R_{\text{water}} = \frac{1}{632.2(2)(0.004)(0.007)} =$$

$$R_{\text{water}} = 8.99$$

Section 2:

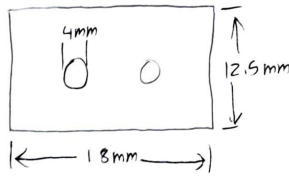
Copper conduction:

$$K_{\text{copper}} = 394 \text{ W/mK}$$

$$A_c = (0.18 \times 0.125) - 2\pi(0.002)^2$$

$$L_c = 0.07 \text{ m}$$

$$R_{\text{cond}} = \frac{L_c}{K A_c} = \boxed{0.089}$$



Air convection

initial conditions:

$$T_{\infty} = 293 \text{ K} \quad T_s = 298 \text{ K}$$

$$T_{\text{avg}} = 295 \text{ K} \approx 20^\circ \text{C}$$

$$\rho = 1.204 \frac{\text{kg}}{\text{m}^3}$$

$$K = 0.02514 \text{ W/mK}$$

$$\gamma = 1.52 \times 10^{-5} \text{ m}^2/\text{sec}$$

$$\text{Pr} = 1.7309$$

$$\beta = 0.0034$$

Vertical: $L_c = 0.0125 \text{ m}$

$$Ra_L = 1030.4$$

(Cengel, 564) for entire range

$$Nu = \left\{ 1.825 + \frac{1.387 Ra_L^{1/4}}{\left[1 + \left(\frac{0.492 \text{Pr}^{1/4}}{16}\right)^{9/16}\right]^{4/3}} \right\}^2$$

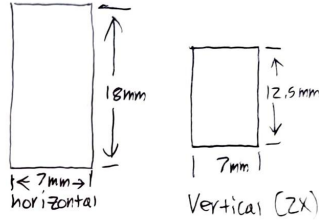
$$Nu_v = 3.45$$

$$h_{\text{horizontal}} = 19.01 \quad SA_h = 1.26 \times 10^{-4} \text{ m}^2$$

$$Nu_h = 1.89$$

$$h_{\text{vertical}} = 6.95 \quad SA_v = 1.75 \times 10^{-4} \text{ m}^2$$

$$R_{\text{air}} = \frac{1}{h_h SA_h} + \frac{1}{h_v SA_v} = \boxed{1240}$$



(Cengel, 563)

$$Ra_L = \frac{g \beta (T_s - T_{\infty}) L_c^3 \text{Pr}}{\gamma^2}$$

horizontal plate:

$$L_c = \frac{SA}{P} = 0.0025$$

$$Ra_L = 9.24$$

No relationship exists for Low Ra horizontal plates. Assume similar relationship to vertical plate.

Section 3:

Water convection

initial conditions:

$T_{water} = 10^{\circ}C$

$\rho = 999.7 \frac{kg}{m^3}$

$\gamma = 1.31 \times 10^{-6} m^2/sec$

$Pr = 9.45$

$k = .58 W/mK$

$\beta = .17 K/m^3$

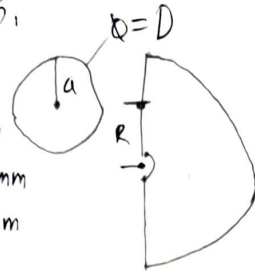
$V = .0483 m/sec$

$Re = 450$

$a = 3 mm$

$R = 3.5 mm$

$D = 6 mm$



(Shan, 22) Dean number $K = Re \sqrt{\frac{a}{R}} = 416.72$

(Shan, 215) $Re_{crit} = 2 \times 10^4 \left(\frac{a}{R}\right)^{3/2} = 18,951$

for $K > 30$ & $Pr >> 1$ (Shan, 216)

$Nu_c = \frac{.869}{3} k^{1/2} (1 + 2.35 k^{-1/2})$

half Torus perimeter

$P = \pi(R-a) + 2\pi R$

half Torus surface area

$SA = \frac{(2\pi R)(2\pi a)}{2}$

$\frac{3}{3} = \frac{2}{11} \left[1 + \sqrt{1 + \frac{27}{4} \frac{1}{Pr^2}} \right]$

$L_c = \frac{SA}{P} = .0088$

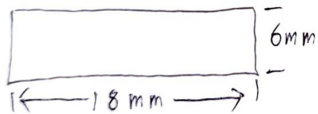
$Nu_c = \frac{h L_c}{k}$

$h = 3396.7 \frac{W}{m^2K}$

$R_{water} = \frac{1}{hSA} = 1.423$

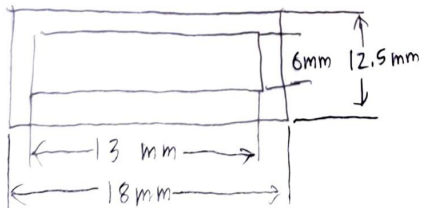
Copper conduction

$k_{copper} = 394 W/mK$



$A_c = (.018 \times .0125) = (.013 \times .006)$

$L_c = .006 m$



$R_{cond} = \frac{L}{kA_c} = .104$

Section 3:

air convection:

initial conditions:

$$T_{\infty} = 293 \text{ K} \quad T_{\text{surface}} = 298 \text{ K}$$

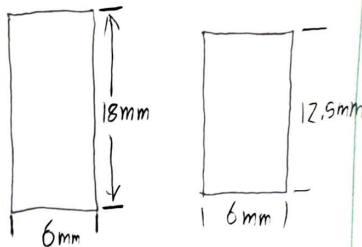
$$T_{\text{avg}} = 295 \text{ K} \approx 20^{\circ}\text{C}$$

$$\rho = 1.204 \frac{\text{kg}}{\text{m}^3}$$

$$k = 0.02514 \text{ W/mK}$$

$$\gamma = 1.52 \times 10^{-5} \text{ m}^2/\text{sec}$$

$$Pr = 0.7309$$



The bottom of the section is attached to aluminum. 3 sides will have natural convection.

Vertical plates:

$$(cengul, 563) \quad Ra_L = \frac{g \beta (T_s - T_{\infty}) L_c^3}{\gamma^2} \quad Pr = 0.7309$$

$$L_c = 0.125$$

$$\beta = \frac{2}{298 + 293} = 0.0034$$

(cengul, 564) for entire range

$$Nu = \left\{ 0.825 + \frac{0.387 Ra_L^{1/4}}{\left(1 + \frac{0.497}{Pr}\right)^{1/4}} \right\}^{2/3}$$

$$Nu_v = 3.45$$

horizontal plate

$$L_c = \frac{SA}{P} = \frac{0.018 \times 0.006}{2(0.006) + 2(0.018)} = 0.00225 \text{ m}$$

$Ra_L = 6$ No relationship exists for horizontal

plates with low Ra_L numbers. Assume similar nusselt number to vertical plate.

$$Nu_h = 1.596$$

$$h_{\text{horizontal}} = 17.83$$

$$h_{\text{vertical}} = 6.45$$

$$R_{\text{conv}} = \frac{1}{17.83(0.006 \times 0.018)} + \frac{1}{6.45(2)(0.006 \times 0.0125)}$$

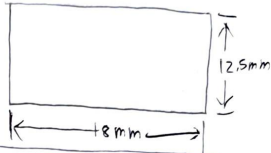
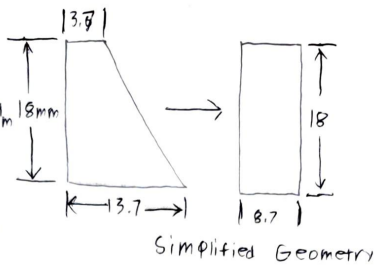
$$R_{\text{conv}} = 14.79$$

Section 4:

Conduction:

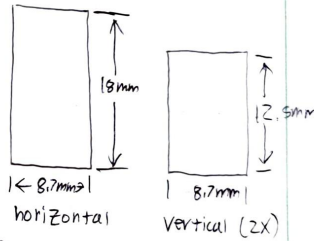
$k_{\text{copper}} = 394 \text{ W/mK}$
 $A_c = (.018 \times .0125) = 2.25 \times 10^{-4} \text{ m}^2$
 $L_c = 8.7 \text{ mm}$

$R_{\text{cond}} = \frac{L_c}{k A_c} = \boxed{.018}$



air convection

initial conditions:
 $T_{\infty} = 293 \text{ K}$ $T_{\text{surface}} = 298 \text{ K}$ $T_{\text{avg}} = 200^{\circ}\text{C}$
 $\rho = 1.204 \frac{\text{kg}}{\text{m}^3}$ $\beta = .0034$
 $k = .02514 \text{ W/mK}$
 $\nu = 1.52 \times 10^{-5} \text{ m}^2/\text{sec}$
 $Pr = .7309$



(Cengel, 9.63) $Ra_L = \frac{g \beta (T_s - T_{\infty}) L_c^3}{\nu^2 Pr}$

Vertical: $L_c = .0125$ $Ra_L = 1030.4$
 (Cengel, 9.64) for entire surface

$Nu = \left\{ .825 + \frac{.387 Ra_L^{1/4}}{\left[1 + \left(\frac{.432}{Pr} \right)^{1/4} \right]^{1/2}} \right\}^2$

$Nu_v = 3.45$
 $h_{\text{vertical}} = 6.46$

$SA_v = (.018 \times .0087) = 1.566 \times 10^{-4} \text{ m}^2$

horizontal: $L_c = \frac{SA}{\beta} = \frac{.018 \times .0087}{(2 \times .018)(2 \times .0087)} = .0087 \text{ m}$

$Ra_L = 14.2$

$Nu_h = 1.772$

$h_{\text{horizontal}} = 14.85$

$SA_h = (.018 \times .0087) = 1.566 \times 10^{-4} \text{ m}^2$

$R_{\text{air}} = \frac{1}{h_v SA_v} + \frac{1}{h_h SA_h} = 1790$

Section 5:

~~Conduction~~ Copper to Copper interface

$h_{\text{contact}} = 55,500 \text{ (Cengel, 165)}$
 $A_c = (.0198 \times .0125) - (.003 \times .0153)$
 $A_c = 2.016 \times 10^{-4} \text{ m}^2$
 $R_{\text{contact}} = \frac{1}{h A_c} = \boxed{.089}$

Conduction

$h_{\text{copper}} = 394 \text{ W/mK}$

$L_c = 4 \text{ mm}$

$A_c = 2.016 \times 10^{-4}$

$R_{\text{cond}} = \frac{L_c}{h A_c} = .05$

Air convection:

Initial conditions:

$T_{\infty} = 293 \text{ K}$ $T_{\text{surface}} = 298 \text{ K}$

$T_{\text{avg}} = 20^\circ \text{C}$

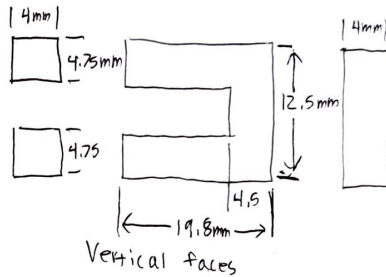
$\rho = 1.204 \text{ kg/m}^3$

$k = .02514 \text{ W/mK}$

$\nu = 1.52 \times 10^{-5} \text{ m}^2/\text{sec}$

$\beta = .7304$

$\beta = .0034$



(Cengel, 563) $Ra_L = \frac{g \beta (T_s - T_{\infty}) L_c^3 \rho}{\nu^2}$

$L_c = \frac{A_s}{p} = \frac{(.0085 \times .0125) + 2(.00475 \times .0193)}{(.0198 + 2(.004))} = \frac{2.896 \times 10^{-4} \text{ m}^2}{.0278 \text{ m}} = .0104 \text{ m}$

$Ra_L = 546.42$

$h = 7.56$

$Na = 3.127$

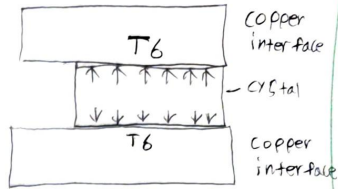
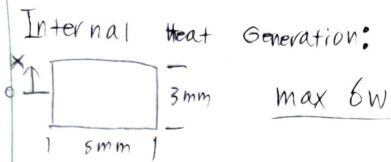
(Cengel, 564)

for entire range $Nu = \left\{ \begin{array}{l} .825 + \frac{.387 Ra_L^{1/4}}{\left(1 + \frac{.492}{Pr}\right)^{1/4}} \end{array} \right\}^2$

$Ra_{\text{air}} = \frac{1}{Na_s}$

$Ra_{\text{air}} = 456.85$

Crystal

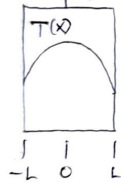


$$\dot{e}_{gen} = \frac{\dot{Q}}{(0.003)(0.005)(0.005)} = 133.33 \frac{\text{W}}{\text{m}^3} \quad K_{\text{crystal}} = 33 \frac{\text{W}}{\text{mK}}$$

$$\frac{d^2T}{dx^2} + \frac{\dot{e}_{gen}}{K_{\text{crystal}}} = \frac{1}{0} \frac{\partial T}{\partial t} \quad \text{Steady state assumption (Cengel, 82)}$$

$$\frac{d^2T}{dx^2} = -\frac{133.33 \times 10^6}{33}$$

$$T(x) = -\frac{133.33 \times 10^6}{33(2)} x^2 + C_1 x + C_2$$



$$T(0) = \text{max} \rightarrow \frac{dT}{dx}(0) = 0$$

$$\left. \frac{dT}{dx} \right|_{x=0} = -\frac{133.33 \times 10^6}{33} x + C_1 = 0 = C_1$$

$$C_1 = 0$$

$$T(L) = T(-L) = T_6$$

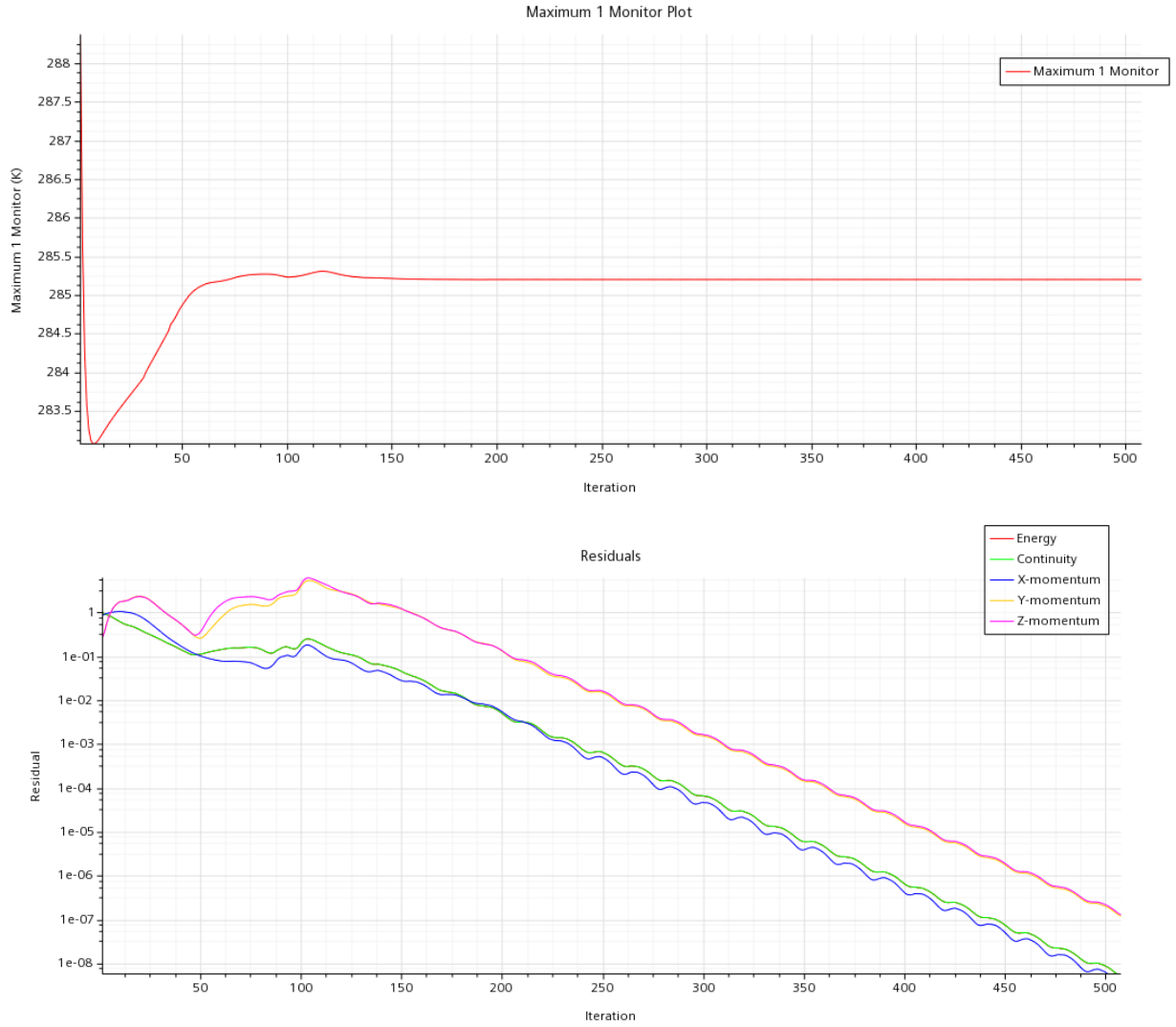
$$T(L) = T(0.005) = -\frac{133.33 \times 10^6}{33(2)} (0.005)^2 + C_1 = T_6$$

$$C_1 = T_6 + 4.55$$

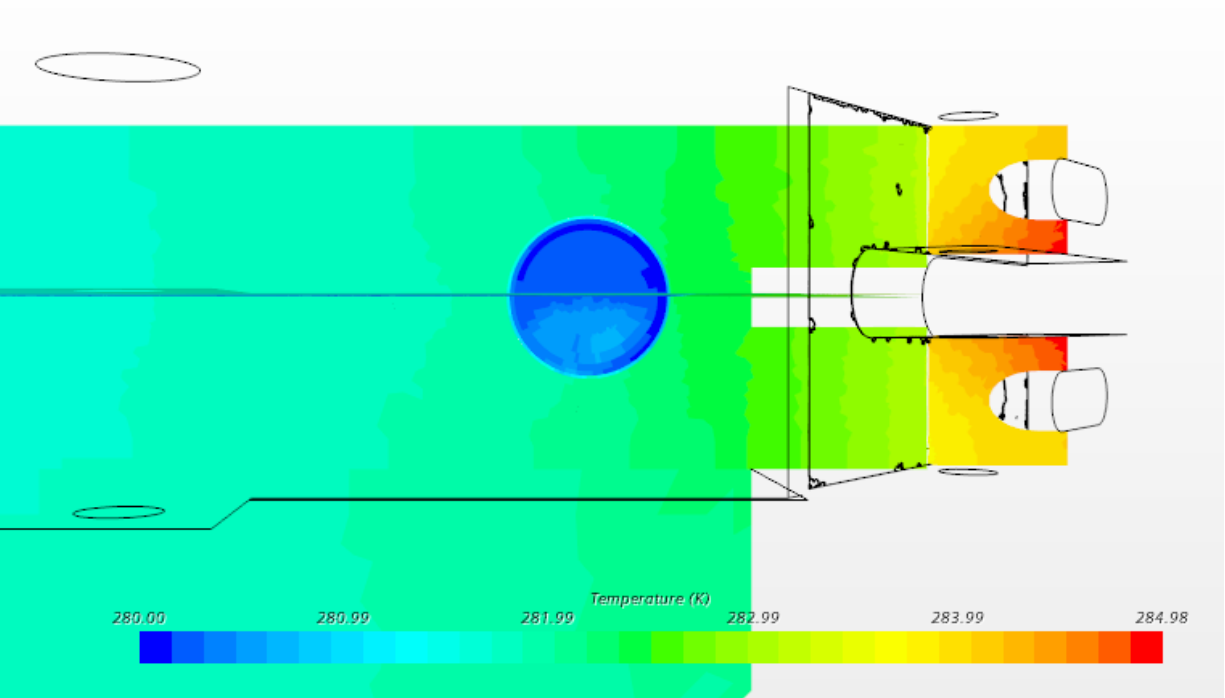
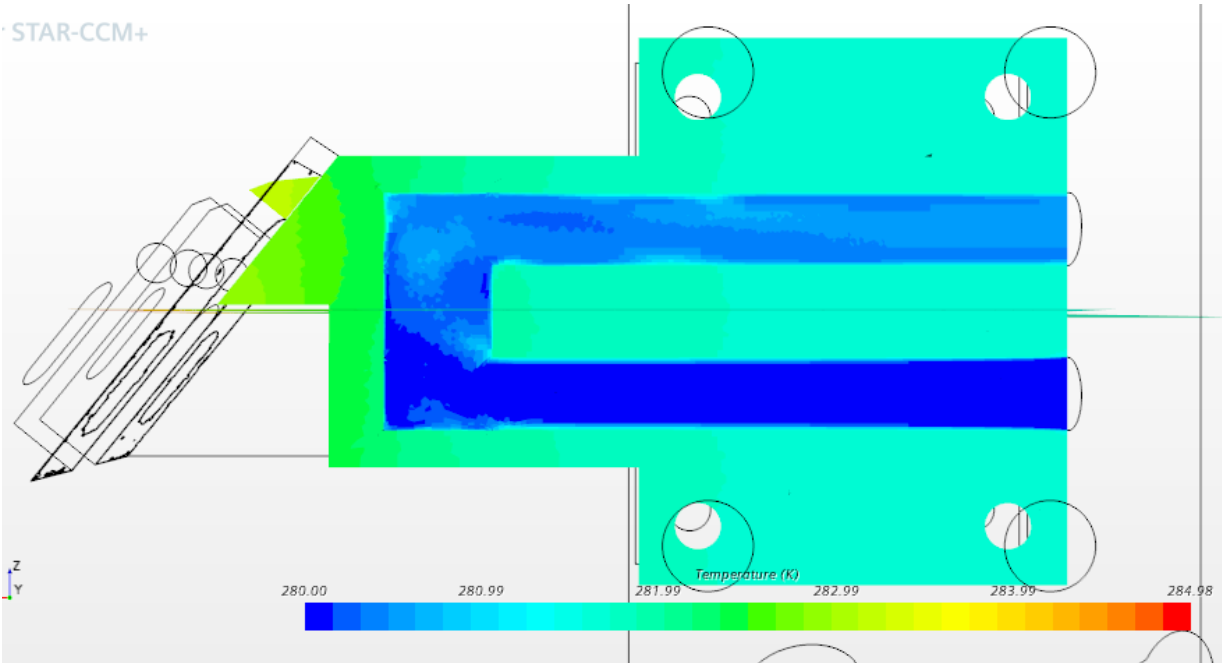
$$T(x) = -\frac{133.33 \times 10^6}{(2)33} x^2 + T_6 + 4.55$$

$$T(0) = T_6 + 4.55$$

A.3 CFD model



STAR-CCM+



Appendix B : PDS

Problem Definition:

The largest benefit to a dual comb spectroscopy laser is its precision and improved data acquisition time. This requires and benefits from its static design and incredibly precise assembly and alignment, as opposed to spectroscopy lasers reliant on mechanical stages. However, the mode locking behavior required to ensure proper functionality of the laser can be incredibly sensitive, and this team hopes to address this problem by adding a PID Controller based active stabilization method. Following the successful assembly of the laser cavity, the team will engage in careful testing, to observe and quantify how changing temperature and reducing vibration affect the signal to noise ratio of the spectroscopy data. The team also wants to test how temperature affects mode locking behavior due to the crystal's properties being temperature dependent.

Design Requirements:

The team has set out to build this laser with a specific customer in mind and thus, many of the system level requirements have been dedicated towards achieving the goal of the main customer. SCU Physics is in need of a Bi-directional Comb Laser, and this project aims to complete this build with that target in mind. Before delving into the system breakdown, four simple design requirements can be discussed as follows. The wavelength range of the laser is 730 to 900 nm, the size of the whole system will be 19 x 19 x 10.5," the time to take measurements will be much less than 1 second, and the accuracy is 0.2 MHz on a scale of 100s of THz.

Laser cavity:

The laser cavity itself is desired to be optimized for performance. The complete design requirements can be seen in appendix B.1.1. The cavity itself should be designed such that it reduces the noise in the data as well as reducing the effects of external influences. This will be done through system isolation as well as fine tuned adjustment tools to achieve an optimized cavity. The data itself has random jitters which is due to the cavity having slight shifts in length from vibration, thermal expansion, and other external factors. Reducing the jitters in the data is of utmost importance and thus will be under heavy consideration. The complete overview of the metrics that are used to quantify the system are listed in appendix B.1.2. The major metric for testing performance will be the output and running time. The output is desired to be pulsed frequency combs and a long running time is preferable. The output metric is directly influenced by cavity isolation, temperature stability, low vibrational/thermal expansion, consistent pump beam, and precise mirror choice. Testing each variable will consist of variable isolation and documenting running time.

The laser cavity is also desired to be constrained by an enclosure for performance/safety reasons. This box is desirable for reducing external factors such as

wind and dust. The enclosure must also absorb stray pulses from the cavity. The laser cavity is also desired to run indefinitely such that replacement parts are not needed under expected application. The cavity must also be placed on a flat level surface such that inconsistencies in the alignment phase cannot be attributed to the mounting surface.

Crystal cooling:

It is also expected for the pump laser to heat up the crystal which causes inconsistencies in the output of the crystal. The reduction of inconsistencies is desired for this type of product. With this in mind, the crystal cooling design should be designed with a reduction of noise in mind. It should also be desired such that the temperature of the crystal should remain constant while the system is in use. It is also desired that the main heat sink should not be intrusive within the main cavity.

The heat sink must also be able to house the crystal such that the laser is able to hit the crystal. The heat sink must be able to sufficiently clamp the crystal such that external influences do not shift the crystal placement. Complete mechanical adjustability of the heat sink is a highly desirable feature that will ease the alignment process. The crystal must also be able to have a direct line of light emission to the cavity mirrors. The heat sink itself should also be designed to withstand the expected application such that a replacement is not needed under the lifetime of the system. It is expected that the water pump system will degrade under normal operating conditions and that the pump system should be designed such that the pipes last longer than 5 years under expected application.

PID system:

The PID loop system is desired to reduce the noise in the system. The actuator is also desired to fit within an enclosure such that a single mirror can be adjusted. It is expected that the electronic equipment that controls the actuator will not fit within this enclosure due to the desire for the PID loop to be easily accessible and comprehensible.

Pump laser:

The pump laser is desired to operate under a 12V power supply. The pump laser is also desired to reduce noise in the data such that the pump laser power level remains incredibly consistent during application. The light also needs to be precisely focused onto the crystal for the system to operate as intended. A level flat beam is a highly desirable trait for when the pump beam is focused onto the crystal.

Overview:

A complete flow down chart of the project is included in appendix B.1.4. The project revolves around system isolation as well as pristine machinability for the most consistent cavity behavior. Many design attributions such as adjustability were deemed

necessary for the alignment phase of the cavity. Cavity alignment is of utmost importance for the success of the project. After alignment has been completed, the expected parts should remain stable under normal operating conditions.

Appendix B.1: Product Design Specification

Design Project: Assembly and Stabilization of a Bidirectional Comb Laser

Appendix B.1.1: Attributes

Cavity Needs				Low=1, High=5
#	Subsystem	Needs	Categorization	Importance (1-5)
1.1	Cavity	PID successfully improves stability	Performance	2
1.2	Cavity	Reduce noise in data	Performance	5
1.3	Cavity	Free Running Behavior	Performance	5
1.4	Cavity	Reduce/limit External Influences on Laser	Performance	4
1.5	Cavity	Capable of stable long term behavior	Performance	5
1.6	Cavity	Sufficient cooling of crystal	Performance	4
1.7	Cavity	Vibrational Stability Achieved	Performance	3
1.8	Cavity	Horizontal Adjustability	Performance	5
1.9	Cavity	Low Airflow	Performance	4
1.10	Cavity	Achieves Mode Locking Behavior	Performance	5
1.11	Cavity	Stable Cavity Repetition Rate	Performance	4
1.12	Cavity	Stable Crystal Placement	Performance	5
1.13	Cavity	Fixed To Standard Optics Table	Performance	5
1.14	Cavity	Flat Beam Alignment	Performance	5
1.15	Cavity	Low Expansion Within Cavity	Performance	3
1.16	Cavity	Flat Optics Table	Performance	5
1.17	Cavity	Compatibility With Standard Optics Systems	Cost	5
1.18	Cavity	Ease of machinability	Cost	2
1.19	Cavity	Product Lifetime	Cost	3
1.20	Cavity	Self contained	Safety	4
1.21	Cavity	PID Is Easily Comprehensible	Appearance	1

1.22	Cavity	Pristine And Visually Appealing	Appearance	1
1.23	Cavity	Reduce Dust Contamination	Appearance	4

Pump laser Needs				Low=1, High=5
#	Subsystem	Needs	Categorization	Importance (1-5)
2.1	Pump	Flat alignment	Performance	5
2.2	Pump	Focused Beam Point of Contact Within Crystal	Performance	5
2.3	Pump	Adjustable Output	Performance	4
2.4	Pump	Beam Is At The Correct Crystal Height	Performance	5
2.5	Pump	Single Light Frequency	Performance	5
2.6	Pump	Long Term Stability	Performance	5
2.7	Pump	Focus Lens Onto The Crystal	Performance	5
2.8	Pump	Contained	Safety	5
2.9	Pump	Product Lifetime	Cost	5

Heat Sink Needs				Low=1, High=5
#	Subsystem	Needs	Categorization	Importance (1-5)
3.1	Heat Sink	Liquid cooling	Performance	4
3.2	Heat Sink	Set Heat Sink Flow Rate	Performance	2
3.3	Heat Sink	Cooling Stability	Performance	5
3.4	Heat Sink	High Thermal Conductivity	Performance	4
3.5	Heat Sink	Mounting Holes	Performance	5
3.6	Heat Sink	Clamping system	Performance	5
3.7	Heat Sink	Open Horizontal Plane For Light Emission	Performance	5
3.8	Heat Sink	Adjustability	Performance	5
3.9	Heat Sink	Ease Of Manufacturability	Cost	2
3.10	Heat Sink	Product Lifetime	Cost	3
3.11	Heat Sink	Pristine And Visually Appealing	Appearance	1

Appendix B.1.2: Performance Criteria

Metric	Needs	Units	Marginal Value	Ideal Value
Repetition Frequency Stability	1.1, 1.5, 1.11, 1.3	MHz	<1	<.5
Crystal Temperature	1.4, 1.5, 1.6, 1.11, 3.1, 3.2, 3.2	K	<300	<293
Material Choice	1.12, 1.15, 1.18, 3.4	W/mK $\mu\text{m}/\text{mK}$ K	>250W/mK >23 $\mu\text{m}/\text{mK}$ >	400W/mK 15 $\mu\text{m}/\text{mK}$ >
Noise Under 1Mhz	1.2, 1.4, 1.7	Db	>-10Db	>-20Db
Reduce Vibrational Effects From 0 to 500 Hz	1.2, 1.4, 1.7	mm/N	>10 ⁻³	>10 ⁻⁴
Precise Mechanical Adjustment	1.8, 1.14, 2.1, 2.2, 2.4, 3.8	mm	1	<1
Fluid Flow Rate	2.6, 3.1, 3.2, 3.3	kg/min	>.1	>.5
Screw/ Hole Spacing	1.13, 3.5, 3.9, 1.17	In/in	.25/ 1	.25/ 1
Size	1.13, 1.21, 2.8	in x in	<22x22	<22x18
Running Time	1.3, 1.5, 1.10, 2.6, 3.3	hours	>12	>24
Output	1.3, 1.10	Wave type	Pulsed Gaussian frequency combs	Pulsed Gaussian frequency combs
Air Flow	1.5, 1.9	M/s	<.05	<.01
Stray Beam Absorption	1.20, 2.7	%	100%	100%
Product lifetime	1.19, 2.9, 3.10	Years	>5	>10
Pump Focusing Lens	2.7	cm	<8	<5
Flat Table	1.16, 1.14	mm	+-.002	+-.001

Appendix 3: Budget

Covered Costs and Preliminary Future Budget: \$7250 in Total

Covered Costs: \$5700

- Various clamps
- Various mirrors/lenses
- Piezoelectrics
- Beamsplitters
- Titanium Sapphire Crystal

Preliminary Future Budget: ~\$1550

- Circa 16"x16" Stainless Steel Breadboard : \$700
- 4 x 1/2" Mirror mounts : \$400-800
- Cooling Tubing : \$50
- Shielding Container : \$100

Appendix C : Customer Needs

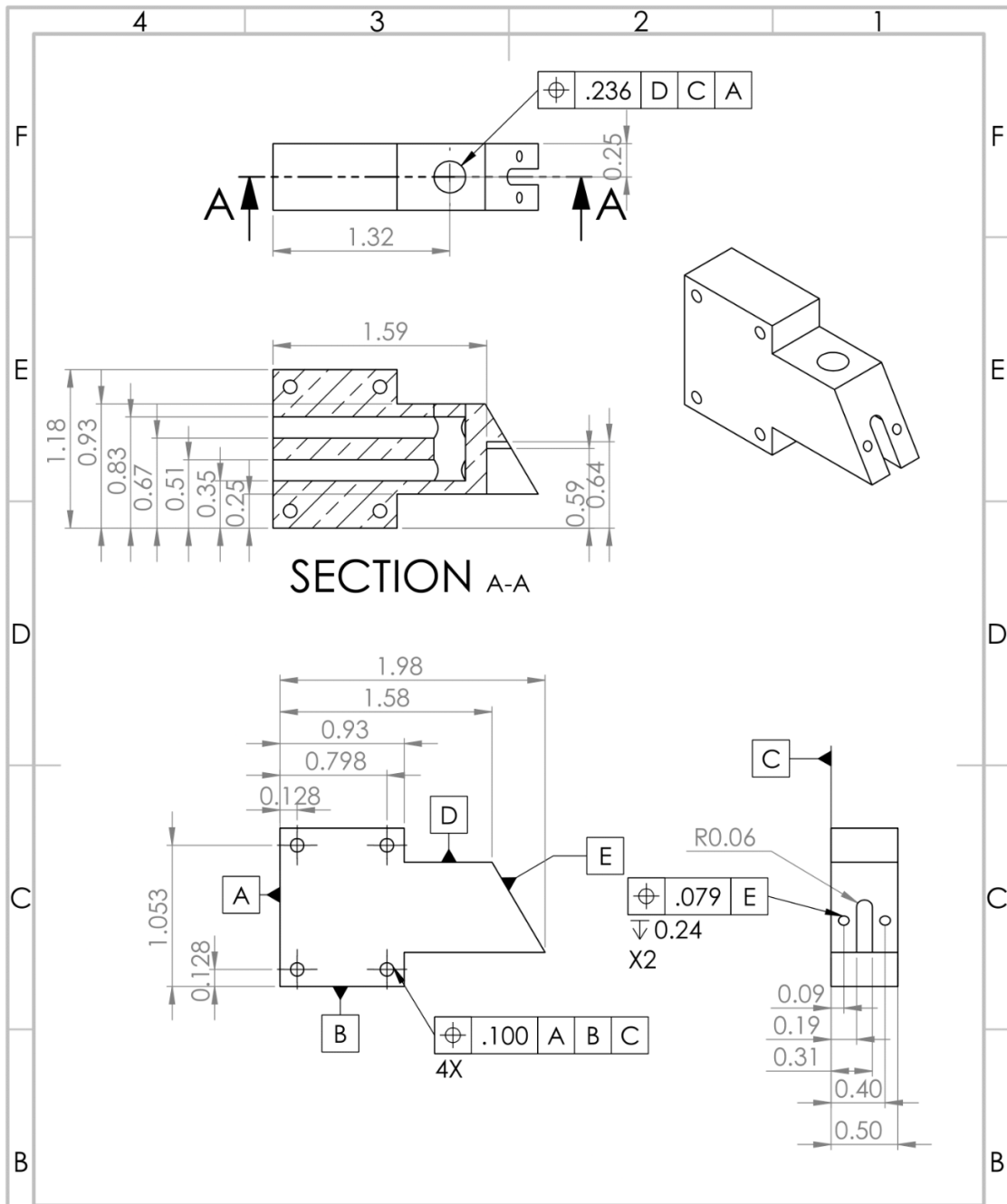
Customer Needs

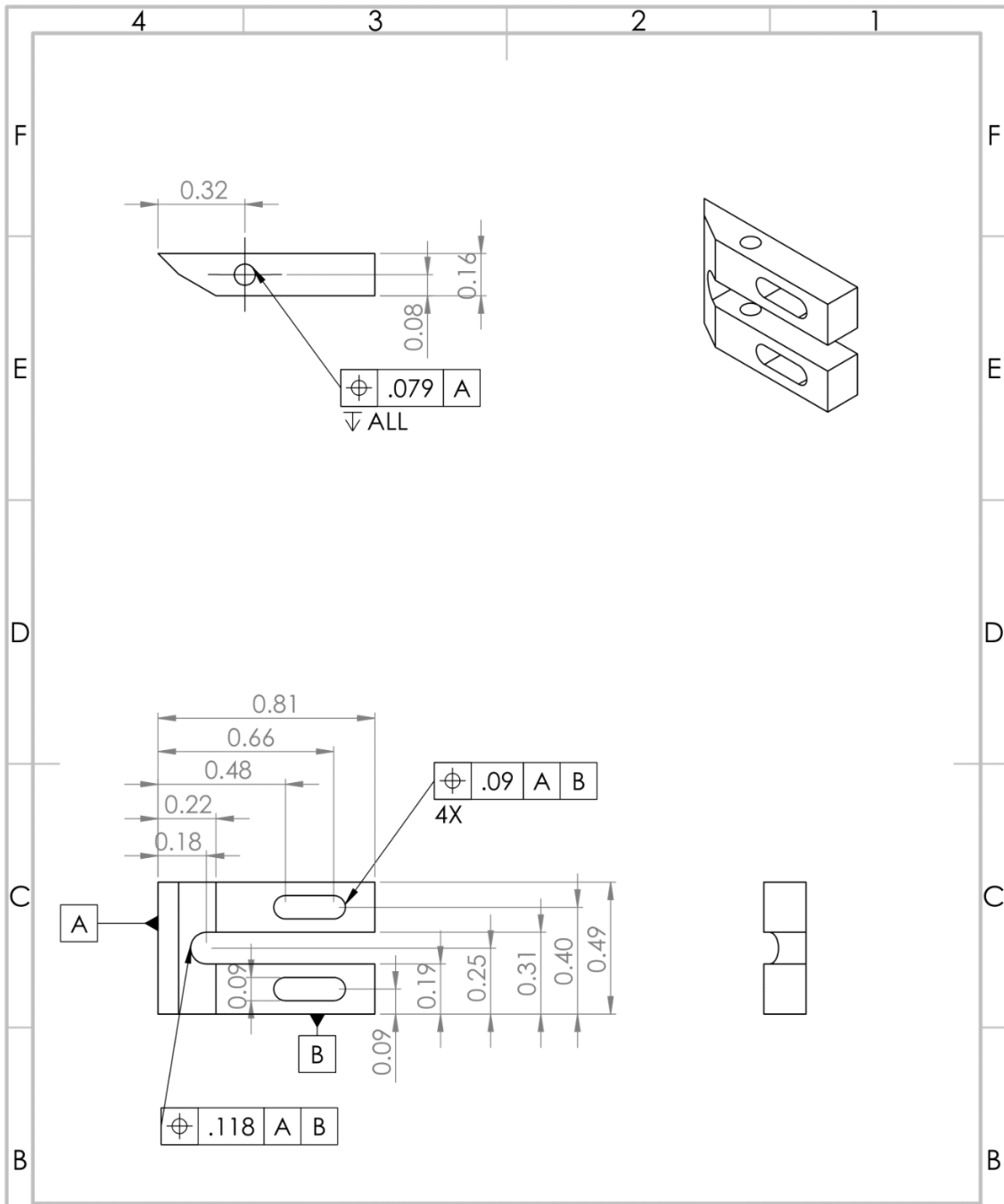
Table 1: Attribute Categorization

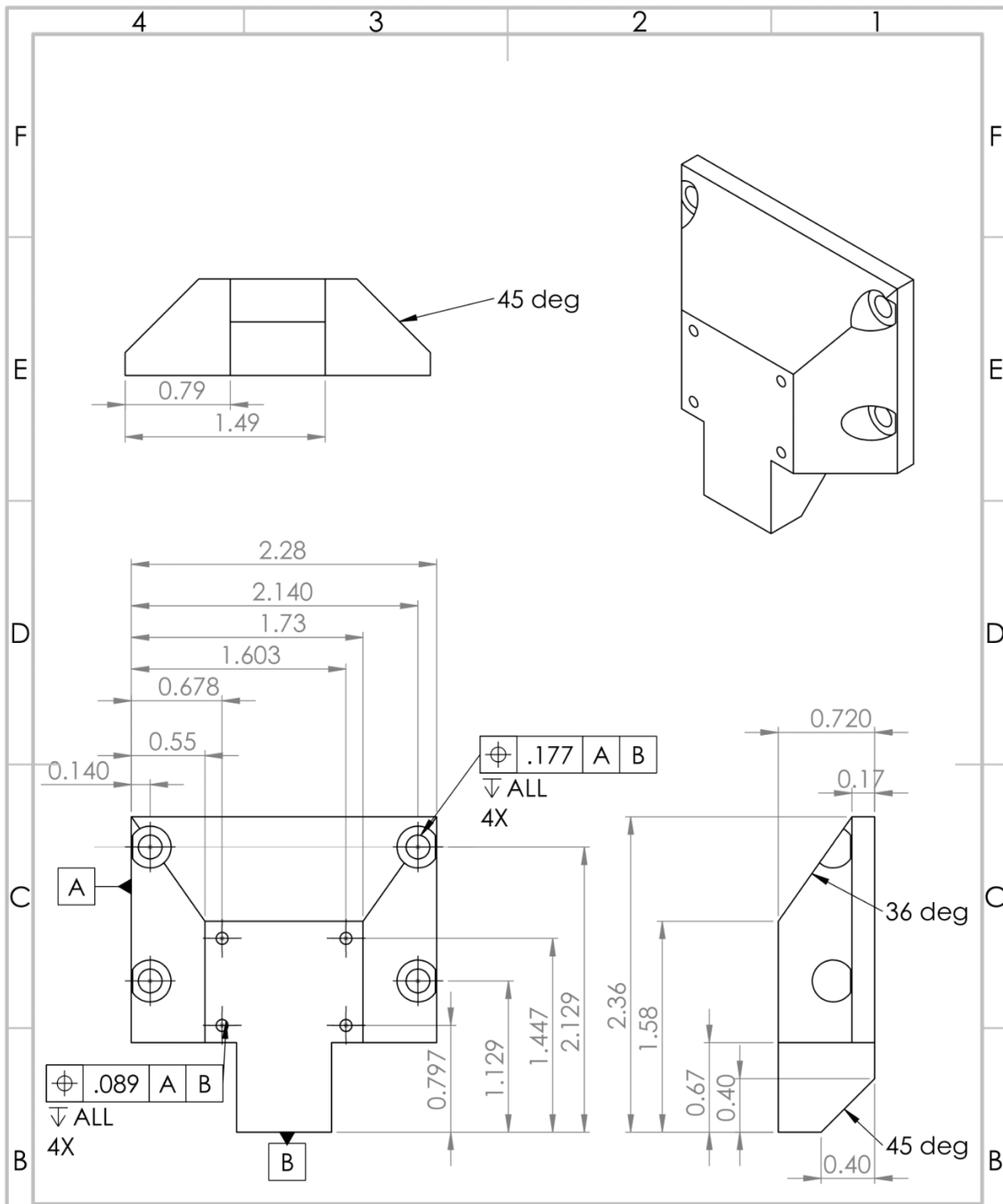
Performance	Safety	Appearance	Cost
1.1 No Free Running Behavior	2.1 Enclosed Container	3.1 PID is easily comprehensible	4.1 No replacement parts needed
1.2 PID successfully improves stability			
1.3 Reduce noise in data	2.2 No sharp edges	3.2 Fixed to the table	
1.4 Reduce/limit External Influences on Laser			
1.5 Capable of running indefinitely	C. Door closed	3.3 Dust free	
1.6 Capable of Power Cycling			
1.7 Sufficient cooling of crystal	C. Safety goggles	3.4 No audible noise	
1.8 Temperature controlled		3.5 Pristine and visually appealing	
1.9 Vibrational Stability Achieved			
1.10 Low airflow		C. Dimensions: 40"x40"x10"	
1.11 Set flow rate			
1.12 Assembly process repeatable			
1.13 mirror adjustability			
1.14 1 GHz repetition rate			
C. Subject to Laser room safety override			
F. PID control achieves mode locking behavior			
F. Identity materials and amount present through absorption spectroscopy			

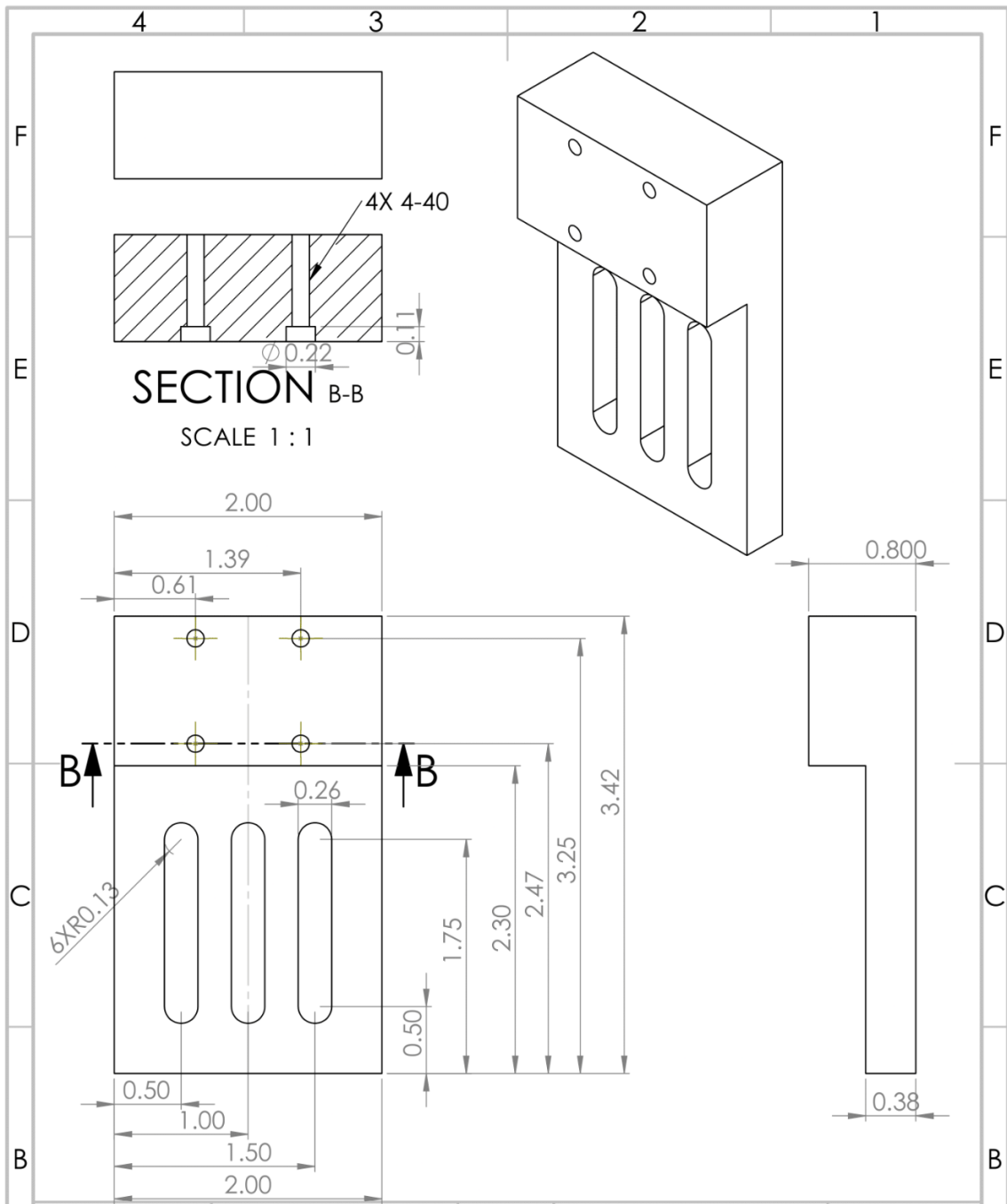
Appendix D : Sketches

D.1: Heat Sink:

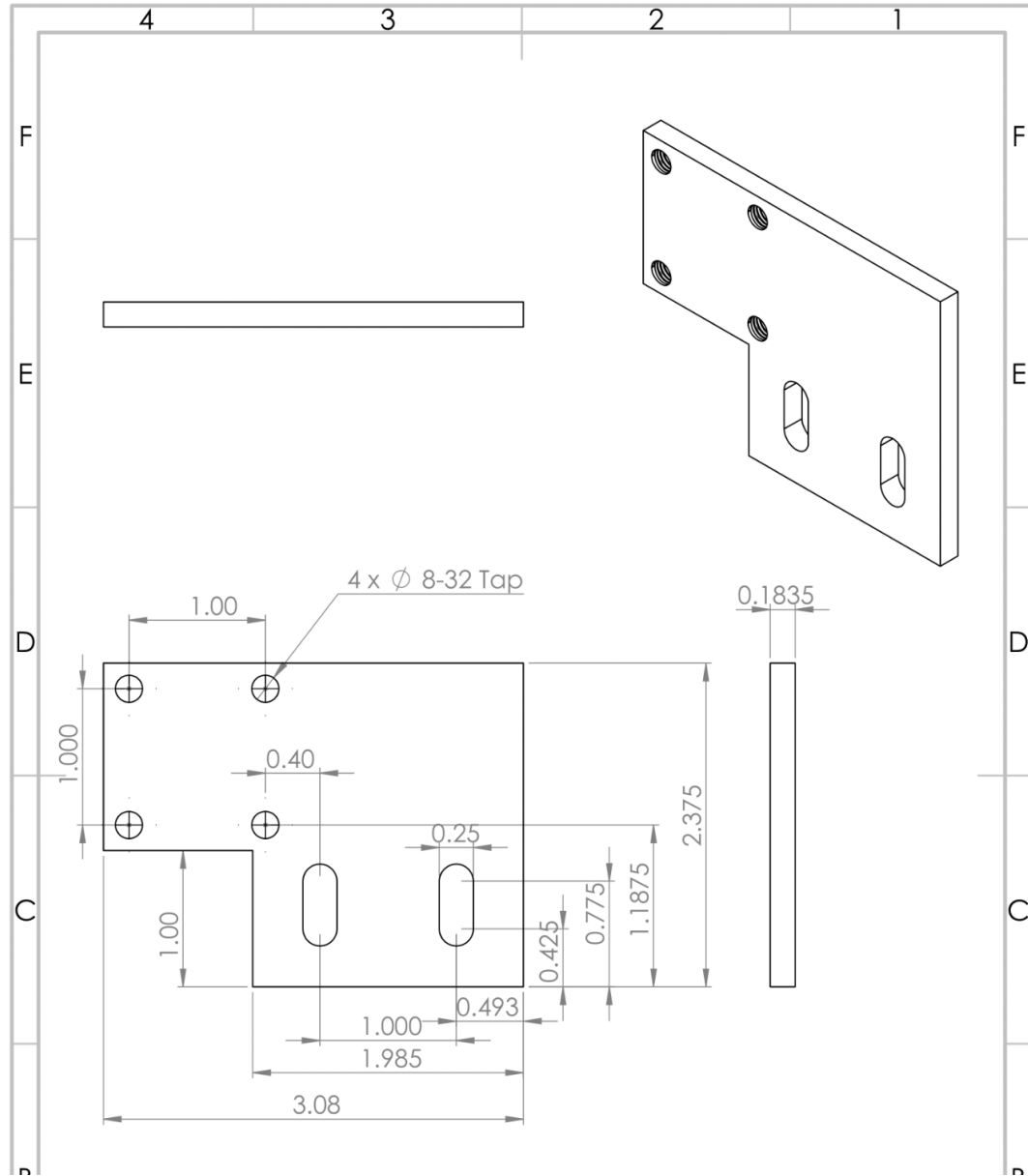


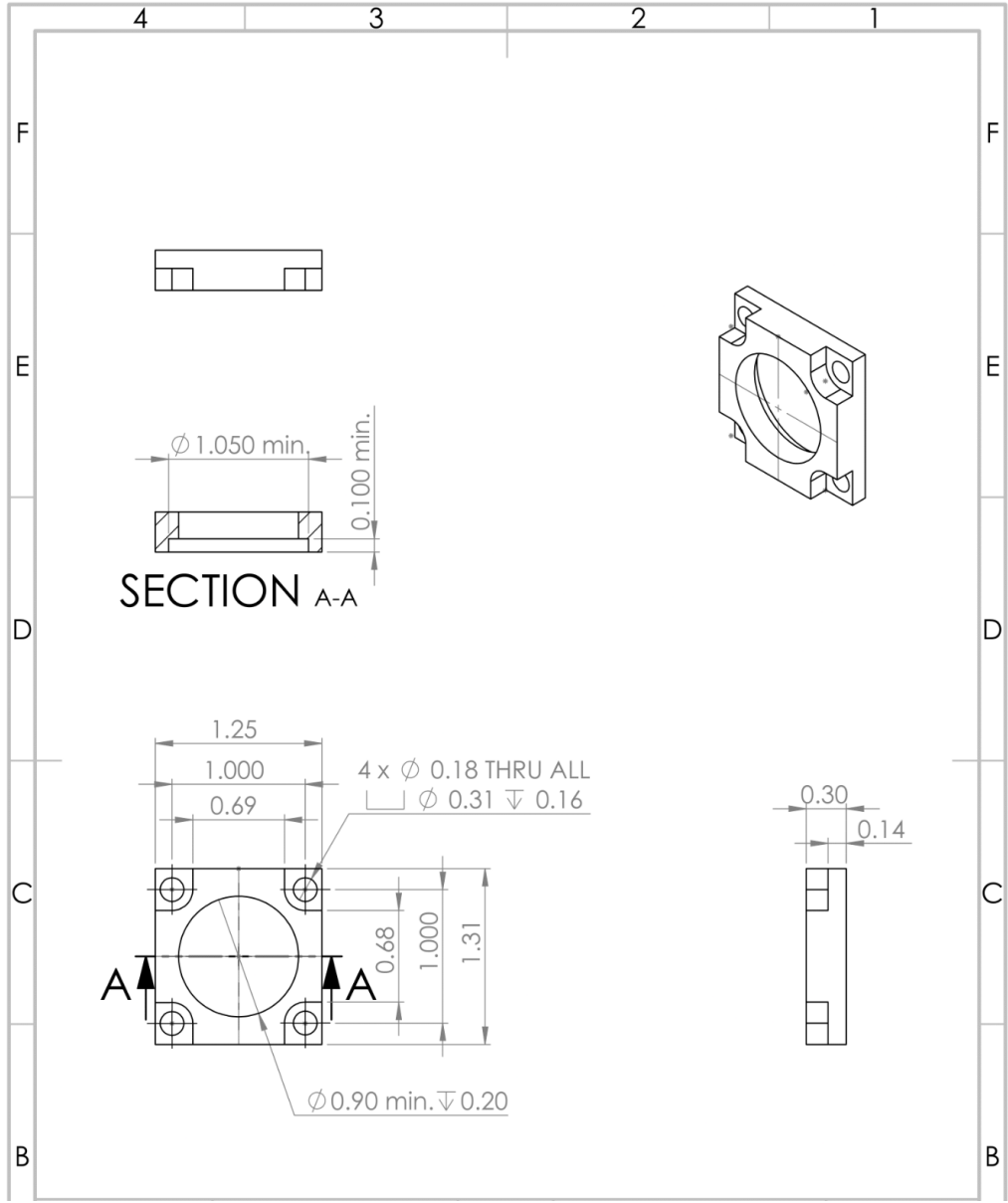




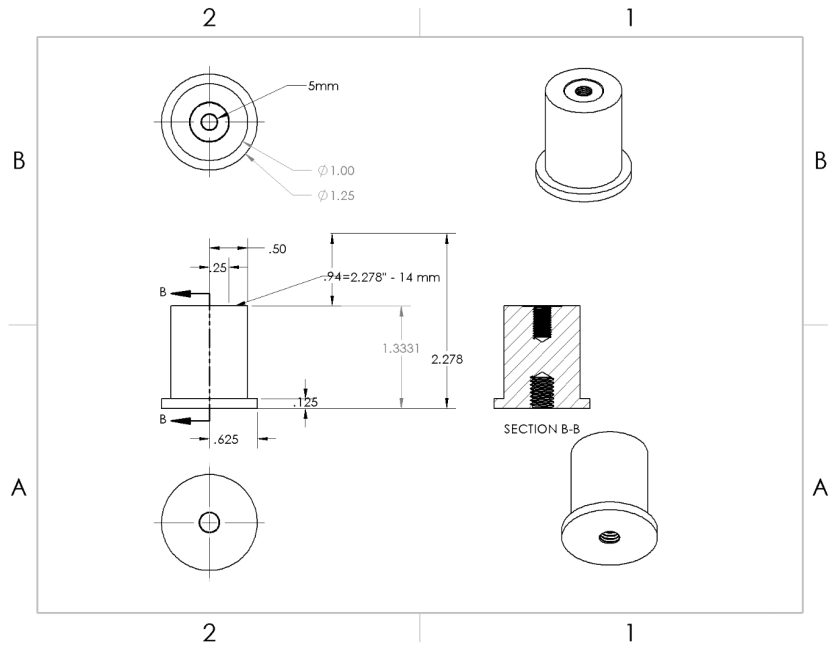


D.2: Focus Lens:

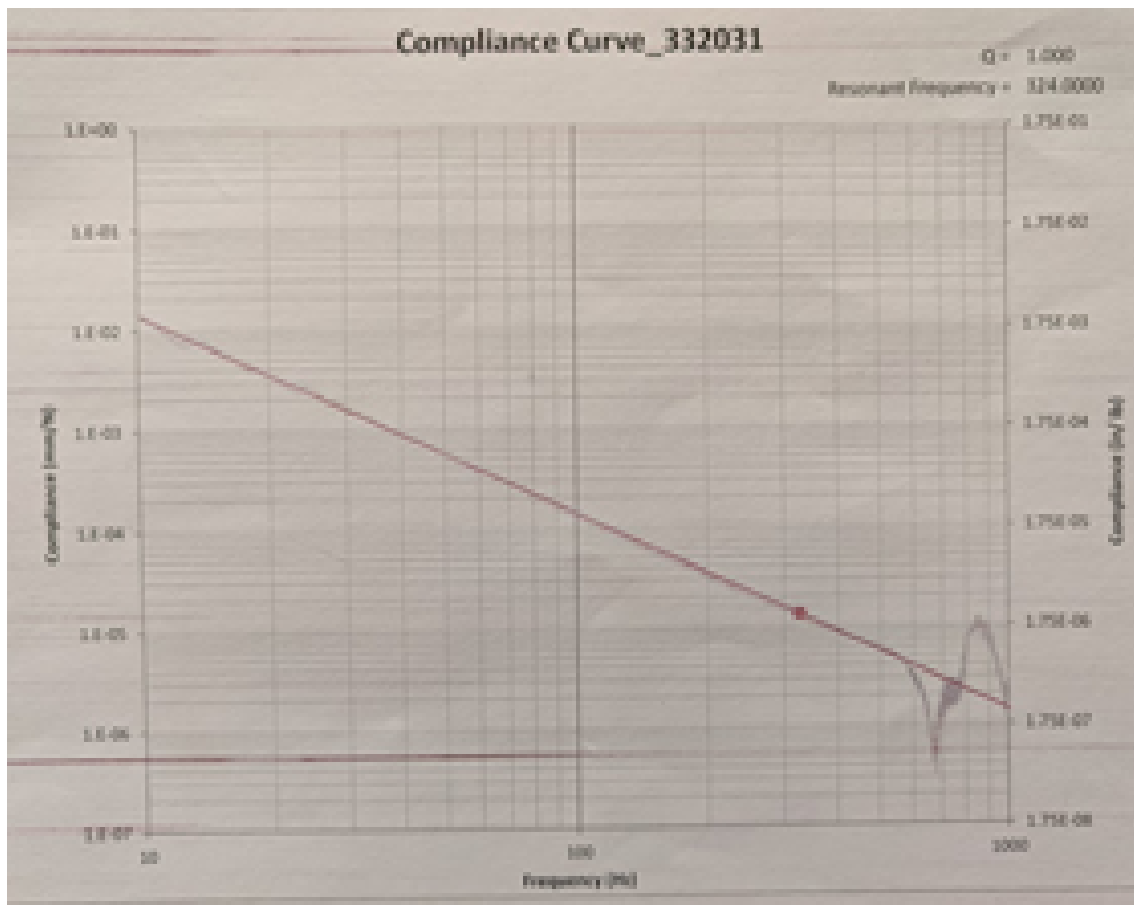
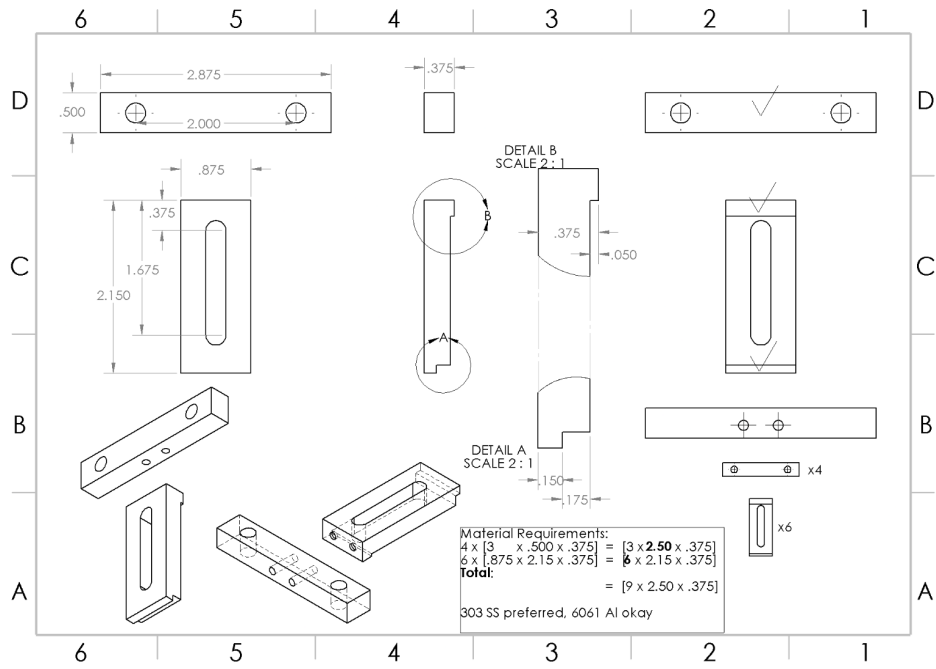




D.3 Chirped mirror:



D.4 BreadBoard Clamps



Appendix E : Gantt Chart

Task	2020		2021							
	Sept-Nov	Dec	Jan	Feb	Mar 1-15	Mar 16-31	Apr 1-15	Apr 16-30	May 1-15	May 16-28
Research	[Gray]		[Red]							
Consult Experts	[Red]		[Red]							
Initial Lab Access	[Gray]		[Red]							
Design	[Gray]		[Red]							
In-House Components	[Gray]		[Red]							
Parts Selection	[Gray]		[Red]							
Manufacturing	[Gray]		[Red]							
Preliminary Assembly	[Gray]		[Red]							
Periscope	[Gray]		[Red]							
Primary Alignment	[Gray]		[Red]							
Cooling System	[Gray]		[Red]							
Box and Hinge	[Gray]		[Red]							
Iterative Redesign	[Gray]		[Red]							
Fine Tune Laser	[Gray]		[Red]							
Improve Mode locking	[Gray]		[Red]							
Lasing/Modelocking Analysis	[Gray]		[Red]							
Temperature Analysis	[Gray]		[Red]							
Solidworks	[Red]		[Red]							
Weekly Hours	[Gray]		[Gray]							

KEY DATE

Gray = Plan, Red = Actual

Appendix F : Budget

Table 9.1: Pre Secured Covered Costs

Secured Covered	
Part	Total Cost
M-SDS25 stage	\$536
UMR5.16 stage	\$289
TSX-1D stage	\$194
curved mirror	\$817
curved mirror	\$817
chirped mirror	\$373
1/2" Waveplate	\$1,040
Titanium Sapphire Crystal	\$1,600
Output coupler	\$320
Piezoelectric Actuator	\$310
∅25.4mm Mirror	\$295
Beamsplitter	\$210
Long pass filter	\$160
Prism mount	\$80
1/2" Beam splitter mount	\$80
Convex lens	\$70
km100pm	\$80
Km100 x 8	\$320
U50-s mirror mounts x 3	\$210
Lens mounting ring	\$32
Miscellaneous additional parts	\$103
Grand Total (incl tax):	\$7,936

Table 9.2: Mechanical Engineering Department Funding

Mechanical Engineering Department Funding	
Part	Total Cost
Stainless Steel Breadboard 18x18x2.4 in	\$800
1/2" Mirror mounts w/ Micrometers	\$800
Grand Total Requested:	\$1,600

Table 9.3: Purchased Parts Costs

Purchased Parts	Total Cost
Plastic Clear Tubing	\$10.50
Polycarbonate Round Tube	\$3.36
Universal-Thread Push-to-Connect Tube Fitting for Air and Water	\$22.64
Pipe Fitting Straight Connector with Hex	\$27.92
Brass Ball Valve with Lever Handle Female	\$13.03
Optical Rail	\$35.00
Brass Round Tube	\$11.56
Tube Fitting for Water - Straight Adapter with HexMale	\$2.76
Universal-Thread Push-to-Connect Tube Fittings	\$19.04
Tube Fitting for Air and Water - Adapter Female	\$3.57
Tube Fitting for Air and Water - AdapterFemale	\$3.57
Tube Fitting for Air and Water - Straight Adapter with HexMale	\$2.76
Lid Stays, Folding Lid Support Hinges	\$23.98
Cast Acrylic - Opaque Black 19x19 in	\$74.20
Cast Acrylic - Opaque Black 10x18 in	\$74.00
Cast Acrylic - Opaque Black 10x19 in	\$78.10
Mirror Mount (2) 100-TPI Allen-Keys	\$201.00
Thorlabs LB1 Beam Block	\$107.12
ARN-2-M AILERON STAY	\$82.50
Breadboard	\$761.00
Grand Total (incl tax):	\$1,557.61

Appendix G : safety requirements

G.1: OSHA Control Measures

Control measures	----- Class -----					
	I	IA	II	IIIA	IIIB	IV
Protective housing	X	X	X	X	X	X
Without protective housing	-- LSO shall establish alternate controls --					
Interlocks on protective housing	a	a	a	X	X	X
Service access panel	b	b	b	b	b	X
Key switch master	—	—	—	—	•	X
Viewing portals	—	—	◇	◇	◇	◇
Collecting optics	—	—	◇	◇	◇	◇
Totally open beam path	—	—	—	—	X	X
Limited open beam path	—	—	—	—	X	X
Remote interlock connector	—	—	—	—	•	X
Beram stop or attenuator	—	—	—	•	•	X
Activation warning system	—	—	—	—	•	X
Emission delay	—	—	—	—	—	•
Class IIIB laser controlled area	—	—	—	—	X	—
Class IV laser controlled area	—	—	—	—	—	X
Laser outdoor controls	—	—	—	—	X	X
Temporary laser controlled area	b	b	b	b	—	—
Remote firing & monitoring	—	—	—	—	—	•
Labels	—	X	X	X	X	X
Area posting	—	—	•	•	X	X
Administrative & procedural controls	—	X	X	X	X	X
Standard operating procedures	—	—	—	—	•	X
Output emission limitations	—	—	—	--LSO determines--		
Education and training	—	—	—	X	X	X
Authorized personnel	—	—	—	—	X	X

Alignment procedures	_	_	X	X	X	X
Eye protection	_	_	_	_	•	X
Spectator control	_	_	_	_	•	X
Service personnel	b	b	b	b	X	X
Laser demonstration	_	_	X	X	X	X
Laser fiber optics	_	_	X	X	X	X

Key:

X = Shall.

a. = Shall if embedded Class IIIA, Class IIIB, Class IV.

b. = Shall if embedded ClassIIIB or Class IV.

_ = No requirement.

• = Should. ◊ = Shall if MPE is exceeded.

G.2 Laser Safety Goggles:

Goggles used in the lab have a rating of 7+ in the optical wavelength range our laser operates in (approx. 700-1100 nm) and (532 nm)

OD (Optical Density)	Transmission in %	Attenuation Factor
0	100%	1:1
1	10%	1:10
2	1%	1:100
3	0.1%	1:1000
4	0.01%	1:10000
5	0.001%	1:100000
6	0.0001%	1:10 ⁶
7	0.00001%	1:10 ⁷
7+	<0.00001%	1:>10 ⁷

Appendix H : Senior Design Presentation Slides

5/28/2021



Senior Design Conference

Bi-directional Kerr-Lens Mode-Locked Ti-Sapphire Laser

Ricky Arnold, Stratos Koutroulis, Dylan Meyer

Advisors: Dr. Bachana Lomsadze, Dr. Drazen Fabris

Senior Design Conference | School of Engineering | Santa Clara University

1

Overview

- Motivation
- Design Challenges
- Laser Knowledge
- Subsystems
- Alignment
- Lasing/Dual Comb
- Future Plans
- Timeline
- Budget Analysis

Senior Design Conference | School of Engineering | Santa Clara University

2

Purpose

Physics Department needs a second Dual Comb Spectroscopy Laser.

- Current one exhibits **drifting behavior**
 - Addressing that problem changes a key part of the design, causing a cascade of other design challenges.
- Additional opportunities to improve many components

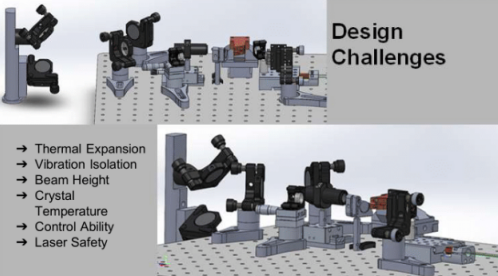
Intended Use

- Dual comb absorption spectroscopy;
 - **high resolution, high accuracy, and data acquisition in under a second**
 - Absorption spectroscopy is the process of mapping a sample's wavelength absorption pattern to identify elements within.

Senior Design Conference | School of Engineering | Santa Clara University

3

Design Challenges



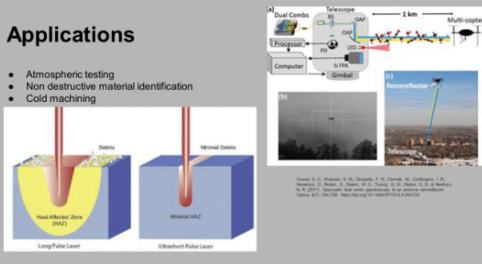
- Thermal Expansion
- Vibration Isolation
- Beam Height
- Crystal Temperature
- Control Ability
- Laser Safety

Senior Design Conference | School of Engineering | Santa Clara University

4

Applications

- Atmospheric testing
- Non destructive material identification
- Cold machining

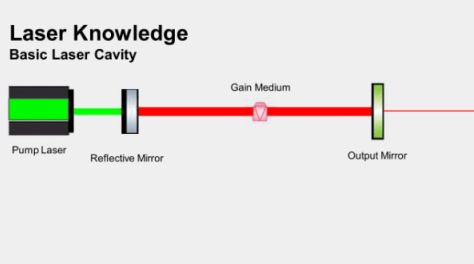


Senior Design Conference | School of Engineering | Santa Clara University

5

Laser Knowledge

Basic Laser Cavity



Senior Design Conference | School of Engineering | Santa Clara University

6

Laser Knowledge

Light Amplification by Stimulated Emission of Radiation

Green pump excites electron to e1.

e1 electron will quickly decay to e2 after ~0.1 ps.

e2 electron can stay in this region for ~3.2µs. It can emit a spectrum of red-infrared light to relax back to ground.

Senior Design Conference | School of Engineering | Santa Clara University

7

Pulsing Animation

Senior Design Conference | School of Engineering | Santa Clara University

8

FOURIER TRANSFORM INFRARED SPECTROSCOPY

Resolution: $df = \frac{c}{dx}$

Senior Design Conference | School of Engineering | Santa Clara University

9

Laser Knowledge

Need: pulses that scan over each other

Senior Design Conference | School of Engineering | Santa Clara University

10

Laser Knowledge

Cavity configuration

Cavity Length: 40.3 cm
Freq: 744 MHz

Senior Design Conference | School of Engineering | Santa Clara University

11

Laser Knowledge

Gain Medium

- Ti:Sapphire crystal
 - Solid state gain medium
 - Brewster cut Ti:Sapphire crystal
 - 3mm x 5mm x 5mm
- Lasing properties
 - Wide emission spectrum and wide wavelength tunability
 - Non linear gain medium
 - Intensity dependent index of refraction (Kerr effect)
 - Self focusing lens effect
 - Self mode locking (Pulsing)
 - Temperature dependent efficiency profile

Senior Design Conference | School of Engineering | Santa Clara University

12

Laser Knowledge Frequency Comb Generation

- 2 stable configurations
 - Continuous wave
 - Pulsed (mode locked)
- Frequency combs
 - Standing wave (In Resonance)
 - Cavity dependent spacing of comb teeth
- Generation of frequency combs which are evenly spaced

Spacing: $\frac{c}{2L}$

Senior Design Conference | School of Engineering | Santa Clara University

13

Laser Knowledge Dual Comb

- Two similar pulses generated from a single cavity
- Slightly altered intensity profile from each arm
- Slight repetition delay between pulses

Senior Design Conference | School of Engineering | Santa Clara University

14

Laser Knowledge Dual Comb Spectroscopy

- $f_{rep} \approx 1\text{GHz}$ and $\Delta f \approx 100\text{-}2000\text{ Hz}$
- Optical frequency = 250-400 THz
- Beat patterns (heterodyne mixing) of pulses
- Mixing of both arms effectively maps a signal in the THz to the MHz
- Compression of comb teeth into the RF domain with a spacing of $\Delta f!$

$\cos(2\pi(f_1 - f_2)) + \cos(2\pi(f_1 + f_2))$

Senior Design Conference | School of Engineering | Santa Clara University

15

Laser Knowledge Chirp

- Group velocity dispersion from intensity dependent profile
- Chirped mirrors fix solution which allows wavelengths to be reflected at different depths within the mirror
- Mirror operates within wavelength range of 700 to 900 nm

Senior Design Conference | School of Engineering | Santa Clara University

16

Solving Design Challenges

- Thermal Expansion
- Vibration Isolation
- Beam Height
- Crystal
- Temperature Control Ability
- Laser Safety

Senior Design Conference | School of Engineering | Santa Clara University

17

Subsystems

- Prefab Optical Components
- Designed and Manufactured Parts
- Heat Sink Analysis
- Operational Safety
- Piezoelectric Stabilization (work in progress)

Senior Design Conference | School of Engineering | Santa Clara University

18

Prefabricated Optical Components

Honeycomb 430 Steel Breadboard
 Pump Laser
 Laser Containments
 Mirrors and Mirror Mounts

Senior Design Conference | School of Engineering | Santa Clara University

19

Designed and Manufactured Parts

Senior Design Conference | School of Engineering | Santa Clara University

20

Subsystem Breadboard

Design Requirements

- Dampen vibration
- Reduce thermal expansion
- Mount standard optical equipment
- Provide enough space for cavity components

Solution

- 18"x18" (457 mm x 457 mm) steel breadboard
- ±0.1 mm flatness over 600 mm x 600 mm
- 6 Clamps mount breadboard to optics table

Senior Design Conference | School of Engineering | Santa Clara University

21

Subsystem Pump Laser

Problem:

- Pump laser beam height: 2.217" (5.63 cm)
- Crystal height: 4.637" (11.78 cm)

Solution:

Design an adjustable periscope

- Bottom mirror: 2" (5.08cm)
- Top mirror: 1.5" (3.81cm)

Adjustable Periscope mounted to the optical table

Application of the Periscope which elevates beam height and flattens beam

Senior Design Conference | School of Engineering | Santa Clara University

22

Subsystem Focus Lens

Focus lens:

- Focal distance: ~4 cm

Solution:

- Circular mount provides rotational adjustability
- Rigid clamping
- Linear stage changes focal location

Bottom Plate | Circular Mount

Senior Design Conference | School of Engineering | Santa Clara University

23

Subsystem Curved mirrors

Design Requirements:

- Vertical/horizontal angle adjustability
- Beam focal point within crystal
- Astigmatism compensation

Solutions:

- Linear Stage
- Mirrors transmit green, reflect red/infrared
- Mirror angled at 19.6°

Senior Design Conference | School of Engineering | Santa Clara University

24

Subsystem

Chirped mirror and output mirror

Senior Design Conference | School of Engineering | Santa Clara University

25

Manufacturing of Parts

- Stainless steel:**
 - Mirror stands
 - Periscope stand
 - Stand base
- Copper:**
 - Heat sink
- Aluminum:**
 - Square spacers
 - Heat sink mount
- Acrylic:**
 - Main cavity container and cutouts
 - Periscope box
 - L-shaped box for pre cavity mirrors

Senior Design Conference | School of Engineering | Santa Clara University

26

Subsystem

Heat Sink Design Requirements

Design Requirements:

- Clamp crystal
- Elevate crystal to 2.275"
- Adjustable
- Keep crystal at room temperature
- small footprint within cavity

Senior Design Conference | School of Engineering | Santa Clara University

27

Heat Sink Analysis

- Water Pump:**
 - 0.17 L/min
 - 20°C water
- Heat Sink:**
 - OFHC Copper
 - 394 W/mK
- Ti:Sapphire crystal:**
 - Max 6 watts of heat
 - 34 W/mK

Assumptions:

- 1D heat flow
- No contact resistance between crystal and copper mount
- Simplified geometry
- Neglected screws
- Curved circular duct approximation

Senior Design Conference | School of Engineering | Santa Clara University

28

Heat Sink Analysis

Analytical Results:

- Max temperature change of 7.2°C at the contact point of the crystal and the heat sink
- Theoretical max temperature change of 11.7°C within the center of the crystal

T1:	T2:	T3:	T4:	T5:	T6:
4.7°C	5°C	5.2°C	5.8°C	6.9°C	7.2°C

Senior Design Conference | School of Engineering | Santa Clara University

29

Subsystem

Heat Sink Analysis CFD results

Results

- Simulations done in STAR-CCM+
- Adequate flow through heat sink

Senior Design Conference | School of Engineering | Santa Clara University

30

Subsystem Heat sink installation

Senior Design Conference School of Engineering | Santa Clara University

31

Subsystem Containment-Pump Beam

OSHA classifications:
Pump laser class 4 laser system
(> CW: 500 mW)

Safety requirements

- Protective housing of pump laser
- Tubes for pump beam
- Protective housing of periscope

Senior Design Conference School of Engineering | Santa Clara University

32

Subsystem Containment-Main Cavity

OSHA classifies main cavity as a class 4 laser system (> pulsed: 10 J/cm²)

Safety requirements

- Containment box
- Beam blocks

Application of beam block

Senior Design Conference School of Engineering | Santa Clara University

33

Laser safety

Both laser systems are classified as a class 4 laser system.

OSHA Technical Manual (OTM) Section III: Chapter 6 safety requirements

- PPE (safety goggles, fully clothed)
- Warning signs
- Laser interlock system
- Alignment safety protocol
- Defined Nominal Hazard Zone (NHZ)
- Administrative controls

Senior Design Conference School of Engineering | Santa Clara University

34

Laser Setup Progress & Future Plans

- Alignment
- Modelocking
- Power Level Testing and Result Analysis
- Application of PID

Senior Design Conference School of Engineering | Santa Clara University

35

Alignment and Mode Locking

Goal:

- For 6 W, mode locked arms are 350 mW each
- Goal is 11.4% efficiency, 5.7% per arm

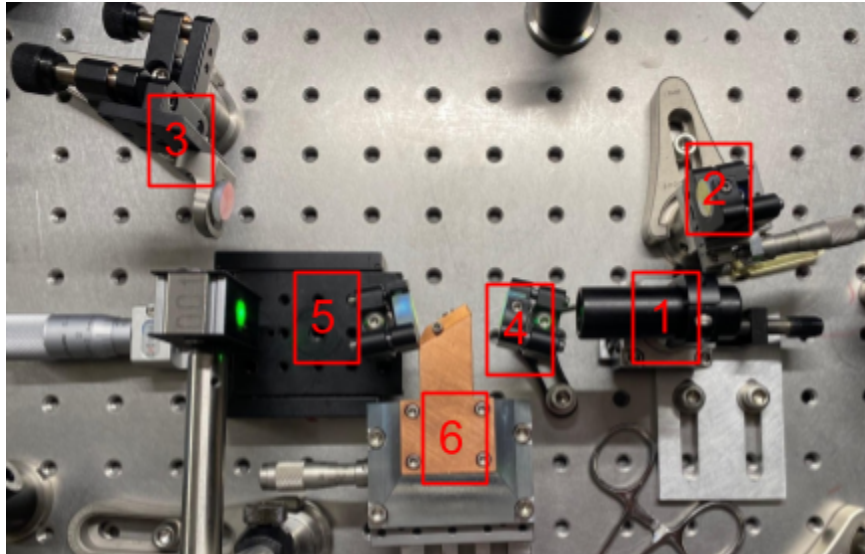
Results:

- At the moment, we have reached 363 mW at a power level of 4.53 W.
- 8% efficiency in a single arm

Senior Design Conference School of Engineering | Santa Clara University

36

Appendix I: Optical Equipment used



Key:	Part name:	Linear stage	Mirror mount	Clamps
1	Focus lens	Newport TSX-1D	SM05M20	N/A
2	Chirped mirror	Newport M-SDS25	Newport U50-S	Newport optical 1" clamping fork
3	Output mirror	Thorlabs KM-100PM	Polaris B05S 1/2"	Newport 1" clamping fork
4	Curved mirror right	N/A	Newport U50-S	Thorlabs MSC2
5	Curved mirror left	Newport 9064-X-M	Newport U50-S	N/A
6	Heatsink/crystal mount	Newport UMR5.16	N/A	NA

Appendix J: Crystal Background Information

Thermal Behavior

For the most part, all of the energy from the beam continues through the crystal and out into the mirrors. However, a small amount stays in the crystal and causes it to heat up a certain amount. In a collaborative effort titled, *Radiative and non-radiative transitions of excited Ti^{3+} cations in sapphire*, a group of 5 researchers discuss the explanation behind the physical phenomenon. The crystal has a fluorescent quantum efficiency of 68% [12]. This number represents the amount of energy in the form of photons emitted divided by the amount initially absorbed.

The lattice structure of a crystal also has implications for the behavior of the crystal during lasing. Sidney Perkowitz discusses this in depth in her article on Phonons. Phonon describes how a crystal lattice oscillates at a uniform frequency. This vibration is caused by atoms in the lattice that bounce off of each other continuously. The bouncing causes the atoms to have their own thermal energy that by itself or in addition to external forces imparted on the crystal, makes the lattice move. The material containing the lattice structures has heat and sound waves moving through it due to this phenomenon. In heat generation and transfer, phonons determine how much heat is required from the outside in order to heat up the material itself [18]. When there are more phonons, it is easier because the phonons are already causing internal heat generation themselves. This can make it more difficult to quantify and control how much heat can be dissipated by a heat exchanger, such as the copper one that is used on this project's particular setup. Phonons give crystals their properties of heat generation and conductivity which can be found in the table in section 1.5 [7].

Medium Characteristics e.g. Wavelength Bands

Within the crystal field, localized ions transition from location to location. These transitions are necessary to understanding the crystal's absorption spectrum referred to in Fig. 1.11. There are six of these transitions found in the Ti to Eg energy levels. When they are summed together, the absorption spectrum is revealed [23]. Understanding the lattice behavior in the crystal is also very important because the lattice oscillation affects the general picture of the absorption spectrum that the summation of the ion transitions provides [23]. Specifically, the lattice oscillation works to broaden and shift the absorption spectrum. This effect is due to the fact that the oscillation affects the electronic energy levels and thus the crystal field. How features of the crystal affect the energy field, therefore, can be seen as the most important parameter when figuring out whether or not the examined feature affects the absorption spectrum. Ti:Sapphire crystals typically have a large absorption band from 450 nm to 570 nm. Thus it works well given the specifications of the laser beam, being 532 nm.

Doping Level

Doping level, or doping concentration, is a feature of crystals used in lasers that provides much insight into the properties and functionality of both a crystal and the laser. Dr. Rüdiger Paschotta talks about this important parameter in his encyclopedia [24]. The value is defined as the concentration of laser active ions in a laser gain medium. There are a few ways to categorize this doping level. The first is treating it as the molar percentage of the dopant, represented as %_{at}. For a Ti:Sapphire crystal, the Ti³⁺ is the dopant that is being used to replace the Al₂ in the Al₂O₃. Another way of thinking about doping level is number density, which helps to evaluate the absorption and gain values of a laser beam.

Additionally, a high doping level in a crystal increases the temperature in a system. In one of his other encyclopedias, one that is focused more generally on Ti:Sapphire lasers, Dr. Paschotta explains that this can lead to mechanical stress and thermal lensing in the system. For a Ti:Sapphire crystal, the doping level is most often fairly low and hover around either 0.15 and 0.25% [7]. A higher value would not be compatible with any good quality of crystal.

Brewster Angle

The last feature of the crystal that affects its performance is the angle at which its cut, in this case, a Brewster angle. Cutting at a brewster angle allows for the beam to follow a straight path with the least possible reflection away from its intended path [25]. The angle also addresses astigmatism, which is a function of the curve of the lenses and the index of refraction of the crystal [26].

Appendix K: Power Extraction Efficiency

When it comes to any machine, efficiency is one of the most important parameters to think about. How well a system deals with the power it is given or how fast it gets results is key to understanding how good the system's design and performance actually is. In a laser system with a gain medium, there are multiple efficiencies to be aware of. There is the electric to optical efficiency, a rate of how well the laser takes the energy from its power source and converts it to a beam. The fact that the crystal fluoresces in all directions and only some of the light is captured by the curved mirrors and used in the two paths also reduces the power used in the system. This efficiency is also complicated due to the fact that we are not hitting the crystal directly, but actually off center. Finally, the measure of the final output beam's power, in this case feedback, can be different than at other stages in the process due to misalignment.

Saturation intensity is the proper term for the efficiency assigned to how much power is lost due to the beam hitting the crystal either directly or off center [27]. For the case of a direct and straight through hit, the saturation intensity is given as

$$I = I_{sat} \equiv \frac{h\omega}{\sigma\tau_{eff}}$$

Should the beam not hit the gain medium perfectly, the equation becomes

$$I_{sat}(\omega) = I_{sat}(\omega_a) \times \left[1 + \left(2 \frac{\omega - \omega_a}{\Delta\omega_a} \right)^2 \right]$$

This value can be used as I_{extr} in the equation for power extraction inefficiency as follows:

$$\eta_{extr} = \frac{I_{extr}}{I_{avail}} = \frac{\ln(G_0) - \ln(G)}{\ln(G_0)} = 1 - \frac{G_{cB}}{G_{0,dB}}$$

This equation is applicable for homogenous saturation in laser amplifiers and the efficiency in it is for the best case scenario for a system with no optics used other than just the laser. For most Ti:Sapphire laser systems, the best extraction efficiencies represent around 57% of the pump power [28]. For the highest power our laser would be set to, this efficiency could give 3420mV of feedback for both arms combined. This is due to the idea of coupling. Our project used optics such as a gain medium and various mirrors, so we have to take them into account. For this case, we calculate the extraction efficiency with optimum output coupling. In other words, the value given the need for other optic parts. It is recognized that a system can never be perfectly aligned due to factors that can't be helped such as human error. However, there can still be a highest value obtainable in this situation. That is,

$$\eta_{opt} = \left[1 - \sqrt{\frac{\delta_o}{2\alpha_{mo}\rho_m}} \right]^2$$

Most Ti:Sapphire laser systems have this extraction efficiency being anywhere between 10 to 30% of the pump power [28]. Taking our max output power of 6W, the maximum efficiency would be 600 to 1800mV. These values, however, are for best case scenarios and many systems never reach the upper end of this spectrum.